4-2023

Molecular and Cellular Investigations of Prader-Willi Syndrome

Anna K. Victor
University of Tennessee Health Science Center

Molecular and Cellular Investigations of Prader-Willi Syndrome

Abstract

Prader-Willi syndrome (PWS) is a complex multigenic neurodevelopmental disorder resulting in hypotonia, developmental delay, hypogonadism, sleep dysfunction and childhood onset obesity affecting 1 in 10,000 to 30,000 individuals. PWS is an imprinting disorder that is caused by a loss of expression of maternally imprinted genes in the 15q11.2-q13 region including NDN, MAGEL2, SNRPN/SNURF, and a cluster of snoRNAs. The majority of cases are caused by inheriting a paternal allele deletion of this region (65-75%) and a smaller number are caused by chromosome 15 maternal uniparental disomy (UPD) (20-30%) or imprinting center defects (1-3%). Here, we used dental pulp stem cells (DPSC), differentiated to neuronal cultures, to investigate the molecular and cellular phenotypes of PWS neurons. DPSC are multipotent stem cells that accurately recapitulate the epigenetic signature of embryonic stem cells and can differentiate to a variety of cell types. Our group has collected over 40 individual PWS lines across the different genetic subgroups. In Chapter 2, we investigated the transcriptional differences in PWS subtypes. While the UPD subtype has milder classical PWS phenotypes, there is an increased risk of developing autism spectrum disorder (ASD) (30% versus 18%) and cycloid psychosis. Using RNA sequencing (RNAseq), we found a global decrease in mitochondrial transcript expression and a mitochondrial aggregate phenotype in PWS UPD +ASD neurons. In Chapter 3, we optimized a bioluminescent assay to visualize the circadian rhythms in PWS neurons. Additionally, we used this assay to analyze circadian rhythms in neurons from individuals with Schaaf-Yang syndrome (SYS), a similar syndrome resulting from mutations in MAGEL2. Using this assay, we found discordant circadian cycling in both PWS and SYS. We also identified two distinct period length phenotypes in PWS neurons that were significantly different than neurotypical control neurons. In Chapter 4, we used a novel approach to single-cell sequencing (SPLiT-Seq) to identify transcriptional differences between neuronal populations from PWS and neurotypical control subjects. In addition to finding several transcripts differentially expressed that are related to PWS phenotypes such as hypogonadism and endocytic recycling, we found a delay in neurogenesis in the PWS neurons. In Chapter 5, we focused our attention on another obesity disorder for comparison. We used RNAseq to determine the transcriptional similarities and differences between PWS, Rapid-Onset Obesity with Hypothalamic Dysregulation, Hypoventilation, and Autonomic Dysfunction (ROHHAD) and Congenital Central Hypoventilation syndrome (CCHS). ROHHAD presents with several key similarities to PWS including rapid-onset obesity and hypothalamic dysfunction. In this study, we found six transcripts differentially expressed in both PWS and ROHHAD and that these transcripts were not related to an obesity pathway or hypothalamic function. Finally, I discussed how the assays and methods described here provide a pipeline for investigating other neurogenetic disorders and how the data discussed in each of these chapters connects to possible defects caused by the spectrum of PWS genetic changes.

Document Type

Dissertation

Degree Name

Doctor of Philosophy (PhD)

Program

Biomedical Sciences

Research Advisor

Lawrence T. Reiter, PhD

Keywords

Autism; Circadian Rhythm; Dental pulp stem cells; MAGEL2; Neurogenetics; Prader-Willi syndrome

Subject Categories

Analytical, Diagnostic and Therapeutic Techniques and Equipment | Congenital, Hereditary, and Neonatal Diseases and Abnormalities | Diseases | Investigative Techniques | Medicine and Health Sciences | Nervous System Diseases

UNIVERSITY OF TENNESSEE HEALTH SCIENCE CENTER

DOCTORAL DISSERTATION

Molecular and Cellular Investigations of Prader-Willi Syndrome

Author:
Anna K. Victor

Advisor:
Lawrence T. Reiter, Ph.D.

A Dissertation Presented for The Graduate Studies Council of
The University of Tennessee Health Science Center
in Partial Fulfillment of the Requirements for the Doctor of Philosophy degree from
The University of Tennessee

in

Integrated Biomedical Sciences: Neuroscience
College of Graduate Health Sciences

April 2023

DEDICATION

I dedicate this dissertation to my wonderful parents, Rick and Renee, and my fiancé, Scott. Without your constant love and support throughout this process, it would not have been possible. I also dedicate this work to my daughter, Penelope, although entering late in my graduate career, she has been a constant source of joy while completing my degree.

ACKNOWLEDGEMENTS

Dr. Lawrence Reiter, words cannot describe my gratitude for your guidance and mentorship throughout my graduate career. Your knowledge and support throughout this process has been invaluable to my growth as both a scientist and a leader.

The members of my committee, Dr. Tiffany Seagroves, Dr. Jamy Peng, Dr. T.J. Hollingsworth, and Dr. Heather Smallwood. Thank you for your support and feedback throughout this process.

Thank you to the Foundation for Prader-Willi Research for their generous funding and continued support of this important work.

Finally, thank you to the Prader-Willi community for supporting our research through the generous donation of tooth samples and genetic data without which this work would not be possible.

ABSTRACT

Prader-Willi syndrome (PWS) is a complex multigenic neurodevelopmental disorder resulting in hypotonia, developmental delay, hypogonadism, sleep dysfunction and childhood onset obesity affecting 1 in 10,000 to 30,000 individuals worldwide. PWS is an imprinting disorder that is caused by a loss of expression of maternally imprinted genes in the 15q11.2-q13 region including *NDN*, *MAGEL2*, *SNRPN/SNURF*, and a cluster of snoRNAs. The majority of cases are caused by inheriting a paternal allele deletion of this region (65-75%) and a smaller number are caused by chromosome 15 maternal uniparental disomy (UPD) (20-30%) or imprinting center defects (1-3%). Here, we used dental pulp stem cells (DPSC), differentiated to neuronal cultures, to investigate the molecular and cellular phenotypes of PWS neurons. DPSC are multipotent stem cells that accurately recapitulate the epigenetic signature of embryonic stem cells and can differentiate to a variety of cell types. Our group has collected over 40 individual PWS lines across the different genetic subgroups. In Chapter 2, we investigated the transcriptional differences in PWS subtypes. While the UPD subtype has milder classical PWS phenotypes, there is an increased risk of developing autism spectrum disorder (ASD) (30% versus 18%) and cycloid psychosis. Using RNA sequencing (RNAseq), we found a global decrease in mitochondrial transcript expression and a mitochondrial aggregate phenotype in PWS UPD +ASD neurons. In Chapter 3, we optimized a bioluminescent assay to visualize the circadian rhythms in PWS neurons. Additionally, we used this assay to analyze circadian rhythms in neurons from individuals with Schaaf-Yang syndrome (SYS), a similar syndrome resulting from mutations in *MAGEL2*. Using this assay, we found discordant circadian cycling in both PWS and SYS. We also identified two distinct period length phenotypes in PWS neurons that were significantly different than neurotypical control neurons. In Chapter 4, we used a novel approach to single-cell sequencing (SPLiT-Seq) to identify transcriptional differences between neuronal populations from PWS and neurotypical control subjects. In addition to finding several transcripts differentially expressed that are related to PWS phenotypes such as hypogonadism and endocytic recycling, we found a delay in neurogenesis in the PWS neurons. In Chapter 5, we focused our attention on another obesity disorder for comparison. We used RNAseq to determine the transcriptional similarities and differences between PWS, Rapid-Onset Obesity with Hypothalamic Dysregulation, Hypoventilation, and Autonomic Dysfunction (ROHHAD) and Congenital Central Hypoventilation syndrome (CCHS). ROHHAD presents with several key similarities to PWS including rapid-onset obesity and hypothalamic dysfunction. In this study, we found six transcripts differentially expressed in both PWS and ROHHAD and that these transcripts were not related to an obesity pathway or hypothalamic function. Finally, I discussed how the assays and methods described here provide a pipeline for investigating other neurogenetic disorders and how the data discussed in each of these chapters connects to possible defects caused by the spectrum of PWS genetic changes.

TABLE OF CONTENTS

LIST OF TABLES

LIST OF FIGURES

LIST OF ABBREVIATIONS

ANS	Autonomic nervous system
AS	Angelman syndrome
ASD	Autism Spectrum disorder
BP	Break point
CCHS	Congenital Central Hypoventilation syndrome
DAVID	Database for Annotation, Visualization and Integrated Discovery
DPSC	Dental pulp stem cells
EDS	Excessive daytime sleepiness
ESC	Embryonic stem cell
ETC	Electron transport chain
GO	Gene ontology
GUID	Globally unique identifier
IC	Imprinting center
iPSC	Induced pluripotent stem cell
MD	Mitochondrial dysfunction
MSC	Multipotent stem cells
NSC	Neural stem cells
OSA	Obstructive sleep apnea
OXPHOS	Oxidative phosphorylation
PARM	Polyalanine repeat mutation
PW-del	Prader-Willi syndrome (deletion subtype)
PW-UPD	Prader-Willi syndrome (UPD subtype)
PWACR	Prader-Willi/Angelman critical region
PWS	Prader-Willi syndrome
REM	Rapid eye movement
ROHHAD	Rapid-onset obesity with hypothalamic dysregulation, hypoventilation and autonomic dysregulation
SCN	Suprachiasmatic nucleus
SCQ	Social Communication Questionnaire
SDB	Sleep disordered breathing
SPLiT-seq	Split Pool Ligation-based Transcriptome sequencing
SYS	Schaaf-Yang syndrome
UMAP	Uniform manifold approximation and projection
UPD	Uniparental disomy

CHAPTER 1. INTRODUCTION

Prader-Willi Syndrome–History and Subtypes

Prader-Willi syndrome (PWS) is a complex neurodevelopmental disorder characterized by hypotonia, obesity, hyperphagia, hypogonadism and developmental delay with a birth prevalence of 1/10,000 to 1/30,000 [1]. Credit for the discovery of PWS is given to Andrea Prader and Heinrich Willi who, in 1956, describe a cohort of patients presenting with extreme obesity, small hands and feet, intellectual disability, insatiable hunger and hypotonia from birth [2]. However, review of historical medical case files identified a case report from 1864 by Langsdon Down in which he describes a 25-year-old female presenting with rapid onset obesity starting at age seven, facial dysmorphia, hypotonia, short stature, small hands and feet, disordered pubertal development, and intellectual disability. Down's case is considered the first description in the medical literature of PWS [3]. Over 20 years later, in 1981, Ledbetter *et al.* identified a microdeletion on the 15th chromosome (15q11.2-q13) as the causative genetic lesion in PWS [4]. The region is defined as the Prader-Willi/Angelman critical region (PWACR). Later, it was determined that this *de novo* deletion arose from the paternal copy of the 15th chromosome [5]. Many studies followed using high resolution chromosome analysis to genotype PWS cohorts, revealing that while the majority of PWS cases were caused by this microdeletion, it could not explain all the cases [6-8].

About 60% of PWS cases can be explained by a deletion on the paternal 15th chromosome. Nicholls *et al.* used restriction length polymorphism analysis to determine parent of origin for the 15th chromosome of PWS subjects without a deletion. They found that, in most of these cases, the subjects inherited two copies of the maternal allele and no paternal copy [9]. They concluded that the majority of remaining PWS (~30%) cases are not caused by a mutation of any of the genes within the region, but rather by the lack of a paternal copy of this region [9, 10]. This type of genetic inheritance, in which only one parental allele is inherited on both chromosomes, is called uniparental disomy (UPD). This suggested that PWS is an imprinting disorder. Imprinting is a genetic mechanism where expression differs based on the parent of origin of the genetic information. In PWS, the genes *SNRPN/SNURF*, *MAGEL2*, *NDN*, *MKRN3* and a cluster of small nucleolar RNAs (snoRNAs) are imprinted on the maternal chromosome and only expressed from the paternal copy. In the 15q11.2-q13 region, there are both non-imprinted and paternally imprinted genes in addition to the maternally imprinted genes. **Figure 1-1** illustrates the PWACR region and the imprinting status of the genes. For normal development, one copy from each parent must be inherited for the correct expression of imprinted genes. Additional studies found another subtype of PWS (4-7%) arising from imprinting center (IC) defects in the PWACR region. This type of PWS is conferred by a mutation in the IC that controls the paternal imprint of genes in the PWACR region [10-12]. In addition to these subtypes, there is variability within the PWS deletion group. There are two deletion classes with different breakpoints on chromosome 15. The larger deletion, Type 1, is from break point (BP) 1 to BP3. The smaller deletion class, Type 2, encompasses BP2 to BP3, leaving the genes *TUBGCP5*, *CYFIP1*, *NIPA1*

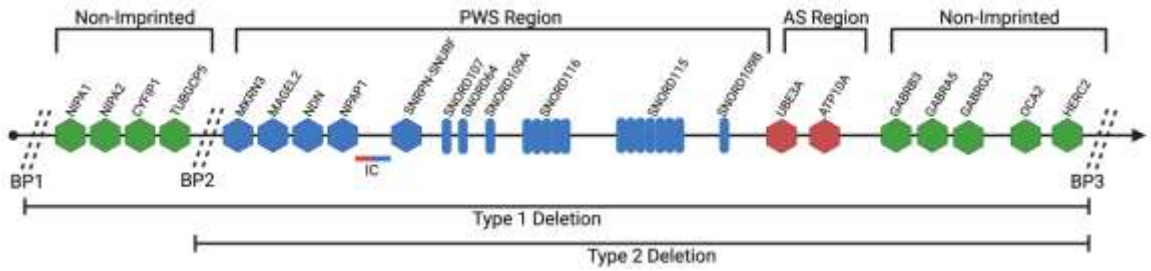

Figure 1-1. Prader-Willi/Angelman critical region (15q11.2-q13).
Within the 15q11.2-13 region, there are genes that are maternally imprinted (blue), paternally imprinted (red), and non-imprinted (green). In Prader-Willi syndrome (PWS), there are two types of paternal deletions, Type 1 and Type 2. Type 1 harbors a larger region spanning from breakpoint (BP) 1 to BP3. Type 2 encompasses a smaller deletion from BP2 to BP3. *UBE3A* and *ATP10A* are within the Angelman syndrome (AS) region. AS is a different syndrome that results from a maternal deletion of this region. Created with BioRender.com.

and *NIPA2* intact [10]. Several groups have found no clinical difference between these two deletion types, likely due to the non-imprinted status of the genes differing between the two types [13, 14]. However, some groups have suggested that deletion of the BP1-BP2 alone can result in a distinct syndrome called Burnside-Butler syndrome (BBS) [15]. The most common phenotypes in BBS are neurodevelopmental delay (~70%), language impairment (~60%) and motor delay (~40%) [16].

The phenotypes resulting from the loss of paternal expression of this region are complex and affect multiple organ systems. PWS conferred by deletion (PW-del) versus UPD (PW-UPD) has differing phenotypic consequences. In the next section, I will discuss the phenotypic outcomes of PWS and how these different genetic subtypes vary from each other.

The Primary Phenotypic Consequences of Prader-Willi Syndrome

Uniparental Disomy Versus Deletion Subtype

Since one would expect both maternal alleles of the imprinted *UBE3A* gene to be expressed~~,~~ there may be a higher dosage of gene expression for *UBE3A* in the PW-UPD group, along with the loss of paternally expressed genes within the region [17]. An increase in *UBE3A* dosage has been suggested as a cause for increased autism spectrum disorder (ASD) [18-20] and other psychiatric disorder susceptibility [21, 22]. Indeed, PW-UPD cases have an increased incidence of ASD versus PW-del subjects (~35% vs 18%) [23-26] as well as an increased likelihood for psychosis later in life [27-30].

Although the UPD genotype appears to confer an increased risk for neuropsychiatric disorders, studies have found that UPD subjects tend to have milder expressivity of the classical PWS features including hypotonia, hypopigmentation, facial dysmorphia and skin-picking [31, 32]. In fact, PW-UPD patients were diagnosed at later ages because of this milder symptomology, specifically the facial dysmorphia [33]. Additionally, PW-UPD subjects show higher verbal and performance intelligence quotient (IQ) scores [34]. Deletion subjects are also more prone to obesity than the UPD group [35]. PW-UPD is significantly correlated to advanced maternal age [36, 37]. Compared to deletion patients, UPD cases arise from older mothers (~37 versus ~30 years of age) [38]. Although these genetic subtypes differ in susceptibility to neuropsychiatric disease and severity of PWS features, they share the core characteristics of PWS, including hypotonia, developmental delay, obesity, hyperphagia, hypogonadism and sleep defects.

Hypotonia

Hypotonia from infancy occurs in nearly all PWS cases. At birth, newborns with PWS have poor suckle, decreased movement, weak cry and poor reflexes [39]. Muscle

biopsy has shown normal muscle tissue, suggesting a central cause for the hypotonia. Due to poor reflexes, decreased appetite and general lethargy, infants often fail to thrive and must receive clinical intervention [40]. Once childhood is reached, feeding behaviors and hypotonia improve. By adulthood, hypotonia is no longer apparent with only slightly decreased muscle tone noted [40].

Developmental Delay

Motor skill development is impaired in 90-100% of PWS individuals [39]. Milestones are achieved usually by double the developmentally appropriate age. Most PWS patients have mild intellectual disabilities which is apparent once the child begins school [40]. Children with PWS have learning disabilities and perform at a lower academic level on all domains than their peers [41].

Hyperphagia and Obesity

During early childhood, children with PWS begin experiencing rapid weight gain with no change in their appetite, however later in childhood, while still rapidly gaining weight, they experience a dramatic increase in appetite known as hyperphagia [42]. They begin to feel insatiable despite the amount of food consumed [40]. They typically display food-seeking and hoarding behaviors in response to this lack of satiety, which often leads to obesity. These behaviors arise likely due to the hypothalamic dysfunction present in PWS causing hyperphagia, but obesity may also arise from autonomic dysfunction involving the sympathetic and parasympathetic systems [42, 43]. Hyperphagia continues into adulthood for most and can lead to morbid obesity along with the life-threatening complications that result from obesity. Obesity-related disease is a common cause of death in PWS subjects [42].

Hypogonadism

Hypogonadism is noted from birth in both males and females with PWS. Most male newborns present with bilateral or unilateral cryptorchidism, while females display hypoplasia of the labia minora [44]. Puberty is delayed in PWS often requiring pharmacological induction with sex steroids [44]. Hypogonadism in PWS is primarily thought to arise from hypothalamic dysfunction resulting in the decreased excretion of gonadotropins, however studies show that hypogonadism arises from both central mechanisms (hypothalamus) and peripheral mechanisms (testicular origin) [44-46].

Sleep Dysfunction

There are a variety of sleep abnormalities in PWS including excessive daytime sleepiness (EDS), central sleep apnea, obstructive sleep apnea (OSA), and sleep-related

hypoventilation, collectively referred to as sleep disordered breathing (SDB) [47]. One study found SDB present in 53% of children and 41% of adults with PWS [48]. Obesity in PWS subjects can often lead to OSA [49]. One group found 80% of their pediatric PWS cohort presented with OSA [50]. PWS patients also have altered ventilatory responses to hypoxemia and hypercapnia [51]. PWS individuals have been shown to lack the appropriate hypoxic ventilatory response when breathing air with low oxygen [52]. These phenotypes are thought to arise from dysfunctional peripheral chemoreceptors and often require clinical intervention.

Interestingly, even after their SDB is treated, many patients still experience EDS [51]. Patients report a high frequency of daytime napping and PWS individuals have been found to have higher self-reported EDS rates than non-PWS individuals with intellectual disabilities [53, 54]. Hypothalamic dysfunction has been hypothesized to be the culprit of EDS in PWS. The hypothalamus regulates non-rapid eye movement sleep (NREM) and rapid eye movement sleep (REM) cycling [53]. The hypothalamus is also home to the suprachiasmatic nucleus (SCN) which regulates circadian rhythms [55]. Additionally, it harbors neurons that secrete hypocretin and orexin and low levels of these hormones have been associated with narcolepsy [53]. The defective regulation of these hormones and REM sleep cycling could contribute to the high rate of EDS seen in PWS.

Insights from Mouse Models of PWS

The genomic structure of the PWACR on the 15th chromosome is highly conserved in mice and correlates to the murine genomic region 7C [56]. Due to the high evolutionary conservation of this region between mice and humans, mouse models are a viable option for studying PWS. Kummerfeld *et al.* recently reviewed the mouse models that have been created to recapitulate the disorder [56]. The first PWS mouse model was a model of the UPD form (both 7C chromosomes were maternally derived). These animals displayed weak feeding reflexes and failure to thrive causing them to die 2-8 days post birth [57]. In 1999, Gabriel *et al.* created a mouse model with the entire PWACR region deleted [58]. Although this model also displayed post-natal lethality, they could be observed for a longer period than previous models, allowing more PWS symptomology to emerge. These mice displayed failure to thrive, growth retardation, reduced movement, respiratory irregularities, and pancreatic apoptosis as well as increased levels of ghrelin and corticosterone [58]. Although these models were ultimately lethal, they demonstrated the importance of this entire gene region to the PWS pathology.

The next mouse models focused on smaller monogenic deletions of individual imprinted genes in an attempt to uncover their roles in the PWS pathogenesis. A *Mkrn3* knockout (KO) mouse displayed decreased weight at post-natal day 45 and an earlier pubertal onset with increased production of gonadotropin-releasing hormone [59]. A *Magel2* KO mouse initially showed growth retardation and failure to thrive resulting in decreased weight; however once weaned they displayed higher body fat percentage and slightly increased weight versus wildtype (WT) litter mates [60, 61]. In addition, this

model exhibited delayed pubertal onset, growth hormone and metabolic defects as well as defects in neuropeptide processing [60, 62, 63]. While the *Magel2* KO mice show many of the early PWS symptoms, they do not exhibit the characteristic obesity and hyperphagia phenotypes. Several *Ndn* KO mouse models were created using varying genetic methods and backgrounds. The most notable phenotypes seen in the *Ndn* KO mice are respiratory distress and circadian rhythm defects [64-67]. One group also reported reduced oxytocin-producing and luteinizing hormone-releasing hormone neurons [64]. Mice harboring a deletion from exon 2 in *Snrpn* to *Ube3a* had poor survivability, but the 20% that did survive displayed growth retardation and hypotonia. However, these mice were fertile and did not develop obesity [68]. Other mouse models with smaller paternal deletions in the *Snrpn/Snurf* gene showed no differences compared to WT mice [56]. Two mouse models were generated with *Snord116* deleted [69, 70]. Both models showed growth retardation and altered sleep cycles [70, 71]. Additionally, the model created by Ding *et al.* had decreased levels of ghrelin, altered diurnal methylation, respiratory rate defects, increased anxiety, and learning and memory impairments [69, 72, 73]. Interestingly, this model showed signs of hyperphagia (increased food intake) but no significant difference in weight when compared to WT littermates [69]. Recently a mouse model harboring a *Snord115* deletion was created [74]. These mice displayed no notable functional differences from their WT littermates [74].

While these mouse models have greatly increased our knowledge of the PWS pathogenesis and the functional consequences of the genes within the PWS critical region, no model was able to fully recapitulate the PWS phenotype. There is a critical need for *ex vivo* models that originate from PWS patients themselves. To this end, we have developed a collection of PWS stem cell lines derived from dental pulp that can differentiate into a variety of cell types, allowing us to study the cellular and molecular consequences of PWS in patient-derived neurons.

Dental Pulp Stem Cells as a Model for the Study of Neurogenetic Disorders[1]

To understand the complex molecular and physiological pathways underlying neurogenetic syndromes, it is often useful to have an *in vitro* model that accurately recapitulates live neurons in the disease state. The use of induced pluripotent stem cells (iPSC) to model the function of cortical neurons from patient derived fibroblasts or blood cells is now well-documented [75-78]. However, there are notable drawbacks to using these de-differentiated, reprogrammed cells as *in vitro* models for molecular studies. Recent studies indicate that iPSC may not accurately represent changes associated with

[1] This portion of chapter republished from final submission with permission. Victor, A.K. and L.T. Reiter, *Dental pulp stem cells for the study of neurogenetic disorders.* Hum Mol Genet, 2017. **26**(R2): p. R166-R171. 10.1093/hmg/ddx208 [137].

neurological pathogenesis since residual epigenetic marks associated with their original cell type which can lead to inappropriate gene expression in the newly derived iPSC neurons [79]. This residual epigenetic signature, along with genomic instability [80], tumorigenic potential [81], and a high mutational load [82] raises concerns for the use of iPSC to model neurogenic disorders that often have complicated genetic and epigenetic etiologies which can alter the molecular changes indicative of the particular syndrome.

Dental pulp stem cells (DPSC) [83, 84] provide an alternative to iPSC and overcome some of the problems associated with epigenetic changes and re-programming [85, 86]. Another significant advantage to using DPSC is that they can be easily obtained from exfoliated or extracted teeth and then transported within 48hrs to the laboratory [87]. The easy collection and transport means that families of children with various neurogenetic syndromes are able to directly contribute to the investigation of these disorders without ever traveling to the clinic or laboratory. It also means that many more teeth representing many more individuals with these syndromes can be collected than for iPSC, which can be difficult to reprogram and often yield clones of a single individual for molecular studies [88-90].

DPSC differentiate into functionally active neurons in the presence of varying neurotrophic factors [91-93]. DPSC have been shown to differentiate into various neural cell types including dopaminergic cells [94-96], glutamatergic and GABAergic cells [97], as well as glial and Schwann cells [98, 99]. Additionally, the ability of pre-differentiated DPSC to integrate into the brains of normal rats and a rat model of traumatic cortical lesion speaks to their therapeutic potential [100]. Kiraly *et al.* showed that these engrafted DPSC retained their neuronal immunohistochemical and electrophysiological characteristics weeks after transplantation. In the traumatic cortical lesion rat model, the pre-differentiated DPSC even migrated to the cortex in response to injury. Pre-differentiated DPSC have also been shown to improve neurological function in a Parkinsonian rat model. These dopaminergic-like neurons increased brain dopamine levels and the neuroprotection of endogenous dopaminergic neurons [101]. These studies suggest great promise for using DPSC in translational research.

Stem Cells of the Dental Pulp

Stem cells are classified into three distinct categories: embryonic stem cells (ESC), adult (post-natal) stem cells (ASC) and induced pluripotent stem cells (iPSC). ASC encompass a broad range of different stem cells including neural (NSC) and mesenchymal (MSC) stem cells [102]. MSC have been shown to differentiate into several terminal cell types such as osteoblasts, adipocytes, and chondrogenic cells [103], making them prime candidates for cell based therapies. MSC have been isolated from a variety of tissues including bone marrow (BMSC) and dental pulp (DPSC).

DPSC reside deep in the dental pulp at the center of the tooth in the pulp cavity and are a part of the dentin-pulp complex (**Figure 1-2**). The regenerative quality of this complex relies on activity within the dental pulp. Gronthos *et al*. discovered a unique

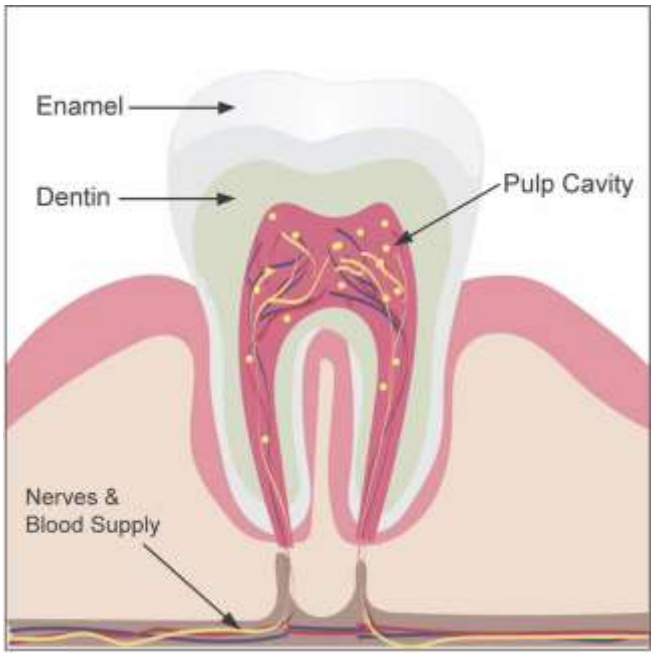

Figure 1-2. Longitudinal section of a tooth depicting the pulp cavity where the dental pulp resides.
Dental pulp stem cells are found within the dental pulp and are represented here as yellow dots.

stem cell population derived from this pulp tissue that resembled BMSC [83]. They found that these cells had self-renewal capabilities and were able to differentiate into adipocytes and neural-like cells [84]. Following the initial discovery of DPSC, a separate population of stem cells arising from the pulp of deciduous ("baby") teeth was characterized. Miura *et al*. isolated stem cells from human exfoliated deciduous teeth (SHED) [104] that shared similarities with MSC found in umbilical cord blood. They also discovered that compared to DPSC, SHED had higher proliferation rates, increased cell population doublings, and a distinct morphology. This difference is not shocking given the different developmental origins between deciduous and adult teeth. Deciduous teeth develop much earlier in the prenatal period than adult teeth. This difference likely effects the stem cell niches in which these cells reside. These microenvironments are controlled by genetic, epigenetic, and environmental forces that regulate the activities of the stem cells [105]. Where a particular stem cell resides and the cell type from which it is derived can contribute to the variability in gene expression observed among stem cells isolated from different tissues.

DPSC have now been compared to other stem cell types used for neurogenetic investigations including ESC, iPSC, and other MSC. Karoaz *et al.* were among the first to compare DPSC to BMSC [106]. They found that DPSC had similar differentiation capabilities as BMSC and expressed both neural and glial specific markers. They also found that DPSC are more developed and metabolically active cells than BMSC, leading to the conclusion that DPSC demonstrate better neural and epithelial stem cell properties. More recently, more robust comparisons utilizing several types of stem cells have been performed. Umbilical cord, dental pulp, and menstrual blood are all relatively accessible sources of MSC. Ren *et al*. compared these three sources on the basis of morphology, proliferation, and differentiation capabilities [107]. Their results show that while stem cells isolated from the umbilical tissue (UC) had higher proliferative capacities, DPSC demonstrated less cellular senescence and higher osteogenic capabilities than either the UC or menstrual blood cells.

Similarly, Kang *et al.* compared gene expression between DPSC and UC [108]. They found that genes related to growth factor activity, receptor activity, and signal transduction were significantly upregulated in DPSC compared to UC. In contrast, genes related to cell proliferation, angiogenesis, and immune responses were expressed in higher levels in the UC. These studies complement each other since the higher proliferation rates of UC correlates with the higher expression of genes related to cell proliferation and the lower senescence of the DPSC likely correlates to the increased expression of genes related to growth factor activity.

Isobe *et al.* compared the differentiation capacity among DPSC, SHED, BMSC, and synovial fluid cells (SFC), all considered MSC [109]. Multipotent capacity was significantly different among these stem cell sources. BMSC and SFC had higher osteogenic and chondrogenic capacity, while DPSC and SHED demonstrated increased neurogenesis. They also observed that SHED showed higher proliferation rates compared to both DPSC and BMSC. Another study comparing DPSC, SHED, and BMSC found that DPSC and SHED express higher levels of embryonic stem cell markers, Oct-4 and

STRO-1, than BMSC. As in other studies, BMSC showed higher osteogenic capabilities than SHED and DPSC. They also present notable differences between DPSC and SHED. SHED had higher osteogenic capabilities and expression of embryonic stem cell markers than DPSC. Between DPSC and SHED, SHED demonstrated higher expression of these markers [110]. Both studies concluded that SHED likely represent a more primitive cell type than DPSC. These comparison studies both found that the levels of MSC-marker expression between the cell types is similar, but the differentiation potential is significantly different, even between SHED and DPSC.

Comparative studies between DPSC and iPSC, the main stem cell culture used to study neurogenetic syndromes, are still limited. However, there have been multiple studies focused on the efficiency and reliability of re-programming DPSC into iPSC [111-114]. DPSC express many ESC markers even prior to reprogramming, thus it has been proposed that these cell types could be a more efficient source of creating iPSC than cells traditionally used for iPSC generation [113]. A transcriptomic analysis of iPSC-derived neurons from both SHED and fibroblasts revealed lower expression of genes involved in hindbrain development (*HOX* and *IRX* families) and higher expression of genes involved in forebrain development (*FOXP2, OTX1, and LHX2)* in the SHED derived iPSC neurons [115]. FOXP2 is involved in language and communication networks and has been implicated in ASD pathology, leading to the conclusion that DPSC derived iPSC may be appropriate for the study of neurodevelopmental disorders [115].

Analyzing the genetic and functional differences between iPSC and DPSC is crucial for determining the best approach to modeling both molecular and neurophysiological changes that occur in neurons in the disease state [112]. Since reprogrammed cells often retain epigenetic marks from their original cell type, understanding the consequences of reprogramming or cellular origin on epigenetic marks is essential while developing reliable disease models. Dunaway *et al.* analyzed how accurately SHED modeled early life and whole genome DNA methylation patterns compared to iPSC [86]. They found that the primitive origin of SHED allows these cells to model the embryonic inner cellular mass and the placenta more accurately. They concluded that compared to iPSC, DPSC are a more reliable model for the study of genome architecture and gene expression changes that occur in neurodevelopmental disease [86].

There is great potential for the use of stem cells to directly treat human disease by returning healthy stem cells with neurogenetic potential to the brain [116, 117]. In order for stem cells cultured *ex vivo* to be considered for therapeutic use, however, they must meet certain criteria including assessment of *in vivo* tumorigenic potential. While the tumorigenic potential of iPSC is well established [118, 119], our lab has shown that immortalized DPSC do not form tumors *in vivo* [85]. The tumorigenic potential of both spontaneous and induced immortalized DPSC was assessed. Karyotype analysis revealed that the spontaneously immortalized DPSC showed no genomic instability. The genomic instability of spontaneously immortalized stem cells from other tissues sources has been shown in multiple studies [80, 120]. The absence of this genomic instability and

tumorigenic potential adds to the growing evidence that DPSC may represent a better stem cell source for both disease modeling and cell therapies.

Multipotent Differentiation Provides Cellular Specificity for a Variety of Syndromes

As neurodevelopmental disorders often involve multiple neuronal and non-neuronal cell types that can contribute to the phenotype, developing target treatments without access to the specific neuronal cell types can limit the effectiveness of these studies. Neural stem cells (NSC) differentiate into neurons and glia *in vivo* and *in vitro*, thus they represent a mixed population of cells that may represent the varied cell types found in the brain. DPSC, which arise for the neural crest, are an excellent proxy for NSC to study in the lab setting. When given the appropriate environmental cues, DPSC differentiate into functional neurons showing neuronal morphology and responsive sodium and potassium channels [121]. Arthur *et al.* first differentiated DPSC into functional neurons using a protocol typically used to differentiate ESC [92]. Using fibroblast growth factor or epidermal growth factor signaling, they were able to differentiate DPSC into neurons that exhibited functional sodium channels. Kiraly *et al.* also developed a protocol for differentiating DPSC into a neural population [93]. In their protocol, the simultaneous activation of protein kinase C and cyclic AMP pathways induced neural differentiation. The DPSC-derived neurons had morphological characteristics similar to neurons derived from other sources (**Figure 1-3**). They were able to show genetic markers associated with neural differentiation and functional sodium and potassium channels, demonstrating strong evidence that the DPSC had differentiated into functional neurons. Using the protocol established by Kiraly *et al.*, we assessed the global gene expression changes resulting from DPSC into mixed neuronal cultures [93]. We found that the differentiation process significantly changes gene expression and that these expression changes occur through the transcription factor RE1-Silencing Transcription (REST). The differentiated DPSC also positive for the neuronal marker MAP2 and expression for the glial marker GFAP was decreased in the mixed neuron/glia cultures versus undifferentiated DPSC but still present [122].

Differentiating DPSC into specific neural subtypes is crucial for modeling neurogenetic disorders as different syndromes affect different neural sub-types in a distinct manner. Several protocols have been published for differentiating DPSC and SHED to dopaminergic cells, or DA neurons. Wang *et al.* were the first to present a protocol for DA differentiation of SHED [94]. This protocol results in about 10% of the cells expressing tyrosine hydroxylase (TH), the enzyme that converts tyrosine to L-DOPA, an essential dopamine precursor. Although dopaminergic induction resulted in a relatively small proportion of TH+ neurons, they also showed that when these DA-like cells were introduced into a Parkinson disease mouse model some Parkinson-like behavioral abnormalities were corrected [94]. Kanafi *et al.* published a two-step protocol using the embryonic midbrain cues, SHH and FGF8 [96]. They found that over 70% of cells were TH+ after induction and maturation. In a related study, they found that while this protocol induced the DPSC into functional DA-like cells, it was not efficient in differentiating the SHED to a terminal DA fate [123]. Fujii *et al.* differentiated SHED

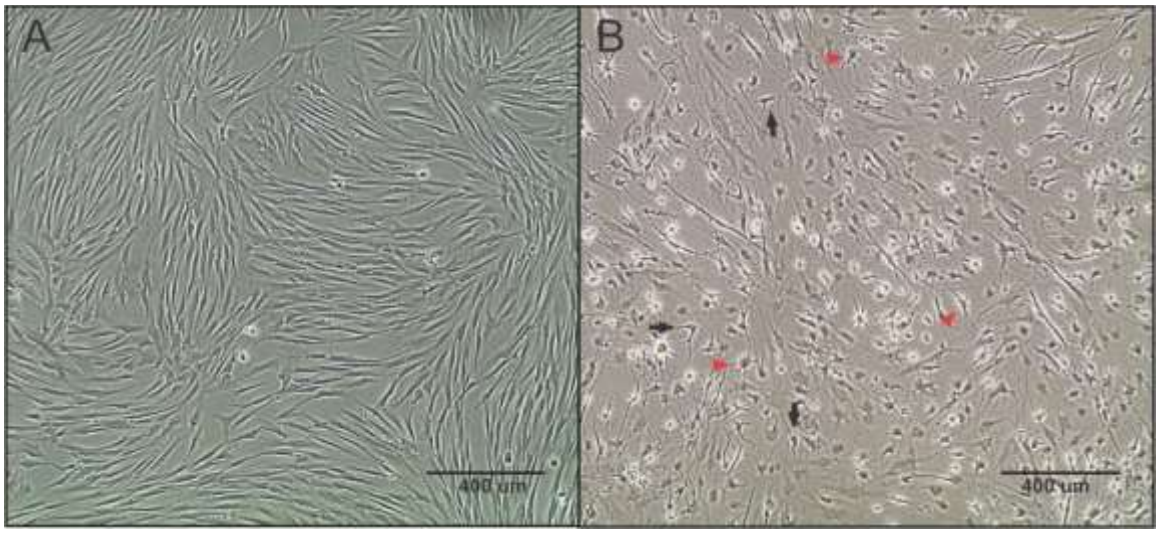

Figure 1-3. Morphological changes during neuronal differentiation of DPSC. **(A)** Undifferentiated DPSC have a spindle-shape similar to fibroblasts. **(B)** DPSC were differentiated and allowed to mature for 3 weeks, resulting in a mixed culture containing both neuron-like and glial-like cells. The neurons (black arrows) show a pyramidal-like, neuronal morphology with shorter projections similar to dendrites and a longer axonal projection on the opposing side. The glial cells (red arrows) show a typical star-shaped morphology with a rounded cell body and small projections extending from the perimeter. Both images were taken at a 10x magnification using phase-contrast microscopy. Dental pulp stem cells (DPSC).

into DA-like neurons using a BDNF stimulating protocol [101]. Compared to other dopaminergic protocols (SHH and FGF8), they discovered that a BDNF protocol resulted in the most TH+ cells (~75%). Because BDNF specifically is involved in the differentiation of new neurons and synapses, they concluded that a protocol with early neurogenesis signals and later maturation of DA neurons was required for efficient dopaminergic differentiation from SHED. This could provide a potential solution for the differentiation of SHED to DA-like neurons.

Although there is little research published showing differentiation of DPSC along neuronal lineages other than DA, one group has been able to differentiate DPSC into a neuronal population that shows increased glutamatergic and GABAergic-like cells [97]. Depletion of PIN1 results in suppression of neurogenesis, while overexpression results in enhanced neurogenesis. PIN1 functions in regulating key signaling molecules involved in cell growth and differentiation. Cho *et al*. observed that upon differentiation, these neuronal populations displayed increased glutamatergic and GABA-ergic markers, while dopaminergic and glial marker expression was decreased resulting in a more glutamatergic and GABA-ergic like neuronal population [97]. These results imply that we may soon develop protocols for a variety of neuronal cell types (dopaminergic, GABAergic, hypothalamic, cortical, etc.), which can be generated from patient-derived DPSC.

Practical Use of Primary Dental Pulp Stem Cell Cultures

All primary cultures, even stem cells, eventually undergo cellular senescence. Long term culturing of primary cells typically causes senescence through telomere shortening or replicative senescence [124], which results in a DNA damage response. Senescent cells remain metabolically active but undergo irreversible growth arrest that is accompanied by characteristic changes in gene expression. Even in stem cells, cellular senescence occurs during prolonged culture periods and results in the loss of differentiation potential and gene expression changes [125]. DPSC also undergoes age-dependent molecular and genetic changes that result in reduced proliferative capacity and differentiation potential [126]. Donor age has also been shown to positively correlate with cellular senescence and impaired regenerative abilities. In order for DPSC to be useful for long-term studies and clinical applications, it will be necessary to overcome cellular senescence in primary DPSC cultures.

The introduction of human telomerase reverse transcriptase (*hTERT*) into cells is one way to immortalize DPSC. In order for *hTERT* immortalization to be considered a practical solution to cellular senescence in DPSC, an investigation into how constitutive *hTERT* expression effects gene expression and differentiation potential of DPSC was warranted [127]. Our lab analyzed the effects of *hTERT* immortalization on the gene expression of SHED derived neurons [122]. Molecular analysis revealed that some of the transcripts that are upregulated during differentiation into neurons were suppressed by constitutive immortalization with *hTERT*. Thus, constitutive *hTERT* expression is not ideal for neurogenetic studies. Although the *hTERT* immortalized SHED demonstrated

characteristics of functional neurons, they do not accurately represent the expression patterns of donor neurons. An inducible immortalization system driving *hTERT* expression in the DPSC stage but turning it off during neuronal differentiation could be a solution. Identifying a protocol that allows for the immortalization of DPSC without affecting the molecular and genetic characteristics of the neurons derived from these cells is critical for the utility of the DPSC model of disease.

Conclusions

There are several reasons to consider DPSC for neurogenetic studies versus stem cells from other tissue sources. DPSC can be obtained non-invasively and even shipped across long distances, remaining viable in culture media for as long as 72hrs [122]. Especially for rare genetic syndromes, the ability to collect samples from distant subjects, even from other countries, is invaluable since it is often difficult to obtain large sample sizes for molecular studies of rare syndromes. More comprehensive comparison studies of various stem cell types, including DPSC, iPSC, ESC, and other MSC, derived from a single donor may help to elucidate the functional and genomic differences between stem cell types. The differentiation potential of DPSC into a variety of neuronal cell types is still largely unexplored. Future studies will require an understanding of the developmental origins and molecular characteristics of DPSC in order to identify the signaling mechanisms needed to differentiate DPSC down different neuronal lineages. Finally, the immortalization of donor DPSC for long-term propagation *in vitro* is required for scaling up the use of DPSC in the study of various disorders of the nervous system. Although the use of DPSC for the study of neurogenetic disorders is relatively new, there is great potential for this stem cell resource both in the study of disease and potentially as a source for therapeutic stem cell treatments targeted to the nervous system.

Hypothesis and Specific Aims

The complex neurological phenotypes present in PWS require novel approaches to understand the molecular pathology. Using our vast library of PWS DPSC lines, I aim to uncover the molecular pathways disturbed in PWS neurons that may be responsible for specific PWS phenotypes. The inherent benefit of this novel model system is the ability to use actual patient cells differentiated to neurons to study the molecular and functional consequences of PWS in the context of variable genetic backgrounds in a large cohort of individuals. My hypothesis is that using these patient-derived neurons, I will be able to uncover molecular and cellular phenotypes specific to PWS symptomology. To that end, I aim to:

1. Determine the gene expression differences between the deletion subtype (PW-del) and the uniparental disomy subtype (PW-UPD) of PWS in order to reveal the molecular underpinnings of the increased ASD incidence in the PW-UPD subtype. Data from these experiments is presented in Chapter 2.

2. Create an assay to measure circadian rhythms in PWS patient-derived neurons in order to detect differences in circadian cycling in PWS neurons that may be contributing to the excessive daytime sleepiness (EDS) seen in many PWS subjects. Data from these experiments is presented in Chapter 3.

3. Use a single cell sequencing approach to identify molecular changes in neurons that result in developmental delay in PWS. This data is presented in Chapter 4.

4. Compare expression data from PWS neurons to neurons from another obesity syndrome, ROHHAD, with similar phenotypes. This data is presented in Chapter

CHAPTER 2. MOLECULAR CHANGES IN PRADER-WILLI SYNDROME NERUONS REVEALS CLUES ABOUT INCREASED AUTISM SUSCEPTIBILITY[2]

Introduction

Prader-Willi syndrome (PWS) is a multifaceted neurodevelopmental disorder characterized by hypotonia, hyperphagia, and developmental delay [128]. PWS is caused by a loss of expression for one or more paternally expressed genes in the 15q11.2-q13. region (PWACR). Most PWS cases are caused by a paternal interstitial deletions in this region, but a smaller percentage of PWS is caused by the inheritance of two copies of maternal chromosome 15, maternal uniparental disomy (UPD) [129]. Due to imprinted expression of critical genes in the 15q11.2-q13.3 region, a set of normally paternally expressed genes are effectively silenced in neurons including *MAGEL2*, *SNORD115/116*, *SNRPN*, and *SNURF* [130]. PWS caused by UPD (PW-UPD) results in a milder phenotype than PWS caused by a paternal deletion (PW-del). However, UPD cases have a higher risk for autism spectrum disorder (ASD) than typically developing individuals [25, 131-134] and later in life can develop cycloid psychosis [29, 135].

The goal of this study was to identify molecular changes that may confer increased autism incidence in PW-UPD subjects through analysis of expression differences among neurons from PW-UPD, PW-del and control individuals. We used our large collection of dental pulp stem cell (DPSC) lines to generate neurons in culture for these studies [136, 137]. DPSC are neural crest stem cells that reside inside the pulp cavity of naturally shed “baby teeth” [83, 84, 104]. They are multipotent stem cells that have been differentiated to various cell types including neurons, osteocytes, glial cells, and adipocytes [99, 138, 139]. In fact, several groups have shown that DPSC-derived neuronal cultures exhibit electrophysiological properties of functional neurons [93, 122, 140, 141]. Previously, we established DPSC growth parameters [122], efficacy [85], and similarity to other stem cell systems [137]. In an earlier gene expression study of DPSC neurons from duplication 15q11.2-q13.1 (Dup15q) and Angelman syndrome (AS) deletion subjects, we identified distinct expression patterns indicative of each syndrome [142]. For the molecular studies presented here, we differentiated these stem cells into neuronal cultures using our previously published protocol [136]. After differentiation, RNA sequencing (RNAseq) was performed to define transcriptional differences among PWS subtypes and neurotypical controls. These molecular studies revealed new details about shared gene expression changes in PWS and unique expression defects related to mitochondria in PWS-UPD neurons that may contribute to increased autism risk.

---

[2] Reproduced from final submission with open access permission. Victor, A.K., M. Donaldson, D. Johnson, W. Miller, and L.T. Reiter, *Molecular Changes in Prader-Willi Syndrome Neurons Reveals Clues About Increased Autism Susceptibility.* Front Mol Neurosci, 2021. **14**: p. 747855. 10.3389/fnmol.2021.747855. [26].

Materials and Methods

Obtaining Teeth for Dental Pulp Stem Cell Culture

Neurotypical control teeth were obtained through the Department of Pediatric Dentistry and Community Oral Health at the University of Tennessee Health Science Center (UTHSC). Teeth from children with PWS subtypes were collected remotely by the caregivers of these subjects after confirmation of the underlying genetic diagnosis. Subjects provided informed consent for tooth collection along with a Social Communication Questionnaire (SCQ) to assess ASD status. Tooth pulp was cultured from teeth and cell lines frozen during early passages in our DPSC Repository as previously described [136]. The DPSC Repository and subsequent molecular studies were approved by the UTHSC institutional review board prior to conducting research.

Generation of Dental Pulp Stem Cell Cultures

DPSC used in this study were isolated and cultured according to our previously described protocol and stored in the DPSC Repository [136]. Briefly, after mincing the dental pulp from inside the tooth cavity, 3 mg/mL Dispase II and 4 mg/mL Collagenase I were added to digest the tissue. Cells were then seeded on poly-D-Lysine coated 12-well plates with DMEM/F12 1:1, 10% fetal bovine serum (FBS), 10% newborn calf serum (NCS), and 100 U/mL penicillin and 100 ug/mL streptomycin (Pen/Strep) (Fisher Scientific, Waltham, MA). Confluent cultures (80%) were passaged with TrypLE^{TM} Express and neuronal differentiation performed only on early passage cells (< passage 4).

Neuronal Differentiation

DPSC lines were seeded at 20,000 cells/cm^2 on poly-D-lysine coated plates or chamber slides (Ibidi, Planegg, Germany) with DMEM/F12 1:1, 10% fetal bovine serum (FBS), 10% newborn calf serum (NCS), with 100 U/mL penicillin and 100 ug/mL streptomycin (Pen/Strep). At 80% confluence, the neuronal differentiation protocol was followed as previously published in Kiraly *et al.*, 2009 [93] with an extended maturation phase (3 weeks versus 7 days) [136]. Briefly, epigenetic reprogramming was performed by exposing the DPSC to 10 μM 5-azacytidine (Acros Scientific, Geel, Belgium) in DMEM/F12 containing 2.5% FBS and 10 ng/mL bFGF (Fisher Scientific, Waltham, MA) for 48 hours. Neural differentiation was induced by exposing the cells to 250 μM IBMX, 50 μM forskolin, 200 nM TPA, 1mM db-cAMP (Santa Cruz, Dallas, TX), 10 ng/mL bFGF (Invitrogen, Carlsbad, CA), 10 ng/mL NGF (Invitrogen, Carlsbad, CA), 30 ng/mL NT-3 (Peprotech, Rocky Hill, NJ), and 1% insulin-transferrin-sodium selenite premix (ITS) (Fisher Scientific, Waltham, MA) in DMEM/F12 for 3 days. At the end of the neural induction period, neuronal maturation was performed by maintaining the cells in Neurobasal A media (Fisher Scientific, Waltham, MA) with 1mM db-cAMP, 2% B27,

1% N2 supplement, 30 ng/mL NT-3, and 1X Glutamax (Fisher Scientific, Waltham, MA) for 21 days.

RNA Sequencing of Dental Pulp Stem Cell Neurons

Once DPSC-neurons were matured for 3 weeks, total RNA was collected using the Zymo Directzol RNA extraction kit (Zymo, Irvine, CA). Extracted RNA was assayed for quality and integrity using the Agilent Bioanalyzer 6000 pico chip (Agilent, Santa Clara, CA). Only RNA with an RNA Integrity Number (RIN) $\geq$ 9.0 was used for RNAseq studies. Library preparation and RNAseq was performed by Novogene (NovoSeq 6000) (Sacramento, CA) using the Illumina platform and paired end reads. 20M reads per sample were collected.

RNAseq Analysis

FASTQ files from Novogene were analyzed for quality and trimmed using FASTQC. All reads were trimmed to remove nucleotides with Phred scores < Q20. The trimmed FASTQ files were aligned to the human genome reference library hg19 using RNASTAR [143]. Once aligned, the SAM files were collected and mined for read count information of each gene present in the reference file. Read counts were normalized using Counts per Million (CPM) method across groups for the entire experiment. Principle component analysis and Pearson's coefficient plots were performed on the normalized transcriptome profile. A Wilcoxon's *t*-test was used to determine significance across groups. All genes that fail to yield a p-value $\leq$0.05 and a fold change greater than 1.5 were removed. Benjamini and Hochberg false discovery rate (FDR) was performed on this trimmed gene list. All genes that failed to yield an FDR rate of $\leq$ 0.05 were removed. The final significant differential gene lists were loaded into the ClustVis web tool to generate heatmaps [144]. Additionally, the targets were loaded into the web based enrichment analysis tool, Database for Annotation, Visualization and Integrated Discovery (DAVID) [145] to identify enriched gene ontology (GO) terms.

Immunofluorescence

DPSC were grown and differentiated on 3-well chamber slides (Ibidi, Planegg, Germany) coated with poly-D-lysine. Cells were fixed using a 4% paraformaldehyde solution for 10 minutes. Once fixed, cells were blocked and permeabilized using PBS with 1% BSA, 10% FBS, and 0.3% Triton X-100 for 1 hour. Primary antibodies were diluted to 1:500 for anti-Beta Tubulin (Millipore, ab9354) and anti-TOMM20 (Santa Cruz, sc-17764) in the blocking solution and incubated overnight at 2-8 °C with agitation. After overnight incubation, the slides were washed 3x with PBS-T for 10 minutes before the secondary antibodies, Goat anti-mouse Alexa Fluor 488 (Life Technologies, A11029) and Goat anti-chicken Alexa Fluor 594 (Life Technologies, A11042) were added at a 1:1000 dilution. Slides were incubated at room temperature for 1 hour and then washed

again 3x for 10 minutes each. Finally, Prolong Gold Antifade with DAPI (Fisher Scientific, Waltham, MA) was applied for mounting. Slides were imaged on a Zeiss 710 confocal microscope at 63x magnification using Z-stacking to image the entire neuron via ZEN software (Black Edition).

Western Blots

Western blots were performed as previously described [142]. Briefly, protein was extracted from 3-week mature neurons using neuronal protein extraction reagent (N-PER) (Fisher Scientific, Waltham, MA) and protease inhibitor cocktail (Roche). Samples were resolved on a NuPage 1.5mm 4-12% Bis-Tris gel (Invitrogen, Carlsbad, CA) according to manufacturer instructions and transferred to an Invitrolon™-PVDF membrane (Invitrogen, Carlsbad, CA). The membrane was blocked using Odyssey Blocking Buffer (Licor, Lincoln, NE) for 1 hour and incubated overnight at 2-8°C in primary antibody with agitation. Primary antibodies used: anti-MAP2 (Santa Cruz, sc-32791), anti-Nestin (Santa Cruz, sc-23927), and anti-GABA A receptor beta 3 (Abcam, ab98968). anti-GAPDH (Abcam, ab157156) was used as a protein loading control. Blots were incubated at room temperature for 1 hour in secondary antibodies for both the 700 and 800 channels using Li-Cor IR secondary antibodies (Licor, 926-32212 & 926-68074) . Blots were imaged on a Li-Cor Odyssey™ Fc Imager. Both the 700 and 800 channels were exposed for 2 minutes.

Image Analysis

All imaging analysis was done using coded cell lines, so the observer was blinded to the genotypes. Only after data collection and analysis were cell lines decoded. For each cell line ($\geq$5 individuals per group), $\geq$15 neurons were imaged for analysis of mitochondrial abundance within the neuron. To quantify mitochondrial area, cells were labeled with anti-Beta Tubulin (total neuronal area) and anti-TOMM20 (mitochondrial area), images were loaded into the Imaris imaging analysis software (Oxford Instruments, Abingdon, UK) and surfaces for each marker were created. The mitochondrial area (anti-TOMM20) was then divided by the total neuronal area (anti-Beta Tubulin) to give the percentage of the neuron that contains mitochondria. After collecting all data, significance testing was performed by both ordinary one-way ANOVA and Turkey's multiple comparisons test with a single pooled variance.

Results

PW-UPD Subjects Have an Increased Incidence of Autism Spectrum Disorder Versus Paternal Deletion and Control Subjects

Several studies have shown an incidence of about 35% for ASD in PW-UPD subjects compared to 18% in PW-del subjects [25, 134, 146]. To measure ASD remotely, we used the Social Communication Questionnaire (SCQ). The SCQ provides a way to ascertain the likelihood a subject may have ASD, especially when face to face evaluation is not possible. Several groups have now validated the SCQ as a screening tool for ASD against other tools like the Autism Diagnostic Interview, Revised (ADI-R) [147-151]. We use the "lifetime" version of the test which has been proven to be a more accurate predictor of ASD [149]. A cutoff score of 15 is considered "possible ASD" according the SCQ lifetime tool. We selected 4 lines from each group (neurotypical control, PW-del, PW-UPD -ASD, and PW-UPD +ASD) for RNAseq analysis and additional lines were used for the immunofluorescence analysis. **Figure 2-1** shows the SCQ scores from these subjects, except for two neurotypical control subjects for which we did not receive an SCQ. For one of the neurotypical control subjects without SCQ data, we did collect the Social Responsiveness Scale (SRS) which revealed the subject did not have any autism characteristics. The PW-UPD group shows two distinct clusters, those scoring above 15 (possible ASD) and those within normal limits (**Figure 2-1**).

Characteristics of Mixed Neuronal Cultures Derived from Control and Prader-Willi Syndrome Dental Pulp Stem Cells

Four DPSC lines representing each of the PWS subgroups (PW-del, PW-UPD -ASD, and PW-UPD +ASD) and 4 neurotypical control subject lines were selected from the repository for RNAseq studies (**Table A-1**). Deciduous ("baby") teeth from neurotypical control subjects were collected locally from the Department of Pediatric Dentistry and Community Oral Health at UTHSC and PWS subjects were collected remotely by parents and guardians of the subjects using our previously published protocols [136]. DPSC lines were differentiated into neurons using a published neuronal differentiation protocol [93, 136]. DPSC from all groups show positive expression for the stem cell marker, NESTIN, while these same lines were negative for neuronal markers MAP2 and GABA A receptor subunit beta 3 (**Figure 2-2A**). After the neuronal differentiation protocol and a 3-week maturation period, the cultures were positive for both MAP2 and GABA A receptor subunit beta 3 (**Figure 2-2A**). DPSC show a flat, fibroblast like morphology (**Figure 2-2B**), but after a month of differentiation, the cultures display a pyramidal neuron-like morphology (**Figure 2-2C**). Both neurotypical and PWS neuronal cultures displayed similar morphologies and cell numbers throughout the differentiation process. We have previously established that a 3-week neuronal maturation period is sufficient to induce significant gene expression changes indicative of terminal neuronal differentiation [122] and reflect underlying disease specific gene expression patterns [142].

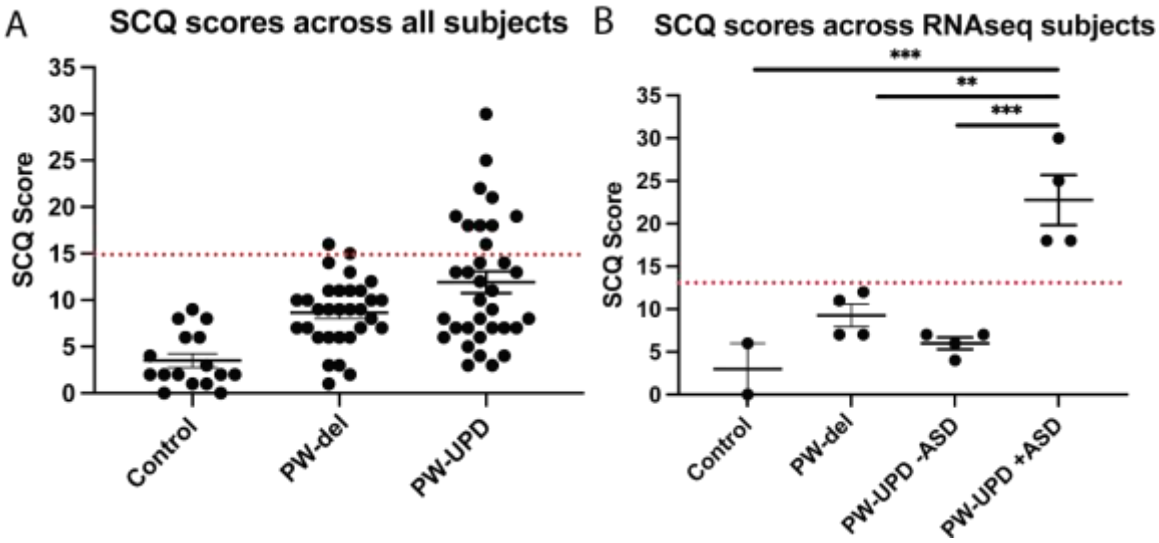

Figure 2-1. Social Communication Questionnaire (SCQ) scores across all subjects. **(A)** SCQ scores across all subjects. **(B)** SCQ scores across individuals used for RNAseq analysis. A cutoff score of 15 (red line) is used as a threshold for "possible ASD". The PW-UPD cohort has two segregated groups. Subjects that meet the criteria for "Possible ASD" (score of 15 or above) and those scoring within normal limits. For 2 of the neurotypical control subjects used, SCQs could not be collected. Significance testing was performed by one-way ANOVA testing. ** = p-value $\leq$ 0.01, *** = p-value $\leq$ 0.005. Autism spectrum disorder (ASD), Prader-Willi syndrome deletion subtype (PW-del), Prader-Willi syndrome uniparental disomy subtype (PW-UPD).

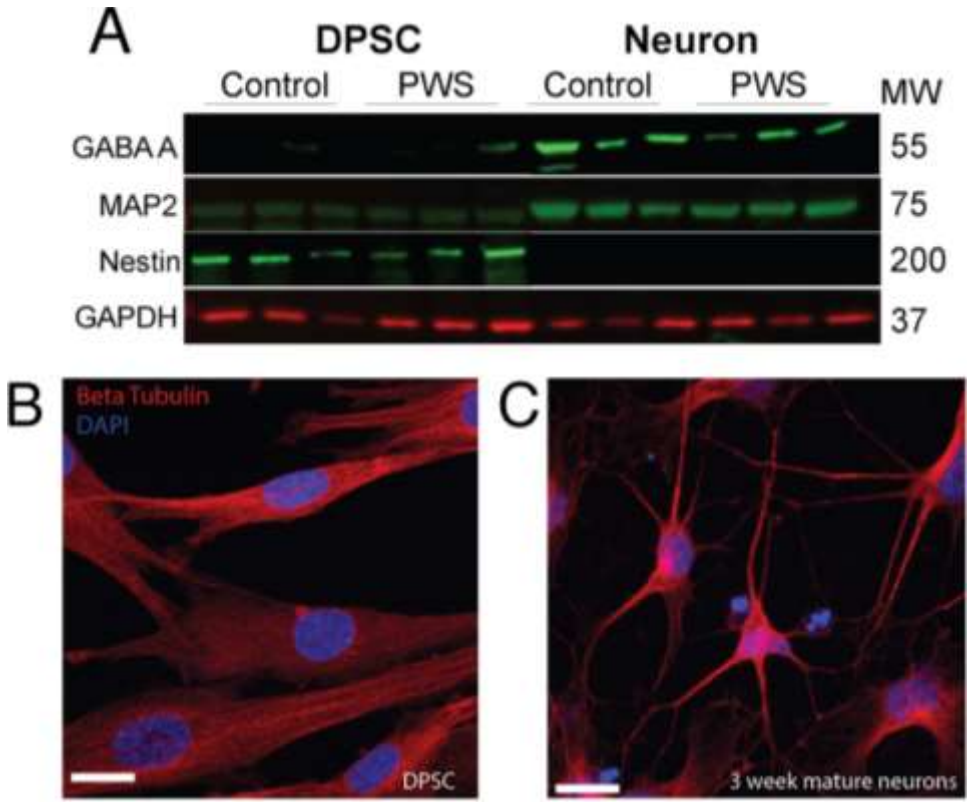

Figure 2-2. DPSC from both PWS and control subjects differentiate efficiently into neuronal cultures.
(A) DPSC from all subjects are negative for neuronal markers, MAP2 and GABA A, but positive for stem cell marker NESTIN. After differentiation and 3 weeks of maturation, the cultures are positive for both MAP2 and GABA A receptor subunit beta 3. (B&C) Representative DPSC versus DPSC-derived neurons visualized with anti-beta tubulin (red) **(B)** DPSC show a flat fibroblast-like morphology as previously reported. **(C)** DPSC-derived neuronal culture contains cells with pyramidal neuron morphology. DAPI (blue) was used as a nuclear stain. 63x magnification. Scale bar is 20µM. Dental pulp stem cells (DPSC), Prader-Willi syndrome (PWS).

Prader-Willi Syndrome Subtypes Show Distinct Transcriptional Profiles and a Shared Prader-Willi Syndrome Expression Signature That Extends to Genes Outside of the PWS Critical Region

RNAseq files from each individual were analyzed by the UTHSC Bioinformatics Core to create lists of significantly (p-value $\leq$ 0.05 and FDR $\leq$ 0.05) different transcripts for each PWS subtype versus control and each subtype versus the other genotypes (see methods for details). Using these lists of significantly differentially expressed transcripts for each group versus control, we created Venn diagrams in BioVenn [152] (**Figure 2-3A**). From this analysis we identified a unique molecular signature for each subgroup and a core PWS signature comprised of 3 transcripts within the PWS critical region (*SNRPN*, *SNURF*, and *MAGEL2*) and 9 transcripts coding for genes located outside of 15q PWS/AS critical region (**Figure 2-3B**). **Table A-2** lists these PWS specific transcripts, their function, and evidence that ties these genes or their function to PWS phenotypes. Analyzing the expression of genes across the PWACR in our subjects shows the expected expression changes from control to PWS subtypes (**Figure A-1**). Specifically, expression of genes that are maternally imprinted in PWS (*MAGEL2*, *SNRPN*, *SNURF*, *NDN*, and *MRKN3*) are absent in our PWS groups, regardless of genetic subtype. These data confirm that DPSC neurons from subjects accurately recapitulate the genetic landscape of PWS in terms of imprinted gene expression.

Significant Down Regulation of Mitochondrial Transcripts in PW-UPD +ASD Neurons

In order to find molecular changes specific to ASD in our dataset, we investigated the significantly different transcripts (p-value $\leq$ 0.05, FDR $\leq$ 0.05) in the -ASD groups versus the UPD +ASD group (**Figure 2-4A**). 380 transcripts met our significance cut off and were interrogated for enrichment analysis using the Database for Annotation, Visualization and Integrated Discovery (DAVID), which assigns enrichment scores for Gene Ontology (GO) and other descriptive terms significantly over-represented in our differentially expressed dataset as compared to the entire human genome [145, 153]. Using DAVID functional clustering for GO terms, we found significant enrichments in mitochondrial compartments, functions, and processes (p-value $\leq$ 0.002) (**Figure 2-4B**). The top enrichment clusters were mitochondrial membrane transcripts and transcripts involved in mitochondrial maintenance and biogenesis. It is important to note that no other enrichments (score $\geq$ 3.0) were found in this dataset. From the transcripts identified in the DAVID enrichment analysis, we created a heatmap across all groups for the mitochondrial genes responsible for the enrichment scores using ClustVis [144] (**Figure 2- 4C).** This heatmap illustrates that most mitochondrial transcripts identified in our enrichment analysis are dramatically decreased in the PW-UPD +ASD group. **Table A-3** lists these transcripts and their function. These data support our premise that mitochondrial dysfunction may contribute to increased ASD risk in PW-UPD sub-group.

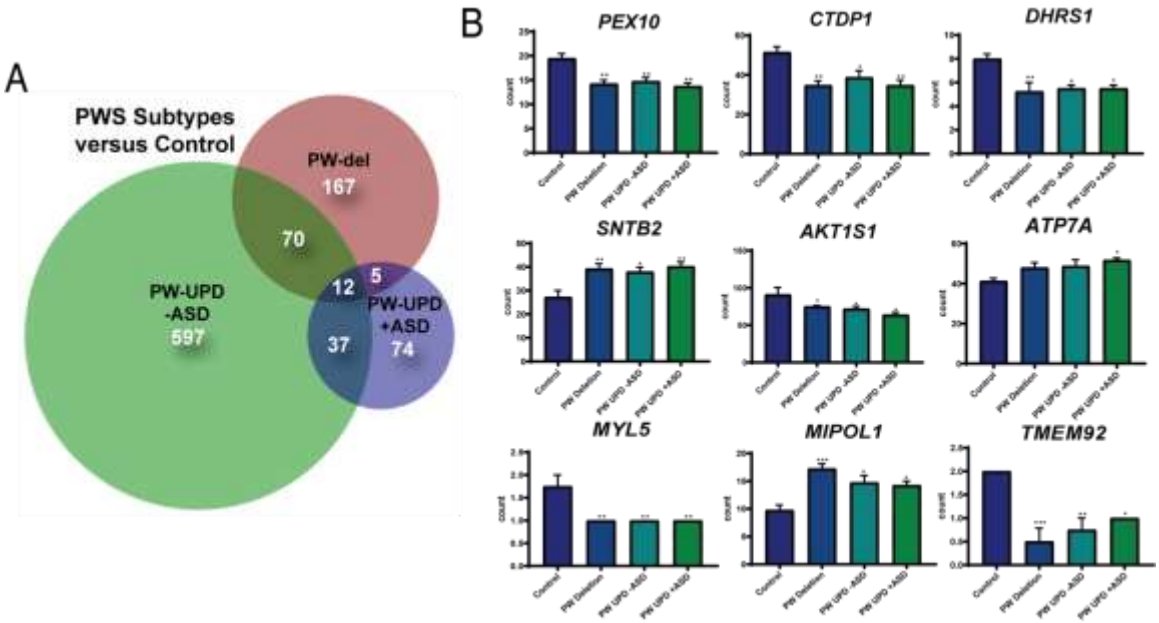

Figure 2-3. DPSC-derived neuronal cultures define PWS subtype specific expression and a core PWS molecular signature.
(A) Venn diagram using all the significantly differentially expressed transcripts (*p*-value $\leq$ 0.05, FDR $\leq$ 0.05) versus control for each PWS subtype created using BioVenn [152]. **(B)** Individual bar graphs showing mean counts per transcript across all groups for each of the transcripts located outside of the PWS critical region and identified as common across all PWS subtypes. These 9 genes, along with *MAGEL2*, *SNRPN*, and *SNURF*, represent a core molecular signature for PWS associated changes in neurons. Significance was determined by individual *t*-tests versus control for each subgroup (*p*-value $\leq$ 0.05). * = *p*-value $\leq$ 0.05, ** = *p*-value $\leq$ 0.01, *** = *p*-value $\leq$ 0.005. Dental pulp stem cells (DPSC), autism spectrum disorder (ASD), Prader-Willi syndrome deletion subtype (PW-del), Prader-Willi syndrome uniparental disomy subtype (PW-UPD).

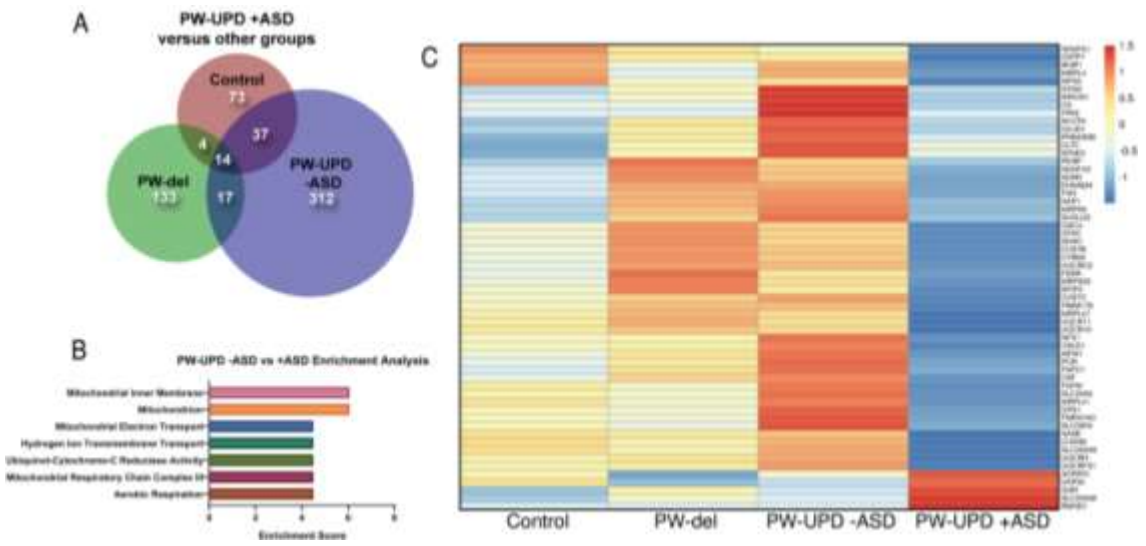

Figure 2-4. RNAseq analysis reveals enrichment in differentially expressed mitochondrial transcripts in the PW-UPD +ASD group.
(A) Venn diagram using all the significantly differentially expressed transcripts (*p*-value $\leq$ 0.05, FDR $\leq$ 0.05) versus PW-UPD +ASD for each PWS subtype and control created using BioVenn [152]. **(B)** The list of differentially expressed transcripts PW-UPD -ASD versus UPD +ASD (*p*-value $\leq$ 0.05, FDR $\leq$ 0.05) was used as input for DAVID [145, 153] pathway analysis. The top enrichments (enrichment score $\geq$ 3.0) were transcripts located within mitochondria and having mitochondrial functions (*p*-value $\leq$ 0.002). **(C)** Heatmap of transcripts identified by DAVID analysis as mitochondrial related. Expression of genes identified as driving the mitochondria enrichment in the PW-UPD +ASD group were used to create this heatmap across all subgroups [144]. Colors indicate read counts from high (red) to low (blue). Most of the mitochondrial transcripts identified in DAVID enrichment set have reduced expression in the PW-UPD +ASD group compared to all other groups. Autism spectrum disorder (ASD), Prader-Willi syndrome deletion subtype (PW-del), Prader-Willi syndrome uniparental disomy subtype (PW-UPD), Database for Annotation, Visualization and Integrated Discovery (DAVID).

PW-UPD +ASD Neurons Display a Cellular Level Defect in Mitochondria

Since enrichment analysis revealed global down regulation of mitochondrial transcripts, we looked for mitochondrial defects at the cellular level in PW-UPD +ASD neurons. Anti-Beta Tubulin was used to outline the area of the neurons (**Figure 2-5A, C**). To visualize mitochondria in neurons, we used the mitochondrial surface marker TOMM20 (translocase of outer mitochondrial membrane 20) [154, 155]. Anti-TOMM20 revealed a mitochondrial phenotype within the +ASD neurons characterized by perinuclear aggregation of mitochondria and decreased mitochondria detected in the neuronal projections (**Figure 2-5B versus D**). To quantify this mitochondrial specific phenotype, we performed a blinded analysis of neuron images from neurotypical control subjects and PWS subjects. For each group $\geq$ 5 individuals were used. Each cell line was coded to ensure no user bias when measuring the mitochondrial area within the neuron. The neuronal cultures were immunolabeled with anti-TOMM20 and α-Beta Tubulin and then imaged through the cell by confocal microscopy. To determine the percentage of neuronal area containing mitochondria, Imaris software (Oxford Instruments, Abingdon, UK) was used on the confocal stacks. Neuron images were uploaded to the Imaris program and surfaces for quantification were created using the anti-Beta Tubulin (**Figure 2-6A, C**) signal to compute total neuronal area and anti-TOMM20 **(Figure 2-6E, G**) to compute the mitochondrial volume within the neuron. **Figure 2-6** shows the Imaris output after using the "surfaces" function to define the area of both components. We were able visually to confine our measurements to single neurons and eliminate any debris from this analysis. For each cell line, $\geq$15 neurons were imaged and analyzed**.** We found a significant difference in the average neuronal mitochondrial coverage between the PW-UPD +ASD group and the other groups **(Figure 2-7)**. These data confirm the hypothesis that mitochondrial dysfunction may underlie the increased ASD incidence of the UPD class.

Discussion

Here we used our DPSC-derived neuronal cultures to define molecular signatures for each genomic subtype of PWS, providing for the first time a molecular signature of gene expression in PWS neurons as well as unique molecular changes in the PW-UPD +ASD group that may be indicative of an underlying mitochondrial defect related to autism. DPSC provide an excellent stem cell source to study neurodevelopmental disorders *in vitro* [137]. They are easy to collect remotely and provide a non-invasive way to obtain patient stem cells from a large number of individuals. In addition, DPSC have been found to more closely mimic the epigenetic landscape of embryonic stem cells compared other stem cell types commonly used for neurogenetic research, such as induced pluripotent stem cells (iPSC) [86].

Expression profiling in this study revealed transcripts that may affect early development in PWS, including genes involved in secretory granule regulation (*SNTB2* and *ATP7A*), mTOR signaling (*AKT1S1*), and peroxisome biogenesis (*PEX10*), all of which have been implicated in phenotypes of neurodevelopmental disorders [156-158].

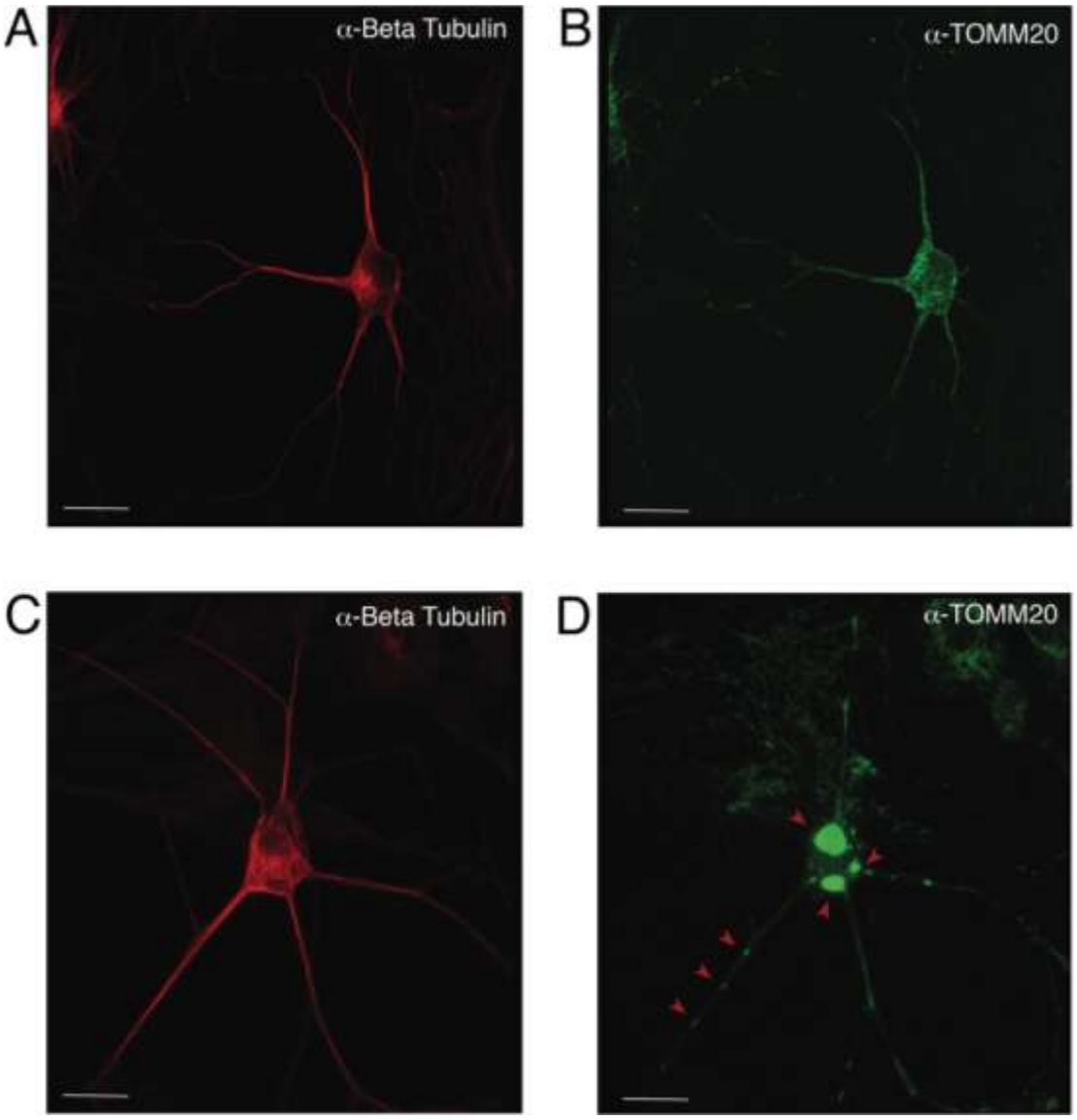

Figure 2-5. Mislocalization and reduced dispersion of mitochondria in ASD neurons.

Neuronal cultures visualized with anti-beta tubulin (red) and the mitochondrial marker anti-TOMM20 (green). The PW-UPD -ASD neuron (**top row**) shows bright and evenly dispersed mitochondria within the neuronal projections. In PW-UPD +ASD neuron (**bottom row**), the red arrows point to mitochondrial aggregates not seen in the PW-UPD -ASD neurons. **A** & **C** show neuronal morphology using anti-beta tubulin staining. **B** & **D** show the anti-TOMM20 staining to identify mitochondria. Confocal stacks were taken at 63X magnification. Scale bar is 20µm. Autism spectrum disorder (ASD), Prader-Willi syndrome uniparental disomy subtype (PW-UPD).

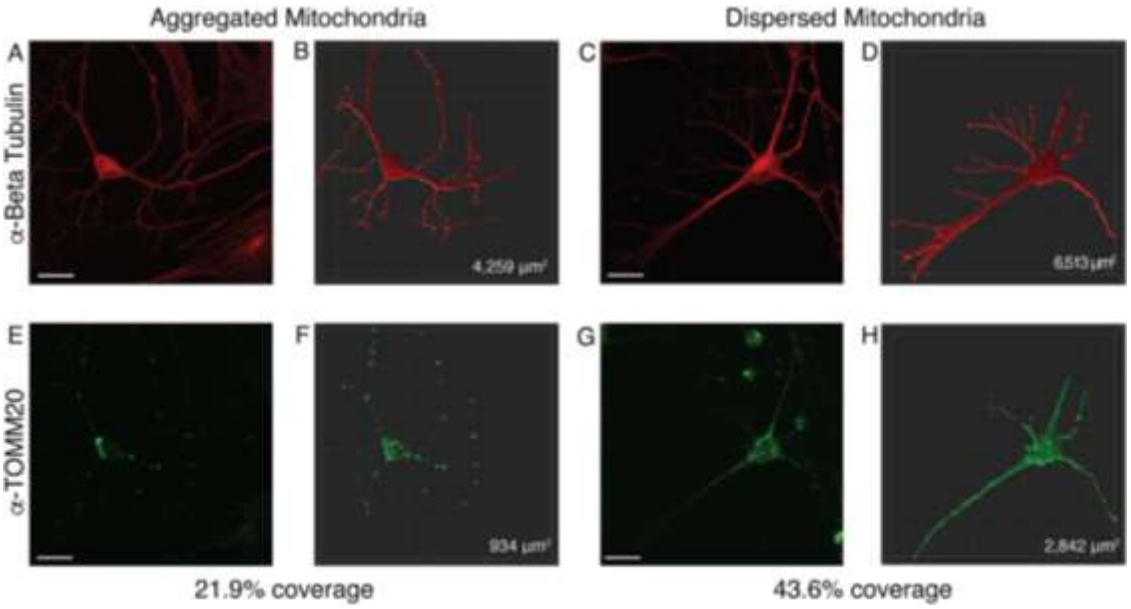

Figure 2-6. Representative image of Imaris volumetric analysis.
Z stacks from neuronal images taken on a Zeiss 810 confocal microscope were loaded into the Imaris software suite for analysis. **A** & **E** show a representative image of a neuron with mitochondrial aggregates while **C** & **G** depict a neuron with dispersed mitochondria. Anti-Beta Tubulin (**A**&**C**) was used to measure the surface area of the neuron, while anti-TOMM20 (**E**&**G**) was used to label total mitochondria content within the neuron. Using the surfaces function in Imaris, a mask for the Beta Tubulin (**B**&**D**) and TOMM20 (**F**&**H**) stained areas was constructed. From these surface masks, the area is calculated by the software (bottom right corner of B, D, F & H) for each surface. The mitochondrial area within the neuron was divided by the total neuronal area to determine a percentage of mitochondrial volume. Images were taken at 63x by confocal microscopy. Scale bar represents 20 µM.

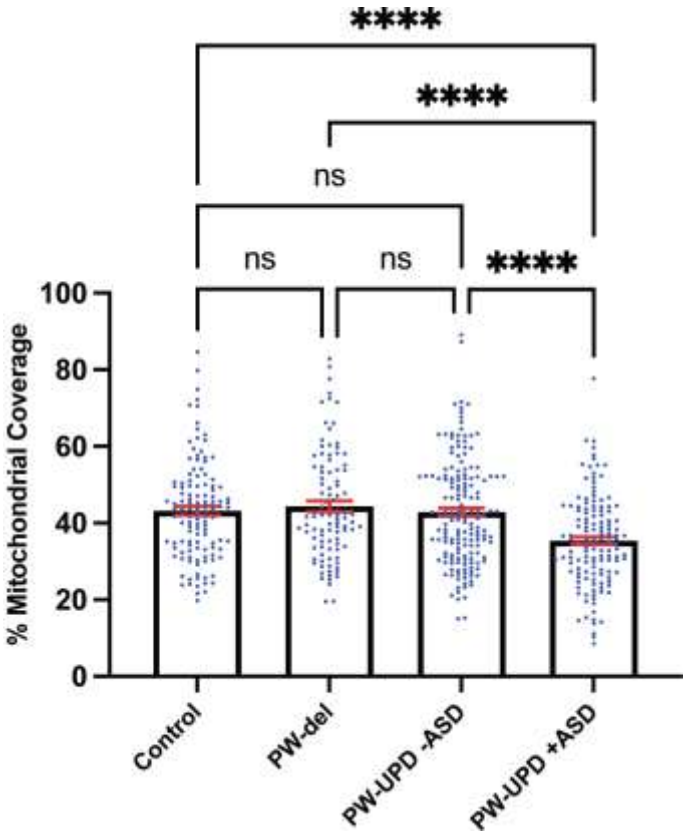

Figure 2-7. PW-UPD +ASD neurons show decreased mitochondrial coverage within neuronal area.

Using Imaris, the total neuronal area (anti-Beta Tubulin) that contains mitochondria (anti-TOMM20) was calculated. Percent of mitochondrial coverage was measured for ≥15 neurons from each cell line and at least 5 cell lines per group in a blinded fashion. Significance testing was performed by both ordinary one-way ANOVA and Turkey's multiple comparisons test with a single pooled variance. **** = *p*-value ≤ 0.001. Autism spectrum disorder (ASD), Prader-Willi syndrome deletion subtype (PW-del), Prader-Willi syndrome uniparental disomy subtype (PW-UPD).

Specifically, prohormone and neuropeptide secretion deficiencies are hallmarks of PWS [62, 159]. These processes rely on efficient secretory granule production and regulation, both of which can be altered by *ATP7A* or *SNTB2,* through its interaction with *PTPRN* [160]. We have previously shown that these MAGEL2 regulated secretory granule defects can be studied in DPSC derived PWS subject neurons. These secretory granule defects have been implicated as a cause of the hormone and neuropeptide deficiencies seen in PWS [62]. *ATP7A* is a copper pump and is integral in regulating copper release at the synapse as well as modulating proteins in the secretory pathway [161]. Due to its widespread function in the brain, it is not surprising that mutations in this gene lead to neurodegenerative and neurodevelopmental disorders [162]. Downstream investigation of these transcripts at the protein level in PWS neurons will be critical to understanding the effect abnormal expression levels of *ATP7A* or *SNTB2* may have on PWS neuropathological development and symptomology. Understanding the function of these genes in the context of PWS could lead to potential therapeutic targets for future interventions involving rescue of endocytic recycling defects driven by loss of MAGEL2 [62].

In addition to uncovering an expression signature common among PWS subtypes compared to neurotypical controls, we also identified transcriptional differences between PW-UPD -ASD and +ASD that may parallel the observed increased autism risk in the PW-UPD cases. In our own cohort of PWS subjects, 33% of PW-UPD individuals scored above the threshold for "possible ASD" on the SCQ (6 out of 18 subjects). This number is comparable to the 35% ASD incidence found in PW-UPD clinical cases [25, 146]. The SCQ has been validated against other ASD tests like ADI-R [148-151, 163] and provides at least an indicator of who may have ASD symptoms.

We identified 380 transcripts that were significantly differentially expressed between +ASD and -ASD groups for PW-UPD subjects (**Figure 2-4A**). Enrichment analysis on these 380 transcripts revealed overrepresented GO terms in mitochondrial compartments, functions, and pathways (**Figure 2-4B**). Many of the transcripts involved in these enrichments produce proteins that are part of the ETC complexes and proteins involved in mitochondrial function, maintenance and biogenesis (**Table A-2**) [164, 165]. Cellular analysis in neurons indicated that +ASD neurons showed a mitochondrial aggregation phenotype (**Figure 2-5**) and have significantly less mitochondrial volume within the neuron (**Figure 2-7**). This further supports our hypothesis that mitochondrial dysfunction (MD) may be involved in the increased ASD incidence in PW-UPD subjects. Additionally, MD has previously been identified in PWS fibroblasts and significant differences in mitochondrial respiration between PW-del and PW-UPD have previously been observed [166].

Mitochondrial dysfunction (MD) has been implicated in both idiopathic [167] and syndromic forms of ASD, including Fragile X [168], Down syndrome [169], Rett syndrome [170], and tuberous sclerosis [171]. In fact, it has been reported that up to 80% of individuals with ASD may also have MD [172]. Neurons consume a large amount of energy to maintain ionic gradients and support neurotransmission [173-175] so it is not surprising that mitochondrial defects have been implicated in both neurodevelopmental and neurodegenerative disorders [176-181]. Inside neurons, mitochondria are the main

energy producers and are integral in maintaining calcium homeostasis at the synapse, which is vital for regulating neurotransmission [182]. Children diagnosed with both ASD and MD have a higher rate of neurodevelopmental regression, seizures, and gross motor delay [183, 184]. Several studies have also shown abnormal levels of metabolic biomarkers such as pyruvate, lactate, glutathione, and ubiquinone in ASD subjects [167, 185-187]. Reduced activities in the electron transport chain (ETC), specifically complexes I and V, have been found in the frontal cortex of ASD individuals [188]. Other studies using post-mortem ASD brain tissue found similar reductions across brain regions of mitochondrial respiratory transcripts and proteins [189-191]. These studies in post-mortem idiopathic ASD brain, although not ideal, add to the evidence that MD may be one of the root causes of ASD in PW-UPD cases.

Performing rescue experiments to re-activate mitochondrial biogenesis, as we did for the restoration of endocytic recycling defects [62], will be a critical future study in our DPSC neuron system. These studies may lead to drug interventions already developed for mitochondrial disorders like Leigh syndrome. In particular, we found a significant decrease in the *PPARGC1A* gene (**Figure A-2)** in the PW-UPD +ASD subjects. The protein produced by this transcript, PGC1α, is a transcriptional coactivator that is responsible for regulating mitochondrial biogenesis [192-194]. Using pharmacological agonists already shown to increase PGC1α expression [195, 196], drug screens can be performed to restore the mitochondrial phenotype we found in the PW-UPD +ASD neurons. Coupled with bioenergetic studies of living mitochondria in our PWS neuronal cultures, we will be able to determine the global effects on mitochondrial function caused by paternal loss of expression in PWS subjects.

Conclusions

In this study we utilized our unique collection of patient-derived DPSC lines to generate neurons for next generation RNAseq analysis from three major genomic subtypes of PWS and compared them to neurotypical control neurons. We found 9 genes outside the PWS/AS critical region on 15q11.2-q13.1 that may contribute to the overall PWS phenotype. We also identified an expression signature in the PW-UPD +ASD group compared to all other groups that appears to indicate a global down regulation of mitochondrial genes is associated with ASD in the PW-UPD subjects. Finally, we showed that this molecular signature translated to a visible and quantifiable change in the appearance and abundance of mitochondria in PW-UPD +ASD neurons. These studies are the first steps at investigating the molecular defects in PWS neurons contributing to both PWS symptomology and increased autism incidence in PW-UPD cases.

CHAPTER 3. ANALYSIS OF CIRCADIAN RHYTHM DEFECTS IN PRADER-WILLI AND SCHAAF-YANG SYNDROME NEURONS

Introduction

Prader-Willi syndrome (PWS) is a neurodevelopmental disorder that results in a constellation of symptoms including hypotonia, failure to thrive, childhood-onset obesity, and developmental delay [40]. PWS is caused by the loss of expression of key genes in the 15q11.2-13 region on the 15th chromosome. Several of these genes are maternally imprinted and only expressed from the paternal allele including *MAGEL2*, *SNRPN/SNURF* and *NDN*. Most cases of PWS result from inheriting a paternal 15th chromosome that is deleted for this critical region, but some cases are caused by inheriting two maternal copies of chromosome 15, or a mutation in the imprinting center that disrupts imprinted expression of these critical genes. PWS can cause a variety of sleep abnormalities including sleep disordered breathing (SDB), excessive daytime sleepiness (EDS), and rapid-eye movement (REM) [49]. Obstructive sleep apnea (OSA) and alveolar hypoventilation are the most common SDB phenotypes reported in PWS. Childhood-onset obesity is a prominent PWS phenotype along with hypotonia and facial dysmorphia (micrognathia and small naso- and/or oropharynx) all of which contribute to the SDB issues found in PWS [48, 49]. Although SDB may be causing EDS, many studies have failed to confirm that EDS is secondary to SDB [197, 198]. In fact, it has been found that even when SDB is corrected, EDS persists in PWS patients, confirming that central hypersomnolence is often a primary clinical phenotype [49, 199].

PWS is described as a hypothalamic insufficiency disorder and, as such, hypothalamic dysfunction has been implicated in EDS. The hypothalamus regulates REM and non-REM sleep cycles and harbors the super chiasmatic nucleus (SCN) which regulates circadian rhythms [53]. The PWACR encompasses several genes that may be involved in disrupting circadian rhythms and hypothalamic function. At least three imprinted genes within the PWS critical region (*NDN*, *SNORD116*, and *MAGEL2*) have been linked to circadian function either through evidence from mouse models or *in vitro* studies [61, 67, 73, 200].

Altered circadian rhythm gene expression was found in *Ndn*-deficient mice [67]. Lassi *et al.* found that in heterozygous *Snord116* mutant mice, REM sleep was altered and there were significant differences in body temperature throughout sleep that they attributed to differing metabolic demands caused by circadian pathway issues [200]. In the same mouse model, another group found significant differences in diurnal rhythmic DNA methylation in PWS mice versus their wild type littermates. In addition, they found that the rhythmic changes in DNA methylation regulated metabolic pathways that were disrupted at different times in the circadian cycle [73].

Kozlov *et al.* created a *Magel2*-null mouse that exhibited altered feeding and breeding behaviors as well as decreased running wheel activity, a measure of daytime wakefulness [61]. Additionally, *in vitro* studies have shown that *MAGEL2* interacts with

and regulates key circadian rhythm genes including *BMAL1*, *PER2*, and *CRY1* [201, 202]. Schaaf-Yang syndrome (SYS), a disorder with overlapping phenotypes to PWS including hypotonia, developmental delay, and obesity, results from truncating mutations in the *MAGEL2* gene [203]. SYS patients also have a high prevalence of sleep disorders including OSA (70-80%), abnormal sleep cycles, and EDS [204, 205]. Understanding the molecular mechanisms leading to sleep abnormalities and EDS in PWS and SYS is vital to finding treatment options for sleep problems in these disorders, alleviating caregiver burden, and enhancing the quality of life for individuals with PWS and SYS.

In this study, we investigated the expression of the essential CLOCK-regulated gene, *Per2*, across the 24hr diurnal cycle in dental pulp stem cell (DPSC) patient-derived neurons from PWS, SYS and neurotypical control subjects. DPSC are multipotent stem cells with the ability to differentiate to a variety of cell types [137]. We have previously used DPSC neurons to investigate disease phenotypes in PWS, Angelman syndrome, and Duplication 15q syndrome [26, 142, 206]. Our lab has established the largest known collection of DPSC lines from the deciduous teeth of PWS and SYS subjects. We regularly differentiate these stem cells into cortical-like neurons for molecular and functional studies. To investigate the endogenous, cellular circadian rhythms in neurons from PWS and SYS subjects, we established DPSC cell lines harboring a *Per2* promoter-driven luciferase reporter (Per2:Luc) for the *in vitro* assessment of circadian rhythm using a bioluminescent assay. We observed two distinct period length phenotypes in PWS neurons, both of which were significantly different from control neurons, and we found that both SYS and PWS neurons display discordant *Per2* circadian cycling. The experiments presented here pave the way for drug discovery assays aimed at finding therapeutic compounds to correct circadian rhythm defects in PWS and SYS patients.

Materials and Methods

Obtaining Teeth for Dental Pulp Stem Cell Cultures

Teeth from children with PWS were collected remotely by the parent or caregivers of these subjects after confirmation of the underlying genetic diagnosis. Subjects provided informed consent for tooth collection and were given instructions for shipping exfoliated teeth. Neurotypical control teeth were obtained from the Department of Pediatric Dentistry and Community Oral Health at the University of Tennessee Health Science Center (UTHSC). As previously described, tooth pulp was collected and cultured to create DPSC lines [136]. Passage 2-4 DPSC lines were then stored in our DPSC repository. The DPSC repository and subsequent molecular studies were approved by the UTHSC institutional review board prior to the start of the study.

Generation of Dental Pulp Stem Cell Cultures

DPSC were isolated and cultured according to our previously published protocol [136]. Briefly, dental pulp was removed from the pulp cavity. The pulp was minced both mechanically and enzymatically using 3 mg/mL Dispase II and 4 mg/mL Collagenase I. Cells were then seeded with DMEM/F12 1:1, 10% fetal bovine serum (FBS), 10% newborn calf serum (NCS), and 100 U/mL penicillin and 100 ug/mL streptomycin (Pen/Strep) (Fisher Scientific, Waltham, MA) on 12-well plates coated with poly-D-Lysine. Once cultures reached ~80% confluency, they were passaged for expansion and aliquots for frozen for banking (passage 2-4) in our DPSC repository.

Creation of Per2:Luc Reporter Lines

Lentiviral luciferase reporters under the control of *Per2* or *Bmal1* promoters were produced as previously described [207]. Concentrated viral particles ($1x10^7$ PFU/mL) were used to infect DPSC with efficiency of ~70%. Briefly, DPSC were seeded at 20,000 cells/cm^2 on a 12-well poly-D-lysine coated plate. Once wells were ~75% confluent, concentrated viral particles ($1x10^7$ PFU/mL) and 5 ug/mL polybrene was added to the cells overnight. After 24-hours, viral supernatant was removed, and cells were allowed to recover overnight in DPSC media. After recovery, transduced cells were selected over a period of 7 days using the selection marker, blasticidin (1 ug/ml). Once transduced cells reached a confluency of ~80%, they were passaged for neuronal differentiation and cell banking.

Neuronal Differentiation

Stably transduced DPSC harboring the Per2:Luc construct were seeded on 35m-mm poly-D-lysine and Matrigel coated plates with DMEM/F12 1:1, 10% fetal bovine serum (FBS), 10% newborn calf serum (NCS), with 100 U/mL penicillin and 100 ug/mL streptomycin (Pen/Strep). Once cells reached confluency (~80%), neuronal differentiation was performed as previously published but with an increased maturation phase of 4 weeks [93, 136]. Briefly, epigenetic reprogramming was performed for 2 days using 10 μM 5-azacytidine (Acros Scientific, Geel, Belgium) in DMEM/F12 containing 2.5% FBS and 10 ng/mL bFGF (Fisher Scientific, Waltham, MA) for 48 hours. Then, neuronal differentiation was induced by exposing the cells to 250 μM IBMX, 50 μM forskolin, 200 nM TPA, 1mM db-cAMP (Santa Cruz, Dallas, TX), 10 ng/mL bFGF (Invitrogen, Carlsbad, CA), 10 ng/mL NGF (Invitrogen, Carlsbad, CA), 30 ng/mL NT-3 (Peprotech, Rocky Hill, NJ), and 1% insulin-transferrin-sodium selenite premix (ITS) (Fisher Scientific, Waltham, MA) in DMEM/F12 for 3 days. At the end of the neural induction period, neuronal maturation was performed in Neurobasal A media (Fisher Scientific, Waltham, MA) with 1mM db-cAMP, 2% B27, 1% N2 supplement, 30 ng/mL NT-3, and 1X Glutamax (Fisher Scientific, Waltham, MA) for 28 days.

Bioluminescence Recording and Data Analysis

Prior to bioluminescence recordings, the neuronal cultures were synchronized using forskolin (50 uM) and IBMX (250 uM) for 2 hours [208]. After synchronization, neuronal cultures were washed with DPBS, and 2 ml of Recording Media were added. Recording Media is composed of 1mM db-cAMP, 2% B27, 1% N2 supplement, 30 ng/mL NT-3, 1X Glutamax (Fisher Scientific, Waltham, MA), and 1 mM luciferin (Biosynth) in DMEM. A LumiCycle luminometer (Actimetrics) was used to record luminescence for 5 days. The LumiCycle Analysis software (Actimetrics, version 2.701) was used to determine period length and create normalized *Per2* and *Bmal1* traces. The baseline drift was removed from the data using the "Running Average" method within the LumiCycle Analysis software. Using this method, the baseline curve is calculated as a running average of the data and this curve is subtracted from the raw data to generate baseline subtracted data on which the period length measurement is derived.

To determine period length, the time frame from 30 hours after beginning the LumiCycle recording up to 110 hours was used. The data within this time frame was fit to a sine wave (dampened) and period length was generated within the LumiCycle Analysis software. Only curves with a goodness of fit $\geq$80% were used for analysis. The LumiCycle analysis software was used to generate traces. Within the software, the baseline subtracted data for each recording was normalized by setting the maximum amplitude to 1 and the data was smoothed using a median filter.

Results

Neuronal Differentiation Is Required for Rhythmic *Per2* Circadian Cycling

The bioluminescent cycling of undifferentiated DPSC Per2:Luc lines was examined using the LumiCycle to monitor expression of *Per2* regulated luciferase across time. Per2:Luc control DPSC lines were grown to confluency, synced, and placed in the LumiCycle to monitor expression of luciferase (**Figure 3-1A**). In these studies, we use IBMX (3-isobutyl-1-methylxanthine) and forskolin to sync cellular circadian clocks in culture prior to measuring rhythms. Both compounds are cyclic AMP activators which have been shown to regulate the transcriptional cycles of the circadian pathway [208, 209]. The DPSC lines show differential *Per2* expression across time, but they are not rhythmic, and no period length could be calculated. Control 1 does not show any pattern of *Per2* cycling and although Control 2 does show a *Per2* peak at ~53 hours, there are no other peaks of expression and no pattern to the expression over time. The same DPSC lines were then differentiated into neuronal cultures and matured for 4 weeks prior to LumiCycle recording (**Figure 3-1B**). After neuronal differentiation, maturation, and synchronization, both lines show rhythmic, overlapping *Per2* oscillations. The single peak seen in panel A for Control 2 does not correspond to any of the peaks seen in panel B. These results suggest that the cell autonomous circadian cycling requires terminal differentiation and is not present in undifferentiated DPSC.

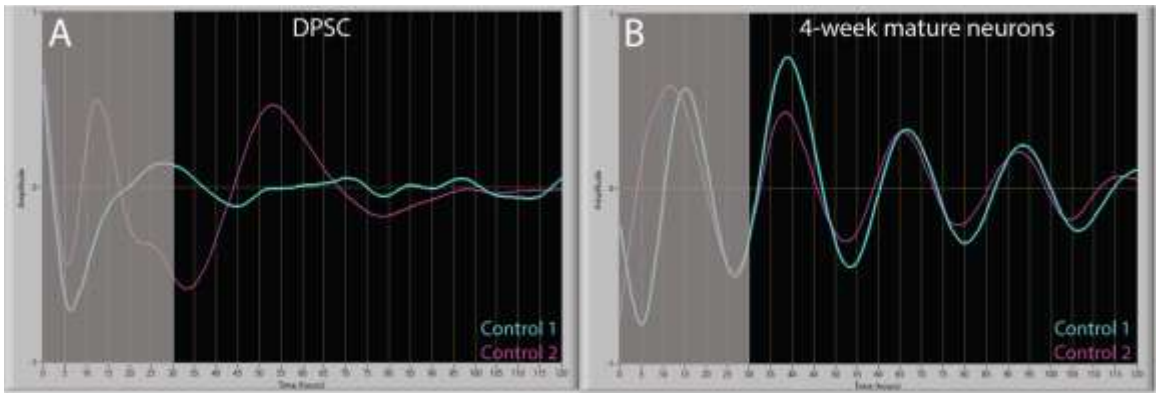

Figure 3-1. Neuronal differentiation required for rhythmic *Per2* circadian cycling.
(A) Undifferentiated DPSC do not show rhythmic *Per2* cycling. **(B)** After neuronal differentiation and maturation, DPSC-derived neurons display *Per2* rhythmic expression. Each colored trace represents an individual DPSC-derived cell line from a neurotypical control subject. Normalization is performed in the LumiCycle Analysis software with peak amplitude set to one for each trace. The first 30 hours are not considered in analysis. Dental pulp stem cells (DPSC).

Neurotypical Controls and Prader Willi Syndrome Neurons Display Anti-Phasic Expression of Both *Per2* and *Bmal1*

Per2 and Bmal1 negatively regulate each other's transcription in the circadian rhythm transcription-translation pathway. To confirm that these genes are being regulated appropriately in both the disease state and control neurons, we created *Bmal1:Luc* stable DPSC lines to observe the expression of *Bmal1* across time. From **Figure 3-2**, it is evident that *Per2* and *Bmal1* expression patterns are anti-phasic and negatively regulate each other. When *Per2* is at its peak, *Bmal1* is at its trough for the observed cycles. The anti-phasic relationship is present in in both our control (**Figure 3-2A**) and PWS (**Figure 3-2B**) neuronal cultures. We also established anti-phasic cycling of *Per2* and *Bmal1* in SYS neurons (**Figure A-3**). These studies demonstrate that critical circadian regulatory systems are present in both disease state neurons and control DPSC-derived neurons.

Prader-Willi Syndrome Neurons Have Two Distinct *Per2* Period Length Phenotypes That Significantly Differ from Control Neurons

Having established that *Per2* and *Bmal1* both show appropriate circadian cycling patterns (**Figure 3-2**) we chose to move forward with characterization of circadian rhythms using only *Per2:Luc* stably expressing cell lines. For these studies, 4 unrelated control and PWS *Per2:Luc* reporter lines were differentiated to neurons and matured for 4 weeks. After maturation, IBMX and Forskolin were used to sync circadian cycling and the lines were placed into the LumiCycle to monitor *Per2* expression for 5 days. **Figure 3-3** shows the cycling traces for these subjects including replicates (at least two replicates per individual). The four control samples (**Figure 3-3A**) have overlapping *Per2* cycling with *Per2* peaks at ~37, 60, and 93 hours. The mean period length for the control group is 27.1 hours. The PWS neurons show two distinct *Per2* period length phenotypes, long (**Figure 3-3B**) and short (**Figure 3-3C**). PWS subjects 1,2, and 3 have replicates showing both phenotypes while PWS 4 only shows the short phenotype. Within the PWS long subgroup, the peaks are ~35, 63, and 90 hours and the individual traces appear to vary more than the control group. The average period length for the long subgroup is 28.1 hours. The PWS short group has variable peaks for each of the individual lines with the first peak from ~33-43 hours, the second peak from ~60-70 hours and the third peak from ~85-95 hours. The average *Per2* period length for the short period subgroup is 26.1 hours. The period length for each trace is quantified in **Figure 3-3D**. Both the short and long PWS subgroups have significantly different period lengths than the control group as determined by an Ordinary one-way ANOVA test. This data confirms that the circadian cycle in PWS neurons is disrupted compared to neurotypical control neurons.

SYS Neurons Have Discordant *Per2* Circadian Cycling Versus Control Neurons

Next, we compared the *Per2* cycling from 2 SYS subjects with different truncating mutations in the *MAGEL2* gene versus the same set of neurotypical control

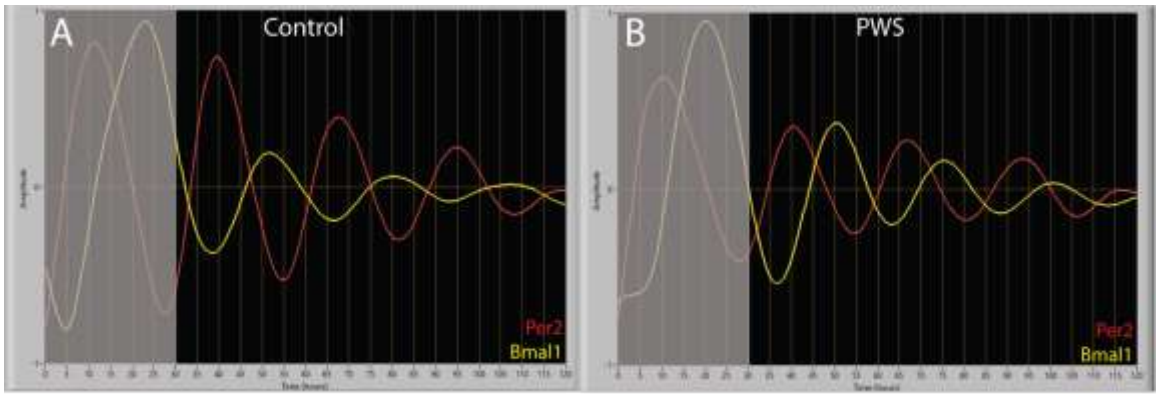

Figure 3-2. Neurotypical control and PWS neurons show anti-phasic expression of *Per2* and *Bmal1*.
Per2:Luc (red trace) and Bmal1:Luc (yellow trace) are CLOCK-controlled genes that negatively regulate each other. *Per2* and *Bmal1* show the expected anti-phasic expression across time in both neurotypical control subjects **(A)** and PWS subjects **(B)**. Normalization is performed in the LumiCycle Analysis software with peak amplitude set to one for each trace. The first 30 hours are not considered in analysis. Prader-Willi syndrome (PWS).

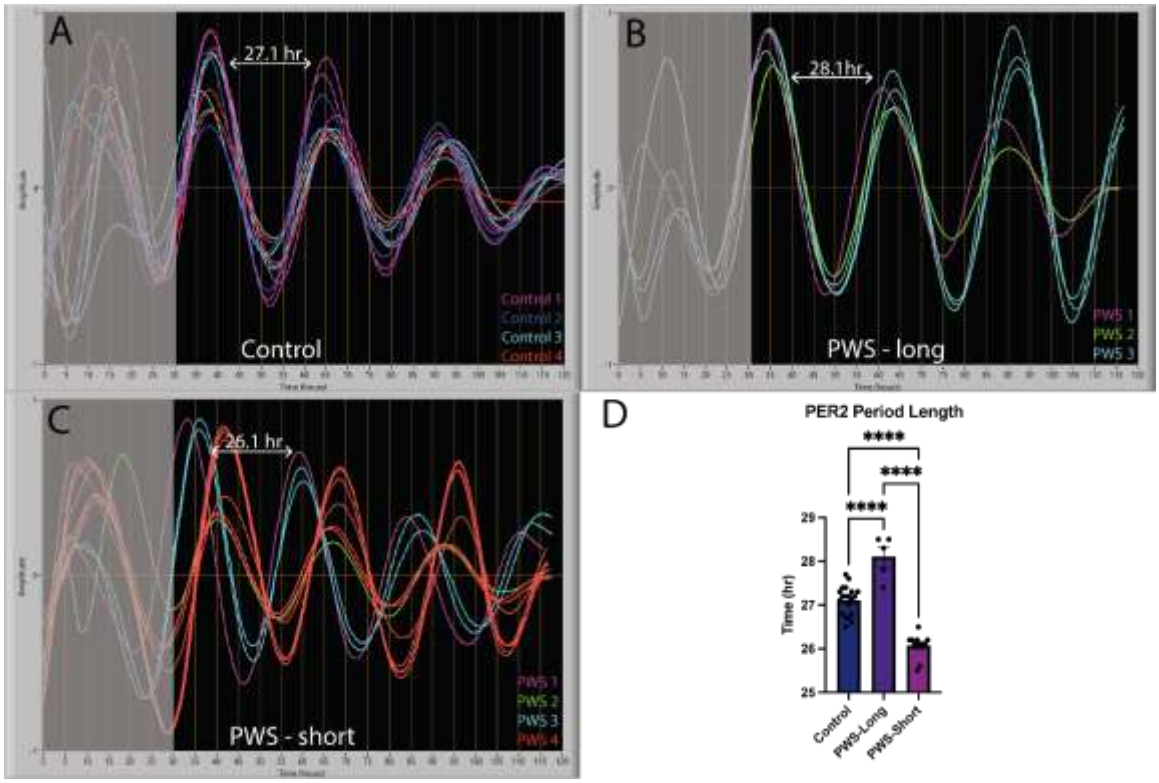

Figure 3-3. PWS neurons show two distinct *Per2* period length phenotypes. *Per2* period length across time was measured in neurotypical control **(A)** and PWS **(B&C)** neurons. PWS neurons display two distinct period length phenotypes: long **(B)** and short **(C)**. **(D)** Period length for each group was quantified in the LumiCycle Analysis software. Each of the PWS subgroups has a significantly different period length versus control subjects. One-way ANOVA was used to determine significance. Each color on the trace diagrams represents a different individual (4 control, 4 PWS subjects). Amplitude normalization is performed in the Lumicycle Analysis software with peak amplitude set to a maximum of 1 for each trace. The first 30 hours are not considered in the analysis. ****=p-value $\leq$ 0.001. Prader-Willi syndrome (PWS).

subjects, as in **Figure 3-3**. We differentiated and matured the neurons for 4 weeks prior to syncing them with IBMX and forskolin and observing *Per2* expression in the LumiCycle compared to neurotypical control subjects (**Figure 3-4A**), the SYS neurons (**Figure 3-4B**) show discordant *Per2* cycling. The two unrelated SYS individuals do not have overlapping *Per2* cycling and even replicates of the same individual have variable *Per2* cycling. The period length for each trace is quantified in **Figure 3-4C**. The mean *Per2* period length for the SYS subjects was 27.08 versus the control length of 27.1. Although there is not a significant difference between the period length from the SYS and control neurons, from the trace figures (**Figure 3-4A, B**), there is an obvious variation in *Per2* cycles even among replicates from the same SYS individual. This is reflected in the standard deviation (SD) differences between the control subjects (SD = 0.33) and the SYS subjects (SD = 0.66). There is also no bimodal distribution in the SYS period lengths indicating long and short subgroups as seen in the PWS data. This indicates that although the data does not show a significant period length in the SYS neurons versus control neurons, there does appear to be a defect causing both inter- and intra-individual variation in *Per2* cycling.

Discussion

PWS is a multigenic syndrome resulting in cognitive and behavioral phenotypes including developmental delay and sleep defects. Many PWS subjects have sleep disordered breathing (SDB) including obstructive sleep apnea. In addition to SDB, PWS subjects experience excessive daytime sleepiness (EDS) and narcolepsy-like symptoms which do not resolve when SDB is corrected. EDS leads to decreased quality of life for both PWS subjects and caregivers.

Within the PWACR, several genes show evidence of having circadian rhythm functions. *Snord116* deficient mice show REM sleep alterations and significant differences in diurnal rhythmic methylation versus wildtype littermates [73, 200]. Both *NDN* and *MAGEL2* are highly expressed in the SCN, making them strong candidates for causing circadian rhythm dysfunction. *MAGEL2* is the only gene within the PWS critical region that is controlled by the *CLOCK/BMAL1* complex (referred to as CLOCK-regulated) and shows circadian expression [61]. While *Magel2*-null mice entrain to light cycles, they exhibit decreased activity amplitude and increased daytime activity as compared to wildtype mice [61]. Additionally, SYS, a syndrome with many phenotypes in common with PWS including sleep dysfunction, both EDS and SDB, results from various truncating mutations in the *MAGEL2* gene [204, 205]. Here, we use our DPSC-neuron system to assay *Per2* expression across time as an output measure for the entire circadian rhythm pathway in PWS and SYS neurons. Identifying molecular defects in circadian rhythm cycling of SYS and PWS neurons is the first step in developing therapeutics to treat the symptoms of defective circadian cycling, i.e. EDS and SDB, in both PWS and SYS.

We show that in DPSC, circadian cycling does not appear to be rhythmic across five-day recordings and does not overlap between control individuals. However, these

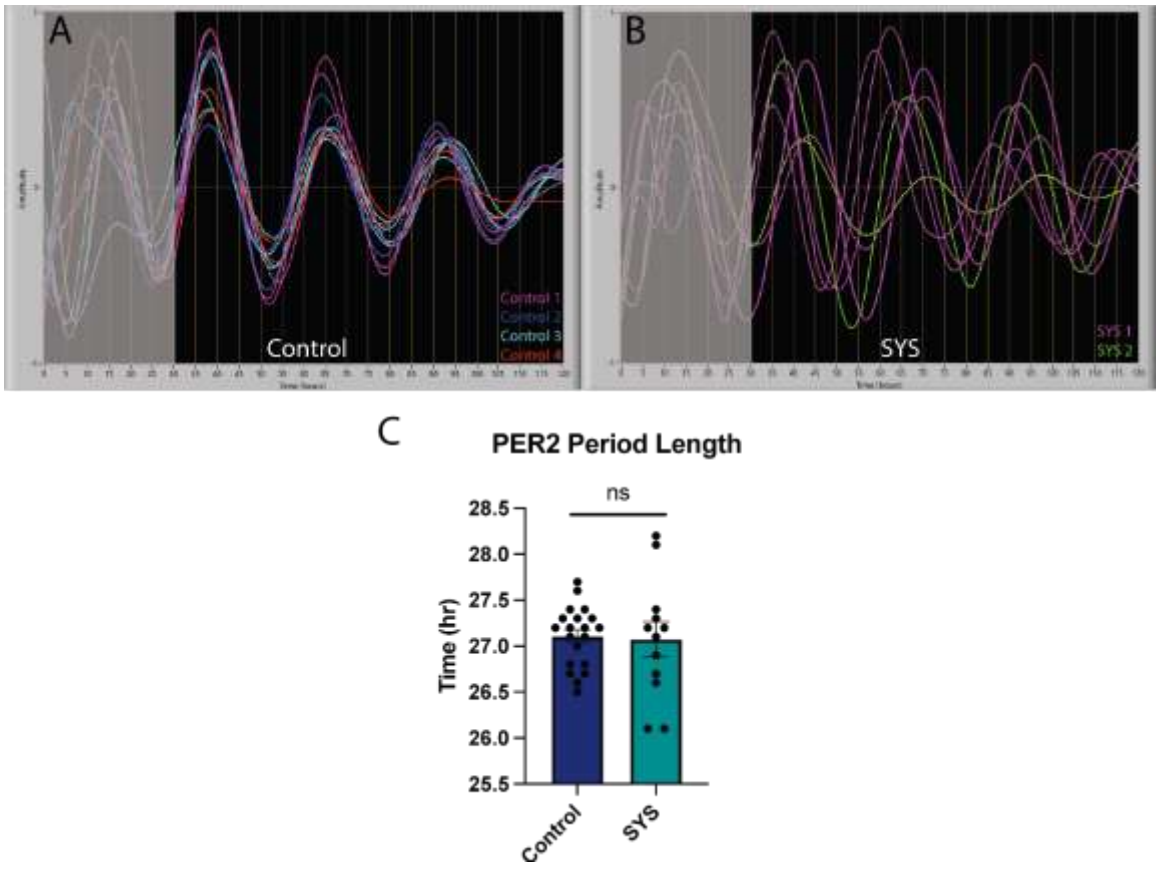

Figure 3-4. SYS neurons show discordant *Per2* cycling.
Per2 expression across time was measured in control **(A)** and SYS **(B)** neurons. The control neurons show overlapping *Per2* expression for replicates and different individuals. The SYS neurons show discordant cycling among the two individuals tested and among the replicates from the same individual. **(C)** *Per2* period length was quantified for SYS and control neurons in the LumiCycle Analysis software. Each color trace represents a different individual (4 control, 2 SYS subjects). Significance was determined using a One-way ANOVA. Amplitude normalization was performed in the LumiCycle Analysis software with peak amplitude for each trace set to a maximum of 1. The first 30 hours are not considered in the analysis. Not significant (NS), Schaaf-Yang syndrome (SYS).

DPSC from the same individuals, when differentiated into neurons, show clear circadian cycling. Our results are consistent with the work of another group who showed that under different synchronizing methods (forskolin, dexamethasone, or temperature), no rhythmic circadian gene expression could be found in iPSC cultures [210]. A different group found that undifferentiated human embryonic stem cells did not display oscillatory expression of clock genes, but once differentiated to cardiomyocytes, circadian rhythmic gene expression emerged [211]. In our system, once neuronal differentiation and maturation occurs, the establishment of the circadian transcription-translation feedback loop can be seen in the rhythmic oscillations of *Per2* expression. Additionally, we show the anti-phasic expression of both *Per2* and *Bmal1* in PWS, SYS and neurotypical control neurons. This confirms that Per2 and Bmal1 in both our control and PWS DPSC-neurons are repressing and enhancing each other, establishing the validity of our DPSC-neuron system for circadian rhythm assays.

The primary genes that regulate circadian oscillations in all animals are *CLOCK*, *BMAL1*, *PER1*, *PER2*, *CRY1* and *CRY2*. This autoregulatory transcriptional network is cell autonomous and occurs in most cell types in the body [212]. During the cycle, CLOCK and BMAL1 form a heterodimer (CLOCK:BMAL) that positively regulates expression of *PER1*, *PER2*, *CRY1*, and *CRY2*. These gene products then form a complex that represses the transcription of *CLOCK* and *BMAL1*, effectively repressing their own expression [212].

Many lines of evidence point to a role for *MAGEL2* in this transcription-translation feedback loop that regulates circadian rhythms. Devos *et al*. showed the Magel2 represses Clock:Bmal1 activity causing a decrease in Per2 expression and that Magel2 interacts with both Per2 and Bmal1 [201]. Additionally, they showed that Magel2 caused the cytosolic localization of Clock to increase [201]. Clock can only exert its effect on Per/Cry expression from the nucleus. MAGE proteins, like MAGEL2, regulate ubiquitination through their interaction with RING E3 ubiquitin ligases and deubiquitinases. Modification of ubiquitin signals acts as a rheostat in maintaining the delicate balance and timing of rhythmic protein expression within the circadian pathway [213]. One of the interacting partners of MAGEL2, USP7, stabilizes CRY1 expression by deubiquitination [202, 214]. Carias *et al*. showed that MAGEL2 modulates the ubiquitination and subcellular localization of CRY1 [202]. While direct interaction with CRY1 has not yet been established, presumably MAGEL2 exerts this effect on CRY1 through its interactions with USP7, finely tuning the cyclical expression of key CLOCK-regulated genes. **Figure 3-5** illustrates the complex hypothesized role of MAGEL2 in regulating the circadian rhythm cycle. In PWS, *MAGEL2* is not expressed. While in SYS, *MAGEL2* is mutated and the significance of these truncating mutations on *MAGEL2* function has not been established. As period length is directly determined by the turnover rate of these CLOCK-regulated proteins, *MAGEL2* loss or functional alteration could have profound effects on overall circadian rhythms. Circadian rhythms not only alter sleep/wake cycles but have an effect on cellular metabolism making any defect in the circadian pathway critically important to correct for overall health [215, 216].

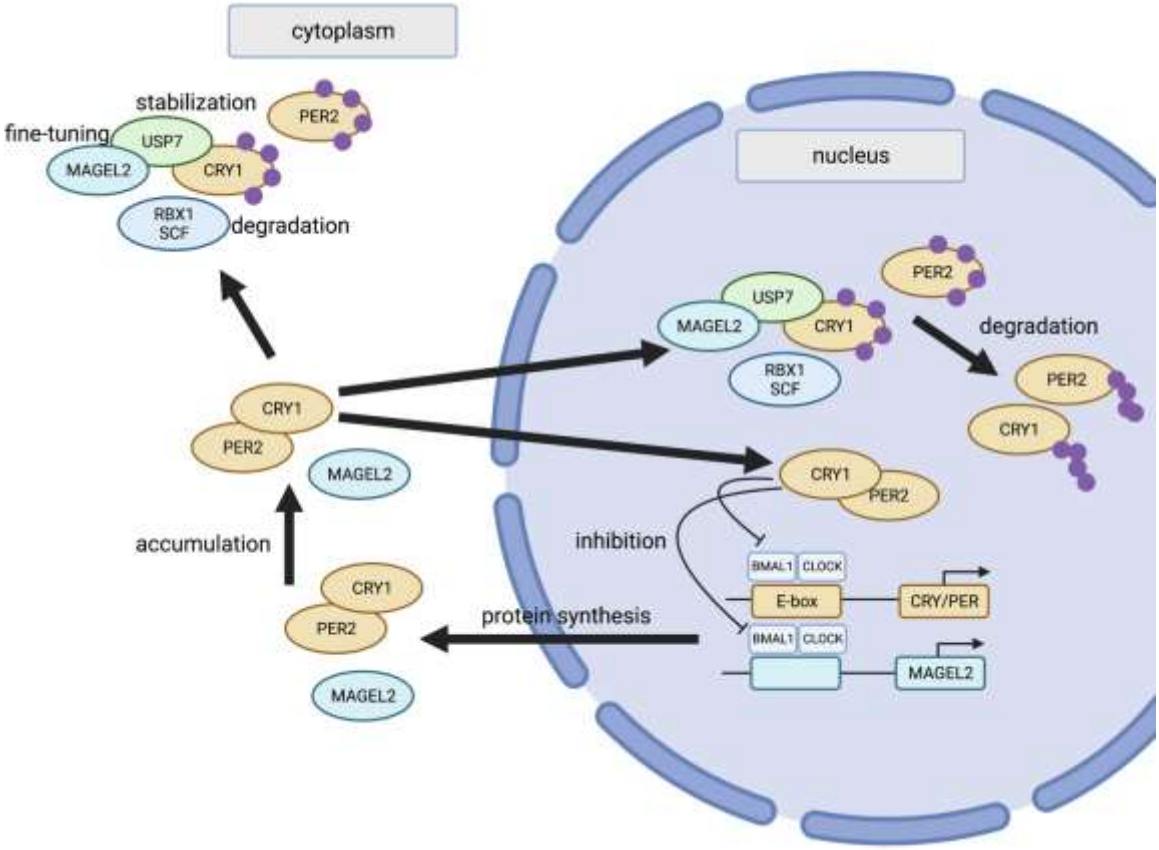

Figure 3-5. MAGEL2 fine-tunes CRY1 stabilization/degradation in the circadian rhythm pathway.
In the transcription-translation feedback loop, BMAL1 and CLOCK bind to promoter elements on CLOCK-regulated genes including *MAGEL2*, *PER2*, and *CRY1* to promote their expression. PER2 and CRY1 form a heterodimer. Once in the cytoplasm these CLOCK-regulated proteins accumulate and post-translational modifications (purple circles) occur through different mechanisms such as ubiquitination and phosphorylation. The RBX1/SCF complex ubiquitinates CRY1, targeting it for degradation, while USP7 deubiquitinates CRY1, stabilizing the protein. MAGEL2 interacts with USP7, likely acting in an opposing manner to destabilize CRY1. Once translocated back to the nucleus, CRY1 and PER2 inhibit the expression of BMAL1/CLOCK, effectively repressing their own transcription. Modified with open access permission from Carias, K. V., Zoeteman, M., Seewald, A., Sanderson, M. R., Bischof, J. M., and Wevrick, R. (2020) A MAGEL2-deubiquitinase complex modulates the ubiquitination of circadian rhythm protein CRY1. *PLoS One* **15**, e0230874. Created with BioRender.com.

In control neurons, the average period length was 27.1 while in PWS, there were two distinct period length phenotypes. The shorter period length subgroup had an average period length of 26.1 hours and the longer subgroup had an average period length of 28.1. For the individual control samples, there was overlap in the timing of *Per2* peaks and troughs for all 4 individuals tested. For the PWS individuals, there was some overlap in *Per2* expression timing, but the deviation was greater, in particular in the PWS-short period phenotype. Interestingly, replicate *Per2* LumiCycle recordings derived from the same PWS individuals (PWS 1, 2, and 3) showed both the long and short period length phenotypes suggesting that the loss of *MAGEL2* in PWS causes the circadian pathway to destabilize and to potentially lose the buffering capabilities of the control neurons. Investigations into MAGEL2's role in this transcription- translation feedback loop will be necessary to determine the MAGEL2 mediated stabilization mechanisms. One of the PWS subjects (PWS 4) only displayed the short phenotype but was not in phase with the other individual traces in the same subgroup. In the SYS neurons, there was discordance in *Per2* cycling between the individual samples and between replicate from the same individual. The *Per2* period length average for the SYS neurons was not significantly different from that of the control neurons, but the difference in the timing of *Per2* peaks and troughs was striking and points to a defect in CLOCK- regulated gene expression versus neurotypical control neurons. The average period length of control neurons was 27.1 hours, which differs from the expected period length of ~24 hours. We hypothesize that this difference arises from the developmental age of the neurons used in these studies. Little is known about circadian rhythms in early neurodevelopment. It will be important to assess circadian function in differentiated DPSC neurons throughout all phases of neurodevelopment and maturity.

Circadian period length is determined by the turnover of CLOCK-regulated proteins. As MAGEL2 has been shown to alter turnover rate, we propose that in both SYS and PWS, MAGEL2 is responsible for regulating the period length and *Per2* expression timing differences we found. A faster turnover rate would reduce the period length. Accordingly, a slower turnover rate would increase the period length versus the control neurons. It is possible that in the absence of MAGEL2 in the PWS neurons, CRY1 is over-stabilized. In endocytic recycling, MAGEL2 opposes the deubiquitinating action of USP7 [217] and likely has this same effect on USP7's interaction with CRY1. This over-stabilization of CRY1 would in theory lead to longer period lengths as CRY1 would not be degraded at the same rate as in the control neurons. One explanation for the shorter period length PWS group is that MAGEL2 may be exerting an effect on the RBX1 complex which ubiquitinates CRY1 and targets it for degradation. Carias *et al.* used BioID assays to determine that MAGEL2 was within 10 nm of the RBX1 containing complex and that when the MAGE homology domain of MAGEL2 was mutated, it no longer interacted with RBX1. The loss of MAGEL2 in PWS neurons appears to abolish the cell's ability to fine tune the transcription translation feedback loop in the circadian pathway. In SYS, MAGEL2 expression is not simply lost, but MAGEL2 itself is mutated and is hypothesized to produce a shortened protein product that could have novel function compared to wild type MAGEL2. The functional significance of each of the various MAGEL2 mutation types in SYS has not yet been determined and future

circadian assays using different SYS mutations may reveal how MAGEL2 function is altered in this specific syndrome.

Conclusion

In this study, we observed for the first time, defects in circadian cycling in primary neurons from SYS and PWS subjects. Using Per2:Luc reporter DPSC lines differentiated to neuronal cultures, we were able to assay *Per2* expression across time as an output of circadian rhythm function. We also found that neuronal differentiation is required for rhythmic *Per2* cycling and that in both PWS and neurotypical control neurons, the transcription translation feedback loop regulating Bmal1 and Per2 in the circadian pathway oscillates as expected. Importantly, we found two distinct period length phenotypes in PWS neurons that were significantly different from control neuron period length. Finally, we observed discordant *Per2* cycling in SYS neurons from different individuals and among replicates from the same individual. We hypothesize that the loss or disruption of MAGEL2 in these syndromes affects the cell's ability to fine-tune the turnover of key circadian rhythm proteins, specifically CRY1. Establishing this assay and observing circadian rhythm defects in PWS and SYS neurons paves the way for future drug discovery aimed at rescuing circadian cycling defects.

CHAPTER 4. PRADER-WILLI SYNDROME NEURONS SHOW NEURODEVELOPMENTAL DELAY AT THE SINGLE CELL LEVEL

Introduction

Prader-Willi syndrome (PWS) is a neurodevelopmental disorder defined by a range of phenotypes including developmental delay, intellectual disability, hypogonadism, sleep disorders and increased autism risk [128, 133, 146]. Motor and language development is impaired in most PWS individuals and about 10-20% of PWS adults experience cycloid psychosis [218]. PWS is caused by a lack of expression of critical genes on the 15th chromosome. This region, 15q11.2-13, is known as the PWS/ Angelman syndrome critical region (PWACR) and has several maternally imprinted genes including *MAGEL2*, *SNRPN/SNURF*, and a cluster of SnoRNAs. Despite the broad range of neurocognitive phenotypes present in PWS, little work has been done at the molecular level to characterize the developmental delay in actual PWS neurons. Indeed, this is a challenging task, given the differences between mouse models of PWS (loss of *MAGEL2*, *SNORD116* or even syntenic deletions) and clinical phenotype diversity of PWS in children. One way around this problem is to study actual neurons from individuals with PWS as they develop from stem cells to mature neurons in culture. Our laboratory has extensive experience studying molecular aspects of multiple neurogenetic syndromes on the autism spectrum using patient derived dental pulp stem cell (DPSC) cultures coaxed into neuronal lineages [137, 142]. DPSC more closely mimic the epigenetic environment of embryonic stem cells [219] and when differentiated to neurons display neuronal markers, ion currents and action potentials [93, 220]. Using this model system derived from primary stem cells of PWS individuals, we can observe the full scope of the PWS critical region deletion on molecular pathways critical during neurodevelopment.

Advances in sequencing technology have enabled us to study heterogenous cultures of neurons at the single cell level (scRNA-seq) in an effort to characterize gene expression changes unique to disease neurons and/or unique to populations of neurons which were previously missed using traditional RNAseq methods. This is vital for analyzing gene expression in heterogenous neuronal cultures such as the patient-derived DPSC-neurons used in our PWS studies. Using SPLiT-seq (Split Pool Ligation-based Transcriptome sequencing), an scRNA-seq technology that uses combinatorial barcoding to label the cellular origin of transcripts [221], we were able to profile both PWS and neurotypical control neurons at the single cell level to identify gene expression differences that were not identified in our previous RNAseq studies [26]. Here, we were able to identify not only that this method is sensitive enough to capture expected expression differences in the PWACR and identify transcripts associated with PWS phenotypes, but we were also able to show an enrichment in transcripts related to translational processes and neurogenesis in PWS neurons. The data presented here provides evidence of a delay in neural development in PWS neurons versus neurotypically developing neurons at the transcriptional level.

Materials and Methods

Prader Will Syndrome and Control Tooth Collection

Teeth for DPSC cultures were collected as previously described [136]. Briefly, teeth from PWS subjects were collected remotely by caregivers after confirmation of genetic diagnosis. Subjects were supplied with a tooth collection kit as well as instructions, a description of the study and a consent form. Neurotypical control teeth were collected through the Department of Pediatric Dentistry and Community Oral Health at the University of Tennessee Health Science Center. Stem cells were cultured from the collected teeth and cell lines from early passages (P2-P4) were frozen for storage in our DPSC repository. Molecular studies performed here and our DPSC repository were approved by the UTHSC institutional review board prior to conducting this research.

Generation of Dental Pulp Stem Cell Cultures

DPSC were isolated and cultured according to our previously published protocol [136]. Briefly, pulp was removed from the tooth cavity and minced both mechanically and enzymatically using 4 mg/mL Collagenase I and 3 mg/mL Dispase. Cells were then seeded with DMEM/F12 1:1, 10% fetal bovine serum, 10% newborn calf serum and 100 U/mL penicillin and 100 ug/mL streptomycin in 12-well plates coated with poly-D-lysine. After cells reached ~80% confluency, they were passaged with TrypLE Express for expansion and neuronal differentiation.

Neuronal Differentiation

DPSC were seeded at 20,000 cells/cm^2 in T-25 cell culture flasks with DMEM/F12 1:1, 10% fetal bovine serum (FBS), 10% newborn calf serum (NCS), with 100 U/mL penicillin and 100 ug/mL streptomycin (Pen/Strep). After reaching ~80% confluency, neuronal differentiation was performed as described by previously by Kiraly *et al*. [93]. Briefly, epigenetic reprogramming was performed for 48 hours using 10 μM 5-azacytidine (Acros Scientific, Geel, Belgium) in DMEM/F12 containing 2.5% FBS and 10 ng/mL bFGF (Fisher Scientific, Waltham, MA). Following epigenetic reprogramming, neuronal differentiation was induced using 250 μM IBMX, 50 μM forskolin, 200 nM TPA, 1mM db-cAMP (Santa Cruz, Dallas, TX), 10 ng/mL bFGF (Invitrogen, Carlsbad, CA), 10 ng/mL NGF (Invitrogen, Carlsbad, CA), 30 ng/mL NT-3 (Peprotech, Rocky Hill, NJ), and 1% insulin-transferrin-sodium selenite (ITS) (Fisher Scientific, Waltham, MA) in DMEM/F12 for 3 days. The cells were then maintained in neuronal maturation media consisting of 1mM db-cAMP, 2% B27, 1% N2 supplement, 30 ng/mL NT-3, and 1X Glutamax (Fisher Scientific, Waltham, MA) in Neurobasal A media (Fisher Scientific, Waltham, MA) for 28 days.

Preparation and Sequencing of Illumina Libraries Using SPLiT-Seq

Single-cell barcoded cDNA was prepared for Illumina sequencing using the Cell Fixation Kit and the Single Cell Whole Transcriptome Kit from Parse Bioscience (Seattle, WA) following the protocol provided by the manufacturer. Briefly, 4-week mature neuronal cultures from 4 individuals (2 control, 2 PWS) were dislodged from T-25 flasks using TrypLE Express and neurons were counted using a hemocytometer and viability was also determined using Trypan Blue. The entire sample was then fixed using the Cell Fixation Kit (Parse Biosciences) for 10 minutes on ice, followed by permeabilization for 3 minutes. Finally, the samples were centrifuged for 10 minutes at 350 x g. The pellet was then resuspended and passed through a 40 uM cell strainer. DMSO was added to the neurons in suspension and the samples were frozen at -80°C using a Mr. Frosty (Nalgene).

To prepare the barcoded cDNA, the neuronal samples were thawed at 37°C and counted using a hemocytometer. Neurons were then added to the Round 1 Barcoding plate at ~2,000 neurons/well for an in-cell reverse transcription reaction using well-specific barcoded primers. After this reaction, the cells were pooled and then split across the Round 2 Barcoding plate where an in-cell ligation reaction added a second well-specific barcode to the cDNA. After the reaction, the cells were pooled again and dispersed across the Round 3 Barcoding plate where another round of in-cell ligation appended another barcode to the cDNA. The cells were then split into sub-libraries of varying cell number, 500-3,000 cells per sub-library. For the experiment detailed here, the sub-library of 3,000 cells was used. After aliquoting the barcoded cDNA into sub-libraries, the cells were lysed and barcoded cDNA was isolated and fragmented using KAPA Pure beads. In the final step, a 4^{th} sub-library specific barcode was ligated to the cDNA by PCR. The isolated cDNA library was sent to Novogene and sequenced using the Illumina HiSeq platform (Novogene).

Data Analysis

scRNA-seq data was analyzed with the assistance of Dr. Daniel Johnson at the UTHSC Molecular Bioinformatics Core. Briefly, FASTQC files were transferred from Novogene using SFTP (secure file transfer protocol). Each FASTQ file was subjected to quality control and correction using FASTQC (bioinformatics.babraham.ac.uk) and FASTX trimmer (hannonlab.cshl.edu/fastx_toolkit/). The trimmed FASTQ files were aligned to the Hg38 for Human using RNA-STAR [222]. The SAM files were then mined for the alignment primary counts and barcode samples using the SPLiT-seq pipeline. The counts were normalized using TMM (Trimmed Mean of M-values) normalization. The normalized data matrix was loading into R to gather statistics and determine differential expression. The mean, variance, standard deviation, and standard error of means were calculated for each gene across each condition. DeSeq2 was used to identify genes with log2 fold change $\leq$ 0.58 and p-value $\leq$ 0.05. P-values were then adjusted for multiplicity using the Benjamini Hochberg method. Only genes with an adjusted p-value $\leq$ 0.05 were considered differentially expressed. Metadata generated from Illumina sequencing data

was input into the GranatumX analysis pipeline [223, 224] to create UMAP graphs for cluster and gene expression visualizations.

Results

SPLiT-Seq Technology Accurately Captures Both Prader-Willi and Sex-Specific Gene Expression Differences

DPSC from 2 control and 2 PWS individuals (1 male and 1 female per group) were differentiated to 4-week mature neuronal cultures prior to creating barcoded single-cell libraries for sequencing. Our barcoded library consisted of ~2,000 cells across the 4 individual lines. After sequencing, 1,873 cells were identified across these 4 lines representing 94% of the input. The mean reads per cell was 145,479 and the median number of genes detected per cell was 3,580. After de-multiplexing and alignments, data was formatted for input into GranatumX to create Uniform Manifold Approximation and Projection (UMAP) plots [225]. GranatumX is an online scRNA-seq analysis pipeline. **Figure 4-1A** shows that the scRNA-seq data clusters by individual. This is to be expected as our neuronal populations have inherent background variability. Cond258 and Cond297 are the PWS individuals and Cond182 and Cond238 are the neurotypical control subjects. **Figure 4-1B** shows the expression of *SNRPN*, a gene within the PWACR, and *XIST*, a gene that is expressed by female cells. The expression of *SNRPN* is only seen in the control populations as expected, since PWS subjects should not be expressing the paternally imprinted *SNRPN* in neurons. The expression of *XIST*, a gene that regulates X chromosome inactivation in females, is only present in the female samples (258 and 182). This data confirms that the SPLiT-seq technique and our DPSC-neuronal model is capturing the expected PWS and sex specific expression.

Single-Cell RNAseq Reveals Significant Differential Expression of Transcripts Related to Neurogenesis, Cognition, Endocytic Recycling, and Hypogonadism in Prader-Willi Syndrome Neurons

Figure 4-2A shows the expression of several transcripts highly expressed in PWS neurons versus neurotypical control neurons. These genes are *SOX11*, *NSG1*, and *IL17RD* and they are expressed in ~90% of the PWS cells and in ~10% of the control neurons. *SOX11* is a transcription factor involved in cell fate and embryogenesis [226]. *NSG1* encodes for a protein specific for endosomal recycling in neurons [227]. *IL17RD* encodes for an interleukin receptor and is associated with hypogonadism. Conversely, **Figure 4-2B** shows the expression of transcripts that were expressed in ~80% of the control neurons and <1% of in the PWS populations. *FOXP2*, a transcription factor, and *NAV2*, a neuronal navigator protein, are associated with neuronal development. *CSMD1* has been associated with cognitive ability, memory, and learning [228]. The PWS samples show only 2 neuronal cells per group that express any of these transcripts. These findings imply that the PWS neurons are more immature than the control neurons at the molecular level

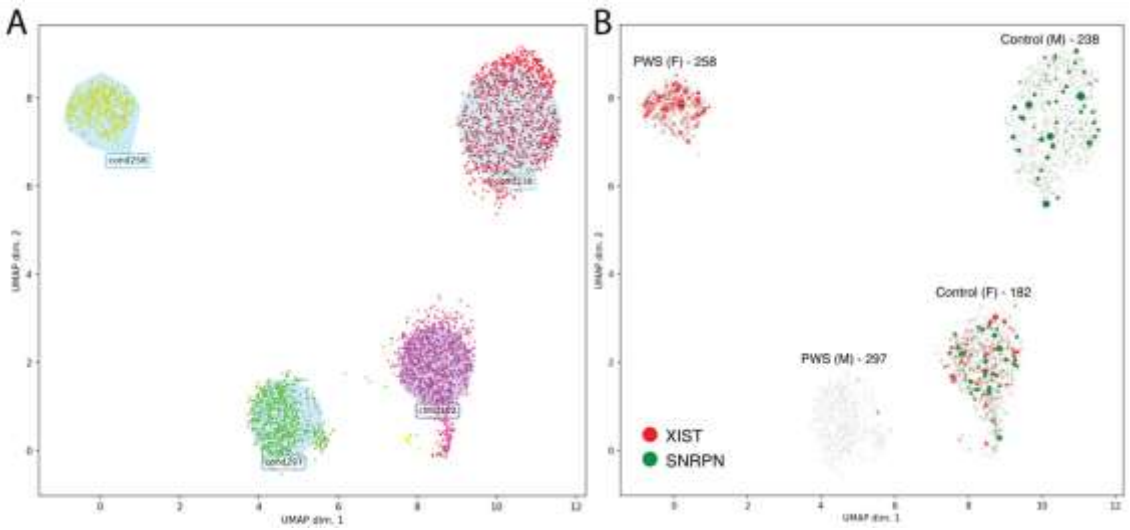

Figure 4-1. Single cell sequencing of DPSC-derived neurons shows expected expression of genetic and sex-specific transcripts.
(A) scRNA-seq using the SPLiT-seq technology shows that DPSC-derived neuronal cultures cluster by individual. **(B)** *XIST*, present primarily in female cells, is expressed in the female samples, but not the males. *SNRPN*, a gene within the PWACR, is only expressed in the control individuals. Dental pulp stem cell (DPSC), Prader-Willi/Angelman syndrome critical region (PWACR).

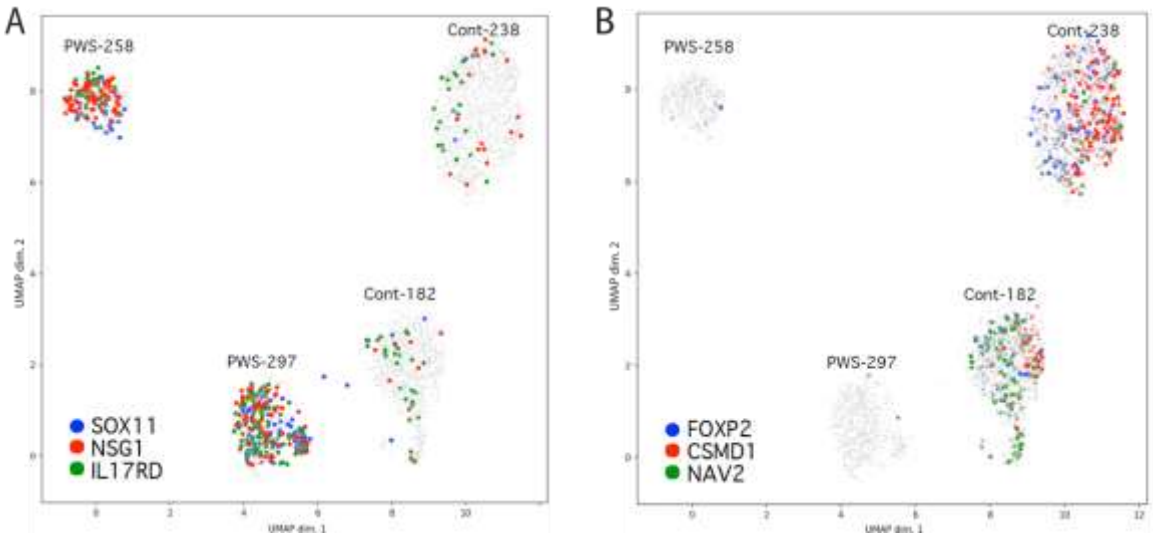

Figure 4-2. Differential expression of transcripts related to PWS phenotypes identified in PWS neurons.

Transcripts related to PWS phenotypes show higher **(A)** and lower **(B)** expression versus control neurons. PWS neurons show differential expression in genes related to hypogonadism (*IL17RD*), endocytic recycling (*NSG1*), cognitive deficits (*CSMD1*) and neurodevelopmental delay (*SOX11, FOXP2,* and *NAV2*). Prader-Willi syndrome (PWS).

(i.e. they do not yet or may never express mature markers like *FOXP2*, *NAV2* and *CSMD1*).

Single-Cell RNAseq Reveals Enrichments in Ribosome, Translation, and Receptor-Related Transcripts in Prader-Willi Syndrome Neurons

Enrichment analysis was performed on the significantly differentially expressed transcripts in the PWS versus control neurons using DAVID (Database for Annotation, Visualization, and Integrated Discovery) analysis. DAVID is an online tool that identifies enriched gene ontology (GO) terms in gene sets and assigns enrichment scores [145, 153]. **Figure 4-3A** lists the GO biological process enrichments identified in our data set. The top enrichments were *cytoplasmic translation* and *translation* (enrichment score = 28.09). 54 of the 58 transcripts identified in the *translation enrichment* are ribosomal proteins integral to the function of the large and small ribosomal proteins. All of these transcripts within the enrichments were reduced in the PWS neurons.

Figure 4-3B shows the expression of multiple ribosomal transcripts on a UMAP plot. The ribosomal transcripts are detected in ~75% of the control neurons versus <10% of the PWS neurons and at much higher expression levels than the neurons that are positive for these transcripts in the PWS samples. Transcripts identified within the *extracellular matrix* enrichment consisted primarily of metallopeptidases and collagen chain components. Interestingly, within this enrichment were transcripts related to neurodevelopment including *NDNF*, *TNR*, and *APP*. The genes identified in the *skin development* enrichment consist of collagen chain components also identified in the extracellular matrix (ECM) enrichment as well as *FRAS1*, *TRAF3IP2*, *ARRDC3*, and *COMP*. Although these transcripts have been identified within the GO *skin development* category, they are expressed in the brain and some have neuronal functions according to their GeneCard profiles [229, 230]. The remaining enrichment categories have many overlapping transcripts that are included in all categories. These transcripts are ephrin, neurotrophic, and growth receptors. The neurotrophic receptors (*NTRK2*, *NTRK3*) showed decreased expression in the PWS populations while the other receptors in these enrichments have variable expression, some showing increased expression and some showing decreased expression versus control neurons. These data reveal molecular pathways that are perturbed in the PWS neurons including a reduction in translation, ribosomal, and neurogenesis related transcripts that may cause a delayed developmental phenotype.

Prader-Willi Syndrome Neurons Have More Stem Cell and Fewer Mature Neuron Markers Than Control Neurons

Within the differentially expressed transcripts identified in our scRNA-seq experiment, there were transcripts related to neurogenesis that were expressed in more neurons in the control samples than the PWS samples (~80% versus <1%). Conversely, transcripts related to stem cell maintenance were expressed in more cells in the PWS

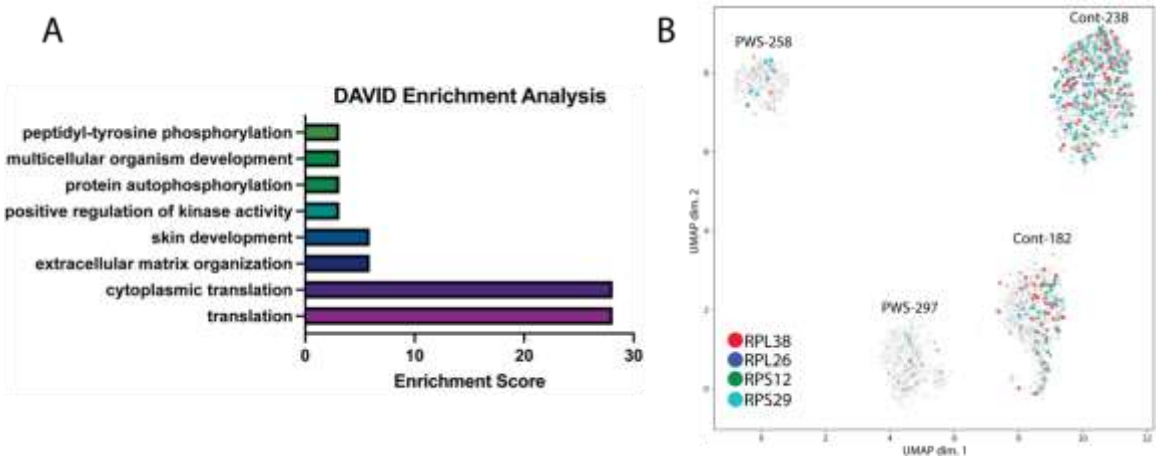

Figure 4-3. Single cell sequencing of PWS neurons versus neurotypical control neurons reveals enrichment in translation and receptor gene ontologies.
(A) DAVID analysis of the scRNA-seq data shows significant enrichments in transcripts related to translation and tyrosine kinase receptors [145]. Within the cytoplasmic translation enrichment, an abundance of ribosomal subunit transcripts was identified. **(B)** Expression of multiple ribosomal transcripts is reduced in the PWS neuronal populations. Prader-Willi syndrome (PWS), Database for Annotation, Visualization and Integrated Discovery (DAVID).

samples. In **Figure 4-2A** *SOX11* was more highly expressed in the PWS neurons (~60% versus <1%), while *FOXP2* and *NAV2* were more highly expressed in the control neurons. In addition to these neuronal and stem cell related transcripts, **Figure 4-4** shows the expression of neurogenesis markers *FOXP1*, *NRXN1* and *NRXN3*. In **Figure 4-4A** the PWS samples ~85% of the neurons are positive for *FOXP1* while the control samples show ~90% of the neurons are positive for *FOXP2*. *FOXP1* and *FOXP2* are critical for early brain development and their expression overlaps in many brain regions [231]. *FOXP1* is expressed in a wide range of neurons across development whereas *FOXP2* is restricted to more distinct neuronal subtypes. The expression pattern for *FOXP1/P2* shown in **Figure 4-4A**, implies that the control neurons are more developmentally mature. *NRXN1* and *NRXN3* are presynaptic proteins found in mature neurons. Their expression increases as neurons develop [232]. In the control samples, both *NRXN1* and *NRXN3* show an increased number of positive neurons (90% versus <1%) versus the PWS samples (**Figure 4-4B**). This further implies the difference in neuronal maturity in the disease versus control state.

Discussion

PWS is a devastating neurodevelopmental disorder that causes global developmental delay, hypotonia, childhood obesity, along with other symptoms. Currently, there are no mouse models that fully recapitulate the disease phenotypes, therefore, cellular models created from actual PWS subjects are critical to understanding the disease molecular etiology. Here we used our DPSC-derived neuronal cultures developed from individuals with PWS to investigate gene expression differences at a single cell level in PWS neurons versus neurotypical control neurons. The method we used here, SPLiT-seq, is a novel approach to single cell sequencing that uses combinatorial barcoding to label the cellular origin of RNA in fixed cells [221]. Using SPLiT-seq, we barcoded cDNA libraries representing a pool of neurons derived from the stem cells of two individuals with PWS and two typically developing individuals. The UMAP output of the scRNA-seq data shows that our samples cluster by individual, rather than cell type, which speaks to the underlying genetic diversity among individuals even with the same syndrome. To confirm that this unique model system and novel scRNA-seq technique was able to accurately recapitulate the genetic landscape of our samples, we queried our data for both *SNRPN*, which is deleted in PWS, and *XIST*, which is expressed only in female cells. Our data shows an expected lack of expression for *SNRPN* in the PWS samples and no *XIST* expression in the male samples, indicating that these cultured neurons do recapitulate the genotype and sex of the individuals used to generate them.

We identified several transcripts that were related to PWS phenotypes in our dataset. These transcripts include *NSG1*, *IL17RD*, and *CSMD1*. The PWS neuronal populations were enriched for *NSG1* and *IL17RD* expression. NSG1 regulates endosomal recycling and sorting of neuronal receptors [233]. Previously, we have shown that aberrant endosomal trafficking in PWS due to the loss of *MAGEL2* leads to a reduction in circulating bioactive hormones which may be the underlying cause of several PWS

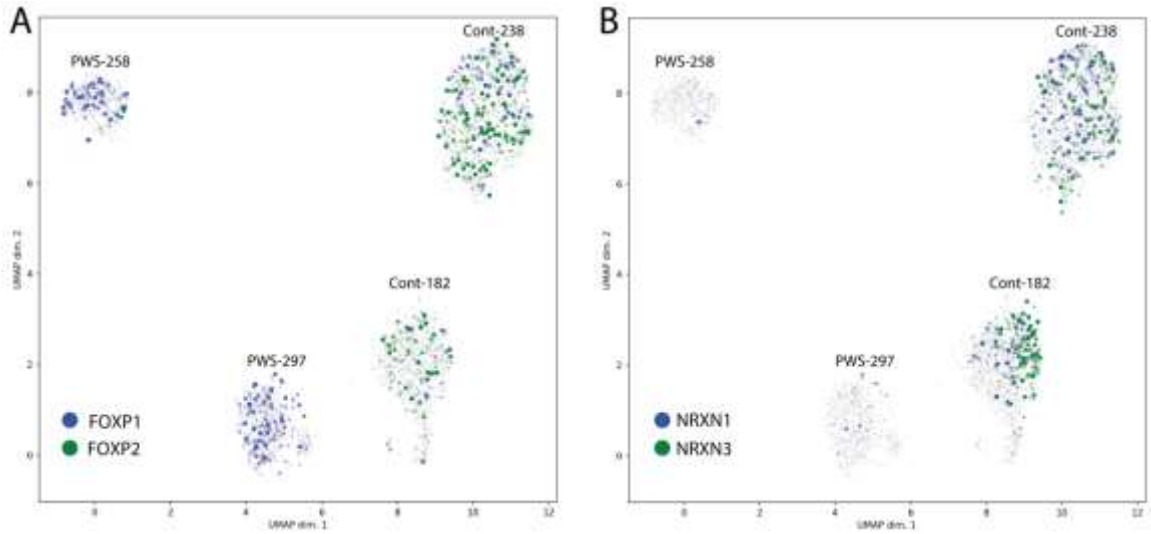

Figure 4-4. PWS neurons show delayed neurodevelopment versus neurotypical control neurons.
(A) *FOXP1* and *FOXP2* are key neuronal development genes. *FOXP1*, a marker of immature neurons, is still present in most PWS neurons. **(B)** *NRXN1* and *NRXN2* are cell surface receptors present at the synapse of developing neurons. These two markers of mature neurons are expressed higher in controls indicating that the PWS neurons are developmentally delayed after 4-weeks in maturation media. Prader-Willi syndrome (PWS).

phenotypes [206]. Indeed, overexpression of NSG1 has been shown to alter the endosomal recycling pathways [234].

IL17RD encodes for an interleukin receptor and is associated with hypogonadism [235-237]. Hypogonadism is a common PWS phenotype and is present in the majority of PWS subjects [130]. Interleukin-17 family members have also been implicated in regulating stem cell fate [238]. *CSMD1*, which was expressed in ~60% of the control neurons but not PWS neurons, is associated with cognitive function and schizophrenia [228, 239]. *Csmd1* knockout mice showed signs of anxiety, depression and blunted emotional responses [240]. Additionally, whole exome sequencing of subjects with Parkinson disease revealed two novel mutations in the *CSMD1* gene [241]. The strong scRNA-seq evidence presented here warrants further investigation into the functional relevance of these transcripts to PWS pathogenesis.

Enrichment analysis showed strong enrichments in transcripts related to translational processes, primarily transcripts encoding ribosomal subunit components. Expression of the ribosomal transcripts identified in these enrichments were significantly decreased in the PWS neuronal populations suggesting a depletion in ribosomes, the site of translation, and subsequently protein production. The decreased expression of many transcripts encoding ribosomal proteins likely precludes the decreased amount of ribosomal biogenesis. The availability of ribosomal pools is critical for developing neurons and establishing neuronal connectivity, a dynamic process involving rapid localized protein turn over [242]. Post-mitotic neurons need an abundance of ribosomes to maintain synaptic plasticity and dendritic/axonal morphology [243]. Increasing ribosomal content during the maturation of neurons has been observed in rat models where continuously increasing ribosomal content was observed from post-natal day 7 to day 42 [243]. The reduced abundance of ribosomes, and subsequent translational insufficiency in PWS neurons, could cause defects in forming and maintaining synapses. Indeed, reduced ribosomal biogenesis has been implicated in various neurodevelopmental disorders including microcephaly and autism spectrum disorder (ASD) [242]. The functional consequences of this decreased ribosomal transcript abundance in PWS neurons requires further investigation to determine if there is simply a delay in neurodevelopment or long-term consequences leading to ongoing cognitive deficits seen in PWS.

In addition to the enrichment in translation found through DAVID analysis, there were also enrichments in transcripts encoding for extracellular membrane proteins, primarily receptors involved in regulation of kinase activity. Several ephrin receptors (EPHA4, EPHA3, and EPHB1) and neurotrophic receptors (NTRK2 and NTRK3) were identified in these enrichments. *EPHA3*, *EPHB1*, *NTRK2* and *NTRK3* were upregulated in the neurotypical control neurons versus the PWS neurons and *EPHA4* was significantly increased in the PWS neurons.

Ephrin receptors are involved in intercellular communication to regulate cellular processes such as differentiation, morphology and proliferation [244]. In a whole transcriptome study on neural progenitor versus mature neurons, *EPHA3* was found the

be significantly increased in mature neurons and associated with axon guidance [245]. EPHB1 is involved in dendritic spine formation and *Ephb1* knockout mice have been shown to develop fewer spines and spines with abnormal morphology [246]. Interestingly, EPHA4, the ephrin receptor with increased expression in PWS neurons, has been shown to maintain stem cells in an undifferentiated state. Khodosevich *et al*. found that *Epha4* knockdown in neurospheres resulted in decreased proliferation and premature differentiation [247]. NTRK2 and NTRK3 are involved in the development of the central nervous system and signaling through these receptors regulates neuronal differentiation. Bartkowska *et al.* found that inhibition of these receptors leads to a decrease in the formation of new neurons and that activation of these receptors was necessary for the proliferation of embryonic cortical precursors [248].

In addition to identifying enrichments in categories related to neural development, we identified additional genes involved in neurogenesis that were significantly differentially expressed between PWS and neurotypical control neurons. *SOX11,* increased in PWS neurons, is a transcription factor involved in embryonic development and cell fate determination. Hoshiba *et al.* found that *Sox11* expression decreased during dendritic formation in cerebral cortex development [249]. However, blocking Sox11 activity limits the ability of post-mitotic neural cells to express neuronal markers [250]. This demonstrates that *Sox11* plays a vital role in early neural development but has inhibitive properties in more mature neurons.

FOXP1 and *FOXP2* are also transcription factors that are important for neural development. *FOXP1* expression has a pre-natal peak that is slightly before the peak of *FOXP2* expression although expression of both is maintained in mature neurons, but in different neuronal populations [251]. Additionally, Vernes *et al.* found that *Foxp2* modulates mRNAs that are involved in both neuronal plasticity and development [252]. Our data shows high expression of *FOXP1* in the PWS neurons and high expression of *FOXP2* in the control neurons of the same age. Both *FOXP1* and *FOXP2* are associated with neurodevelopmental disorders [251]. Whether the distinct *FOXP1/FOXP2* expression patterns shown in our data is related to a delayed neural development in the PWS neurons or possibly a cause of one of the PWS cognitive phenotypes needs further study and clarification.

NAV2, *NRXN1*, and *NRXN3* were expressed in most of the control neurons sequenced but were absent in the PWS neurons. Nav2, essential for neurodevelopment, reaches peak expression during late gestation and early pre-natal life, when neurons are migrating and differentiating [253]. Recently, a *NAV2* mutation was identified as the causative lesion in a female with neurodevelopmental issues and brain malformations [254]. *NRXN1* and *NRXN3* encode for pre-synaptic neurexin receptors that play key roles in signal transduction [255]. The presence of these transcripts indicates the formation of synapses in the control neuronal cultures. Taken together the absence of key neuronal markers and presence of early neural markers in the PWS neurons versus to the control neurons shows that the PWS neurons are developmentally delayed at the molecular level.

These results indicate preliminary evidence of a delayed neural phenotype in PWS neurons but must be followed up with a larger scRNA-seq experiment using additional neurotypical control and PWS subjects to confirm the delayed neurogenesis. Additionally, it will be important to compare the neural subpopulations between PWS and control groups to determine if there are significant differences in neuronal subtypes. The heterogeneity that is apparent at both the transcriptional and morphological level warrants further investigation and classification of each cellular subtype in these DPSC-neuronal cultures. Determining whether the transcriptional differences we found here are the result of slower development in the PWS neurons or a characteristic of PWS is critical to understanding the phenotype presented here. ScRNA-seq experiments across developmental time points (4-weeks, 6-weeks, 10-weeks, etc.) will be vital for determining if PWS neurons ever "catch-up" to control neurons. These experiments will inform any DPSC-neuron experiments moving forward.

Conclusion

The heterogeneity of the cognitive phenotypes in PWS warrants further investigation into the early development of PWS neurons. Using a novel scRNA-seq method, SPLiT-seq, we sequenced DPSC-derived primary neurons from PWS and neurotypical control subjects to investigate the transcriptional differences in immature neurons. We identified enrichments in transcripts related to translation, primarily ribosomal transcripts, that were downregulated in the PWS neurons, indicating reduced translational capacity versus the control neurons. Importantly, we found key neuronal markers that were present in the control populations but absent from the PWS populations. There was also an increase in transcripts related to early neurodevelopmental timepoints in the PWS neurons, implying a lack of maturity. Our data indicates a possible delay in neurogenesis in PWS. It will be important to determine if this delay is corrected at any point during neural development in PWS subjects or whether this transcriptional defect persists and is causative of PWS cognitive phenotypes.

CHAPTER 5. ANALYSIS AND COMPARISIONS OF GENE EXPRESSION CHANGES IN PATIENT-DERIVED NEURONS FROM ROHHAD, CCHS, AND PWS[3]

Introduction

Rapid-onset Obesity with Hypothalamic dysfunction, Hypoventilation, and Autonomic Dysregulation (ROHHAD) is a devastating disorder that affects children primarily between the ages of 1.5-7 years old with a rapid onset of symptoms [256-258]. ROHHAD is an ultra-rare neurocristopathy with only 200 cases described or identified to date [258]. The ROHHAD acronym describes the typical order in which this disease unfolds. Rapid-onset obesity, 20-30 pounds over a 3-12 month period, is typically the first symptom that appears for ROHHAD patients [258]. This rapid-onset obesity is followed by hypothalamic issues including altered salt/water balance, hypothyroidism, growth hormone insufficiency, altered pubertal onset, and additional hypothalamic symptoms [257]. The autonomic nervous system (ANS) dysfunction in ROHHAD includes gastrointestinal (GI) dysfunction, ophthalmologic issues, thermal dysregulation, and cardiac dysrhythmia [257]. Nearly half of all ROHHAD patients will present with a neural crest tumor, typically a ganglioneuroma or ganglioneuroblastoma, but rarely a neuroblasoma [258]. Alveolar hypoventilation is the most devastating symptom, as it can have a stealth onset and result in cardiorespiratory arrest, potentially leading to severe morbidity or sudden death in previously healthy children [256].

Currently there is no known genetic cause for ROHHAD. The leading theories for the cause of ROHHAD are genetic, epigenetic and autoimmune based [258-261]. Potentially causative genes that have roles in nervous system development have been investigated including *BDNF*, *ASCL1*, *NDN*, *ADCYAP1*, *OTP*, *PACAP*, and *HTR1A* [257, 262, 263]. None of these genes could be correlated to ROHHAD symptomology. Barclay *et al*. sequenced the exomes of seven ROHHAD trios and found that no two subjects had the same *de novo* variants [259]. Monozygotic twins discordant for ROHHAD were also sequenced with no genetic coding differences noted [259]. The authors suggest the possibility of varying epigenomes between the identical female twins leading to this discordance. The presence of anti-hypothalamus and anti-pituitary antibodies in cerebrospinal fluid of ROHHAD patients suggests a possible immune system mediated pathogenesis, although only three case studies have been reported [261, 264]. Additionally, immunosuppressive drugs have been found to have a positive effect on the neurological function in one ROHHAD subject [265]. To date, no underlying genetic or immunologic etiology has been identified that can explain the ROHHAD phenotype.

---

[3] Reused from prepared manuscript with authors' permission. Victor, A.K., T. Hedgecock, M. Donaldson, D. Johnson, C.M. Rand, D.E. Weese-Mayer, L.T. Reiter, *Analysis and Comparisons of Gene Expression Changes in Patient-Derived Neurons from ROHHAD, CCHS, and PWS.* (2023).

Currently, ROHHAD is diagnosed based on clinical presentation after a related syndrome, Congenital Central Hypoventilation Syndrome (CCHS) is ruled out. Similar to ROHHAD, CCHS is a rare neurocristopathy with approximately 3000 cases identified since 1970 [258]. CCHS subjects typically present with hypoventilation from birth and all subjects require ventilatory support [258, 266-268]. Unlike ROHHAD, CCHS is caused by a genetic lesion in *PHOX2B*, a transcription factor, primarily from polyalanine repeat expansion mutations (PARMs). The lengths of the PARM repeats correlate linearly with severity of symptoms while a subset of CCHS patients possessing non-PARMs in the *PHOX2B* gene present with more severe CCHS phenotypes [258, 266]. CCHS presents with both ANS dysfunction and hypoventilation, however, there is no rapid-onset obesity and only rarely hypothalamic dysfunction. In terms of ANS dysregulation, CCHS and ROHHAD exhibit overlapping symptoms including ophthalmologic issues, GI dysmotility, and increased pain perception thresholds [266-268]. Some CCHS patients, typically with an NPARM mutation in *PHOX2B*, also present with neural crest tumors. The overlapping phenotypes in these syndromes imply a similar molecular etiology, although formal molecular links between ROHHAD and CCHS have not yet been identified.

Prader-Willi syndrome (PWS) is a hypothalamic disorder with some overlapping phenotypic features to ROHHAD including the rapid-onset obesity [269]. PWS is caused by the loss of paternal specific expression of the genes *SNRPN, SNURF, SNORD116* and *MAGEL2* in the PWS critical region (15q11.2-q13.3) on the 15th chromosome. Although the trajectory of the rapid-onset childhood obesity in PWS is less steep than that seen in ROHHAD, and the age at onset differs, the obesity is a defining feature of PWS and is accompanied by extreme hyperphagia [128]. Autonomic and hypothalamic dysfunction are present in both PWS and ROHHAD syndrome. Hypothalamic dysfunction overlapping both syndromes includes hypothyroidism, growth hormone insufficiency, and altered pubertal onset. Autonomic dysfunction overlapping the two syndromes includes GI dysmotility, ophthalmologic manifestations, elevated pain threshold and thermal dysregulation [128, 257, 258, 263, 270]. Due to these overlapping clinical features, the PWS critical region has been studied in a ROHHAD cohort. Using both next-generation sequencing and methylation sensitive assays of the paternally expressed genes in the region, no variation or loss of heterozygosity was found in the ROHHAD cohort for this region of interest [269]. Although no genes within the 15q11.2-q13.3 region were found to be perturbed in ROHHAD, the similarities between these syndromes leave open the possibility that the same molecular pathways are co-regulated and warrants further gene expression studies in patient-derived neurons.

To understand the molecular overlap among ROHHAD, CCHS, and PWS, we performed RNA sequencing (RNAseq) on neurons derived from dental pulp stem cells (DPSC) collected from ROHHAD and CCHS individuals as well as neurotypical controls. DPSC are multipotent stem cells of neural crest origin and have been differentiated to a variety of cell types including chondrocytes, adipocytes, and neurons [137, 271, 272]. DPSC have been found to recapitulate the epigenetic environment of embryonic stem cells more accurately than induced pluripotent stem cells and are obtainable without the need for invasive biopsies or viral reprogramming [136, 219].

Many groups have differentiated DPSC to neuronal lineages showing morphological, transcriptional, and functional characteristics of terminally differentiated neurons [81, 97, 123, 273-284]. Our group and others have had success modeling neurogenetic syndromes using these stem cells differentiated to neuronal cultures [93, 154, 170, 285, 286]. Using this unique patient-derived stem cell model, we have observed molecular signatures and cellular phenotypes of various syndromes in primary neurons including Prader-Willi, Angelman, and Duplication 15q syndromes [26, 206, 287]. Here we utilize this system to differentiate patient derived DPSC lines to neuronal cultures for RNAseq in order to identify the molecular similarities and find genotype/phenotype correlations among ROHHAD, CCHS and PWS. Early diagnosis and clinical intervention is critical for ROHHAD patients, so identifying molecular markers distinguishing ROHHAD from clinically related syndromes is as important as identifying the molecular commonalities between these syndromes with known genetic lesions.

Materials and Methods

Obtaining Teeth for DPSC Cultures

Neurotypical control teeth were obtained through the Department of Pediatric Dentistry and Community Oral Health at the University of Tennessee Health Science Center (UTHSC). Teeth from children with ROHHAD and CCHS were collected remotely by the caregivers of these subjects after confirmation of the underlying diagnosis. All subjects provided informed consent for tooth collection (IRB#2009-13905 at Lurie Children's Hospital). All 6 ROHHAD subjects have received a ROHHAD diagnosis. 8 of 11 patients were evaluated clinically at Lurie Children's Hospital and their diagnoses confirmed with CCHS-related *PHOX2B* mutations in CCHS subjects (n=5) and with clinical phenotyping in ROHHAD subjects (n=3). The excised deciduous teeth were broken to reveal the pulp, cells cultured and cell lines frozen during early passages for our DPSC Repository as previously described [136]. The DPSC Repository and molecular studies on DPSC-derived neurons were approved by the UTHSC institutional review board prior to conducting research (IRB #10-00878-XP).

Generation of Dental Pulp Stem Cell Cultures

DPSC used in this study were isolated and cultured according to our previously described protocol and cell lines stored in the DPSC Repository [136]. Briefly, the dental pulp was removed from inside the tooth cavity and minced. Following removal, the pulp was digested with 3 mg/mL Dispase II and 4 mg/mL Collagenase I for 1 hour. Cells were then seeded on poly-D-Lysine coated 12-well plates with DMEM/F12 1:1, 10% fetal bovine serum (FBS), 10% newborn calf serum (NCS), and 100 U/mL penicillin and 100 ug/mL streptomycin (Pen/Strep) (Fisher Scientific, Waltham, MA). Once confluent (80%) cultures were passaged using TrypLE^{TM} Express. Only early passage cells ($\leq$ passage 4) were used for subsequent neuronal differentiation and molecular studies.

Neuronal Differentiation

DPSC lines were seeded at 20,000 cells/cm^2 on poly-D-lysine coated flasks with DMEM/F12 1:1, 10% fetal bovine serum (FBS), 10% newborn calf serum (NCS), with 100 U/mL penicillin and 100 ug/mL streptomycin (Pen/Strep). At 80% confluence, the neuronal differentiation protocol was followed as previously published in Kiraly *et al.*, 2009 [93] with an extended maturation phase (4 weeks versus 7 days) [136]. Briefly, DPSC were placed in 10 μM 5-azacytidine (Acros Scientific, Geel, Belgium) in DMEM/F12 containing 2.5% FBS and 10 ng/mL bFGF (Fisher Scientific, Waltham, MA) for 48 hours. Following epigenetic reprogramming, neuronal differentiation was induced by exposing the cells to 250 μM IBMX, 50 μM forskolin, 200 nM TPA, 1mM db-cAMP (Santa Cruz, Dallas, TX), 10 ng/mL bFGF (Invitrogen, Carlsbad, CA), 10 ng/mL NGF (Invitrogen, Carlsbad, CA), 30 ng/mL NT-3 (Peprotech, Rocky Hill, NJ), and 1% insulin-transferrin-sodium selenite premix (ITS) (Fisher Scientific, Waltham, MA) in DMEM/F12 for 3 days. At the end of the neural induction period, neuronal maturation was performed by maintaining the cells in Neurobasal A media (Fisher Scientific, Waltham, MA) with 1mM db-cAMP, 2% B27, 1% N2 supplement, 30 ng/mL NT-3, and 1X Glutamax (Fisher Scientific, Waltham, MA) for 28 days.

RNA Sequencing of DPSC-Neurons

After neuronal maturation for 28 days, total RNA was collected from the DPSC-neurons using the Zymo Directzol RNA extraction kit (Zymo, Irvine, CA). Prior to sequencing, RNA was assayed for integrity and quality using the Agilent Bioanalyzer 6000 pico chip (Agilent, Santa Clara, CA). Only RNA with an RNA Integrity Number (RIN) $\geq$ 9.0 was used for RNAseq studies. Library preparation and RNAseq was performed by Novogene (NovaSeq 6000 PE150) (Sacramento, CA) using the Illumina platform and paired end reads. 20M paired-end reads per sample were collected.

RNAseq Analysis

FASTQ files from Novogene were analyzed for quality and trimmed using FASTQC. All reads were trimmed to remove nucleotides with Phred scores < Q20. The trimmed FASTQ files were aligned to the human genome reference library hg19 using RNASTAR [288]. Once aligned, the SAM files were collected and mined for read count information of each gene present in the reference file. Read counts were normalized using Counts per Million (CPM) method across groups for the entire experiment. Principle component analysis and Pearson's coefficient plots were performed on the normalized transcriptome profile. A lmfit and voom was used to perform differential expression analysis [288]. All genes that fail to yield a *p*-value $\leq$0.05 and a fold change greater than 1.5 were removed. Benjamini and Hochberg false discovery rate (FDR) was performed on this trimmed gene list. All genes that failed to yield an FDR rate of $\leq$ 0.05 were removed. The PWS RNAseq dataset used here is from our previously published work [26] and accessible through the GEO database (GEO#: GSE178687). To generate Venn

diagrams the final list of significantly differentially expressed genes were uploaded into an online Venn diagram tool (http://bioinformatics.psb.ugent.be/webtools/Venn/). Heatmaps were created using the ClustVis web tool [144]. Additionally, the targets were loaded into the web based enrichment analysis tool, Gene Ontology Enrichment Analysis and Visualization Tool (GOrilla) to identify enriched gene ontology (GO) terms [289]. The GOrilla software takes the full list of transcripts ranked by False Discovery Rate (FDR) and identifies GO terms that appear densely at the top of the ranked list. GOrilla assigns an enrichment score based on the total number of genes in the dataset (N), the total number of genes associated with a specific GO term (B), the number of genes in the top of the dataset (n), and the number of genes in the intersection (b). The enrichment score is calculated by the formula: (b/n)/(B/N).

Western Blots

Protein was collected from 4-week mature neuronal cultures using N-PER Protein Extraction Reagent (Fisher Scientific, Waltham, MA) supplemented with a protease inhibitor cocktail (Fisher Scientific, Waltham, MA). Samples were resolved on a 4-12% Bis-Tris gel run at a constant 125V for 3 hrs, then transferred for 23 minutes onto a PVDF membrane using Genscript eBlot machine (L00686). Membranes were blocked at room temperature for 1.5 hrs in TBS-T with 5% nonfat milk and incubated at 4°C overnight in primary antibodies at 1:2000. Primary antibodies used: α-ADORA2A (ProteinTech, 51092-1-AP) and α-PHACTR1 (ProteinTech, 23446-1-AP), and loading control α-GAPDH (Santa Cruz, sc-47724). Following overnight incubation with primary antibodies, three 25-minute washes with TBS-T were performed and membranes were incubated with secondary antibodies for 30 minutes at room temperature. Secondary antibodies used: HRP-conjugated α-rabbit (Cell Signaling, 7074P2) at 1:5000 dilution and HRP-conjugated α-mouse (Cell Signaling, 7076P2) at 1:10000 dilution. Following secondary antibody incubation, three 25-minute washes in TBS-T were performed followed by a final 25-minute wash in TBS. Pierce ECL Western (Fisher Scientific, Waltham, MA) reagents were used for GAPDH exposure. SuperSignal West Atto Ultimate Sensitivity ECL (Fisher Scientific, Waltham, MA) reagents were used to develop the ADORA2A and PHACTR1 membranes. Developed films were then digitized as non-compressed .tiff files using a V600 Epson scanner. Files were processed using ImageJ Fiji using the gel quantification plugin. The mean control sample measurements were used to normalize each lane for ADORA2A and GAPDH blots respectively. ADORA2A was then normalized against GAPDH for final protein fold change values. These values were then analyzed in Prism software (GraphPad) using one-tailed t-tests between each individual and the control group.

Results

Molecular and Phenotypic Overlap Between ROHHAD, CCHS, and PWS

Table 5-1 lists the defining ROHHAD features and the presence or absence of these in CCHS and PWS. The rapid-onset obesity, although a less steep trajectory in PWS and differing age at onset, is present in both ROHHAD and PWS. Additionally, PWS and ROHHAD share hypothalamic dysfunction including growth hormone insufficiency, hypothyroidism, and altered pubertal onset (precocious in ROHHAD but delayed in PWS). ROHHAD and CCHS share the hypoventilation phenotype which is the most severe symptom in both syndromes as well as neural crest tumors in a subset of individuals. All three syndromes display ANS dysregulation including gastrointestinal issues and ophthalmologic manifestations.

To understand the molecular similarities and differences among these three syndromes, RNA sequencing (RNAseq) analysis was performed on DPSC-derived neuronal cultures from neurotypical controls (n=3) and subjects with ROHHAD (n=3) or CCHS (n=2). Throughout this work, we use the term transcript to describe gene-level expression differences. **Table 5-2** lists the GUIDs and clinical characteristics for each subject used in the molecular studies (RNAseq and western blots). For the PWS dataset, we used our previously published RNAseq data from DPSC-neurons (GSE178687) [26]. Differential gene expression analysis for each of the syndromes versus the neurotypical control subjects were analyzed by the UTHSC Bioinformatics Core and significantly (*p*-value $\leq$0.05, FDR $\leq$ 0.05, Fold change $\geq$ 1.5 or $\leq$ 0.5) differentially expressed transcripts were identified. Using this list of significantly different transcripts versus control neurons as well as our previously published RNAseq data from PWS neurons versus control (n=4) [26], we created a Venn diagram (**Figure 5-1A**). Venn analysis shows ROHHAD neurons have their own unique signature, but also share molecular commonalities with CCHS and PWS. In addition, our data shows that these syndromes share three significantly differentially expressed transcripts versus control. These transcripts are *FOXK1*, *ZNF18*, and *FBH1*. The normalized RNAseq expression for these shared transcripts across syndromes is shown in **Figure 5-1B**. The RNAseq data for each experiment was normalized to the average of the neurotypical control samples in the corresponding experiments. *FOXK1* and *ZNF18* are both transcriptional regulators. *FBH1* is critical for repairing stalled or damaged replication forks during DNA replication. Broadly, these results indicate very little overlap among all three syndromes, but significant overlap between CCHS and ROHHAD gene expression signatures. It should be noted that, although each experiment was normalized to neurotypical control expression, the PWS experiment occurred separately and, as such, batch effects may be present.

Table 5-1. Overlapping clinical phenotypes of ROHHAD, CCHS, and PWS.

Clinical Observation	ROHHAD	CCHS	PWS
Obesity	Yes	No	Yes
Hypoventilation	Yes	Yes	Sometimes
Hypothalamic dysfunction	Yes	Rarely	Yes
Hypothyroidism	Sometimes	Rarely	Sometimes
Growth hormone insufficiency	Yes	Rarely	Yes
Altered pubertal onset	Sometimes	No	Sometimes
Autonomic dysfunction	Yes	Yes	Yes
Bradycardia	Sometimes	Sometimes	No
Gastrointestinal dysfunction	Yes	Yes	Sometimes
Hirschsprung disease	No	Often	No
Neural crest tumors	Yes	Sometimes	No
Ophthalmologic manifestations	Yes	Yes	Yes
Altered pain perception	Yes	Yes	Yes
Thermal dysregulation	Yes	Yes	Yes
Seizures	Sometimes	Sometimes	Sometimes
Neonatal hypotonia	No	Sometimes	Yes
Neurocognitive delay	Rarely	Variable	Yes

Rapid-onset obesity with hypothalamic dysfunction, hypoventilation, and autonomic dysfunction (ROHHAD), Congenital Central Hypoventilation syndrome (CCHS), Prader-Willi syndrome (PWS). *Data Sources*: Ceccherini, I., K.C. Kurek, and D.E. Weese-Mayer, *Developmental disorders affecting the respiratory system: CCHS and ROHHAD.* Handb Clin Neurol, 2022. **189**: p. 53-91. 10.1016/b978-0-323-91532-8.00005-7 [258]. Barclay, S.F., et al., *ROHHAD and Prader-Willi syndrome (PWS): clinical and genetic comparison.* Orphanet J Rare Dis, 2018. **13**(1): p. 124. 10.1186/s13023-018-0860-0 [269].

Table 5-2. Subjects included in molecular experiments listed by GUID with corresponding clinical phenotypes.

GUID	Experiment	Diagnosis	Sex	Age of Onset	Ventilatory Support	Seizures	Cardiac Arrest	Neural Crest Tumor
GRDRMK467CLT	RNAseq	ROHHAD	F	4.0	Awake/Asleep	Yes	No	Yes (GN)
GRDRJR976DWY	RNAseq	ROHHAD	M	6.0	Asleep	Yes	No	No
GRDRPN312JYM	RNAseq/Western Blot	ROHHAD	M	1.5	Asleep	No	No	No
NIH-INVYZ061FERBJ	Western Blot	ROHHAD	F	4.0	Asleep	Yes	No	Yes (GN)
GRDRUD154GNH	Western Blot	ROHHAD	M	2.6	Asleep	No	No	No
GRDRGZ805WLY	Western Blot	ROHHAD	M	3.5	Asleep	No	No	No
GRDRHC489JUK	RNAseq	CCHS (20/33)	M	Neonate	Asleep	Yes	No	No
GRDRPU870HZG	RNAseq/Western Blot	CCHS (20/25)	F	Neonate	Asleep	Yes	No	No
GRDRHC22YV2	Western Blot	CCHS (20/26)	F	Neonate	Awake/Asleep	Yes	Yes	No
GRDRWX199GXE	Western Blot	CCHS (20/27)	F	Neonate	Awake/Asleep	Yes	No	No
NIH-INVLG921GKWXE	Western Blot	CCHS (20/33)	M	Neonate	Awake/Asleep	No	No	Yes (NB)

Rapid-onset obesity with hypothalamic dysfunction, hypoventilation, and autonomic dysfunction (ROHHAD), Congenital Central Hypoventilation syndrome (CCHS). *PHOX2B* expansion number listed in parentheses. Age of onset listed in years. Type of neural crest tumor: GN (ganglioneuroma) or NB (neuroblastoma). GUID (globally unique identifier).

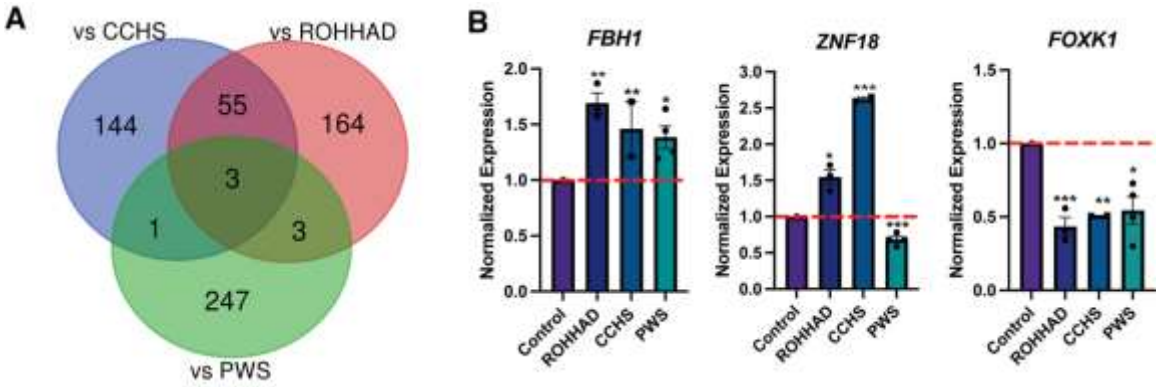

Figure 5-1. ROHHAD, CCHS, and PWS neurons share 3 differentially regulated genes versus control neurons.

(A) Venn diagram of the significantly differentially expressed transcripts (*p*-value ≤ 0.05, FDR ≤ 0.05, fold-change ≤0.5 or ≥1.5) versus control for ROHHAD, CCHS, and PWS. Three transcripts were identified as differentially regulated versus control subjects in all 3 syndromes, while 55 differentially expressed transcripts were shared between ROHHAD and CCHS vs control. **(B)** Average RNAseq expression for each group across the three 3 genes shared by ROHHAD, CCHS and PWS vs controls. Expression was normalized to the average of the control expression in each study. The dashed red line indicates control expression level. PWS data were gathered from our previous RNAseq experiment [26]. Significance determined during RNAseq data analysis (*p*-value ≤ 0.05 and FDR ≤ 0.05). * = *p*-value ≤ 0.05, ** = *p*-value ≤ 0.01, *** = *p*-value ≤ 0.005. Rapid-onset obesity with hypothalamic dysfunction, hypoventilation, and autonomic dysregulation (ROHHAD), Congenital Central Hypoventilation syndrome (CCHS), Prader-Willi syndrome (PWS).

Gene Ontology Enrichment in Receptor, Acetylglucosaminyltransferase and Immune-Mediated Processes in ROHHAD Neurons

RNAseq analysis identified 225 genes to be significantly differentially expressed in ROHHAD versus control neurons. Using GOrilla enrichment analysis, we found significant gene ontology (GO) enrichments in these data. GOrillia enrichments are presented in **Figure 5-2A**. The top enrichments (enrichment score $\geq$ 5) were ATPase transmembrane transporter activity (*ATP6V1G2*, *ABCB9*, *TAPBP*, *ABCD4* and *TCIRG1*), acetylglucosaminyltransferase activity (*MGAT1*, *GCNT3*, *LFNG* and *B3GALNT1*) and phagocytic vesicle membrane (*HLA-A*, *TAPBP*, *PIKFYVE* and *TCIRG1*). A heatmap of the genes found in these enrichments across each subject sequenced is shown in **Figure 5-2B**. Most of these genes have significantly reduced expression versus control, while three show increased expression. Gene functions are listed in **Table A-4** [230]**.** Several of the genes identified in the enrichment categories relate to immune system processes and neuroinflammatory syndromes. These enrichment studies on ROHHAD specific neuron gene expression indicate that at least three molecular pathways may contribute to disease etiology: ATPase transmembrane transporters, acetylglucosaminyltransferases, and phagocytic vesical membrane proteins.

Molecular Overlap Between PWS and ROHHAD May Not Be Related to Rapid-onset Obesity

The RNAseq data collected in this experiment compared with our previously published RNAseq data [26] revealed six genes that are significantly different in both PWS and ROHHAD versus control. The Venn diagram in **Figure 5-1A** shows this overlap. Three of the six genes found in this intersection are unique to PWS and ROHHAD and are not significantly different in the CCHS versus control dataset. These genes are *ID1*, *CNN3*, and *OAZ3*. To compare expression across two datasets, the RNAseq data for ROHHAD and PWS subjects was normalized to the average control expression of the transcript in each dataset. This normalized expression was used to create bar graphs for each gene (**Figure A-4**). For *ID1*, PWS and ROHHAD neurons show differing expression trends versus control. In PWS, *ID1* expression is significantly higher, while in ROHHAD expression is significantly lower. One of the primary reasons for comparing PWS to ROHHAD in this experiment was to see if any of the overlapping genes were related to the rapid-onset obesity phenotype seen in each syndrome. The three overlapping genes in our dataset do not currently have any links to an obesity pathogenesis. *ID1* is a transcriptional regulator. *OAZ3* plays a role in cell proliferation and maintenance. *CNN3* is involved in cytoskeletal function and is actin-binding. These results suggest that the obesity in ROHHAD may not share a molecular pathway with PWS and may be distinct in origin. Further validation of this hypothesis in other relevant cell types will be necessary to confirm the independent obesogenic pathology in PWS and ROHHAD.

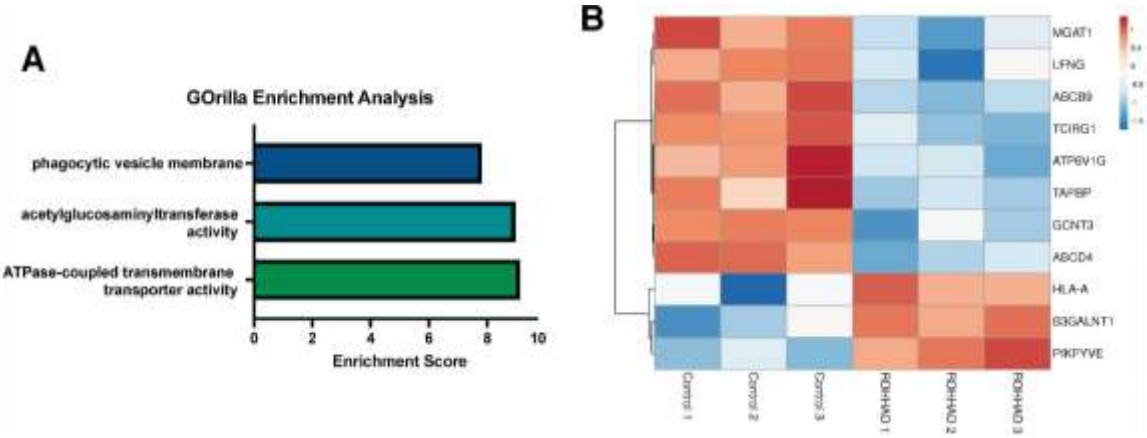

Figure 5-2. Enrichment analysis of ranked gene expression differences between ROHHAD and control neurons shows significant enrichment in phagocytic vesicle membrane, acetylglucosaminyltransferase activity and transmembrane transporter activity.

(**A**) GOrilla enrichment analysis was used to determine the gene ontology (GO) enrichments in our Control versus ROHHAD dataset [289]. GOrilla analysis identified 3 GO categories (enrichment score ≥ 5) that are significantly enriched (p-value ≤ 0.05) at the top of our ranked gene list. **(B)** A heatmap was created using the RNAseq expression counts for each ROHHAD and control individual for genes identified in each of the enrichment categories using ClustVis [144]. Rapid-onset obesity with hypothalamic dysfunction, hypoventilation, and autonomic dysregulation (ROHHAD).

Gene Expression Analysis Reveals Shared Molecular Signature Between ROHHAD and CCHS Neurons

The Venn diagram in **Figure 5-3A** shows that there are 58 genes significantly differentially expressed in both ROHHAD and CCHS versus control. Using the mean RNAseq counts per group, a heatmap was created using ClustVis [144]. The heatmap (**Figure 5-3B**) indicates that most of these genes are significantly decreased versus control in both ROHHAD and CCHS. Eight of these genes show higher expression in ROHHAD and CCHS versus control. For all genes identified in this overlap, the expression trend versus control is the same for both ROHHAD and CCHS. A list of these genes and their function is listed in **Table A-5** [230]. Several of the genes identified encode for proteins that have functions related to neuronal development, including *ADAM8*, *KAT6B* and *ADIRF*. Additionally, *ASCC1*, *COL13A1*, *SYTL3*, *TANGO2*, *PHACTR1*, and *ADORA2A* encode proteins that have functions related to ROHHAD and CCHS phenotypes. These expression studies have revealed molecular overlap between ROHHAD and CCHS neurons versus neurotypical controls. This implies that similar or the same pathways may be disturbed in both syndromes leading to shared phenotypic characteristics.

ADORA2A Protein Does Not Consistently Change in ROHHAD but Shows Reduction in CCHS with Increasing *PHOX2B* PARM Number

One gene that changed at the transcript level in neurons and could play a role in both ROHHAD and CCHS is the *ADORA2A* gene, which encodes an adenosine receptor. We used western blot analysis of ADORA2A protein in ROHHAD and CCHS DPSC-derived neurons versus neurotypical controls to verify that changes in gene expression are reflected at the protein level (**Figure 5-4A**). There was no consistency amongst ROHHAD individuals for ADORA2A protein regulation (**Figure 5-4B**). Two individuals, 5WLY and ERBJ, showed significant reduction (~55% and ~85%) in ADORA2A levels compared to the average control groups. One individual, 4GNH, showed a nonsignificant increase (~132%) in ADORA2A. The remaining ROHHAD individual, 2JYM, having no significant change in protein levels.

In contrast, CCHS individuals exhibited a decrease in ADORA2A protein expression that was inverse to an increase in PARM number. The 20/25 PARM individual (0HZG) showed a significant reduction (~51%) in ADORA2A protein. Whereas the 20/26 (2YV2) individual showed a nonsignificant reduction of 23%. The PARM 20/27 (9GXE), and 20/33 (KWXE) individuals showed significant reduction (~62%) of ADORA2A protein regulation (**Figure 5-4C**). **Figure A-5** shows an additional ADORA2A western blot using a nitrocellulose membrane performed prior to the optimized one shown in Figure 4. We also examined another protein of interest, PHACTR1, however, it showed no consistency amongst controls, ROHHAD, and CCHS DPSC-derived neuron lines (**Figure A-6**). These studies indicate a correlation between PARM number and ADORA2A expression and suggest that ADORA2A may be regulated by the PHOX2B transcription factor, the function of which is affected by

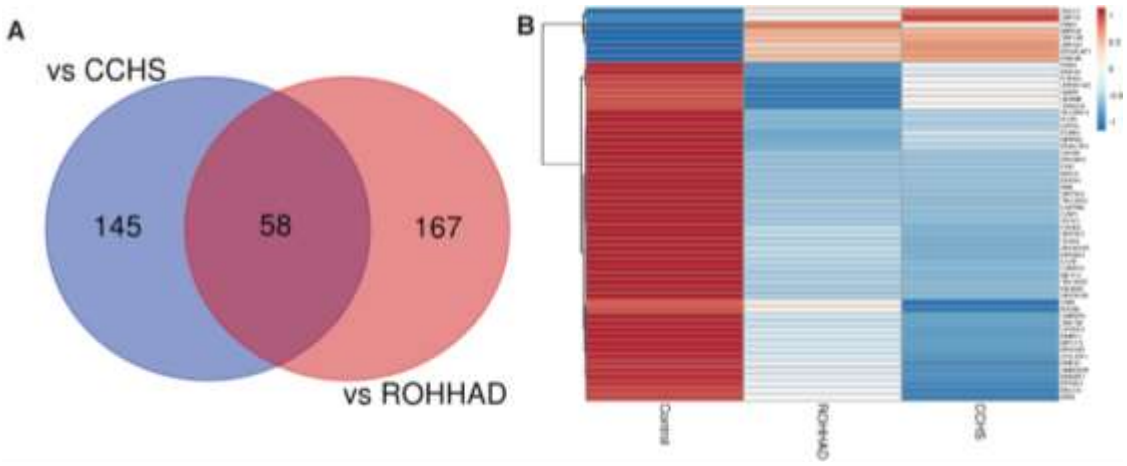

Figure 5-3. ROHHAD and CCHS share 58 differentially expressed genes versus neurotypical control subjects.
(A) Venn diagram created using the list of differentially expressed transcripts (*p*-value ≤ 0.05, FDR ≤ 0.05, fold-change ≤0.5 or ≥1.5) versus control subjects. **(B)** Heatmap of the 58 overlapping transcripts differentially expressed in ROHHAD and CCHS neurons versus control neurons. Heatmap was created using ClustVis [144]. Rapid-onset obesity with hypothalamic dysfunction, hypoventilation, and autonomic dysfunction (ROHHAD), Congenital Central Hypoventilation syndrome (CCHS).

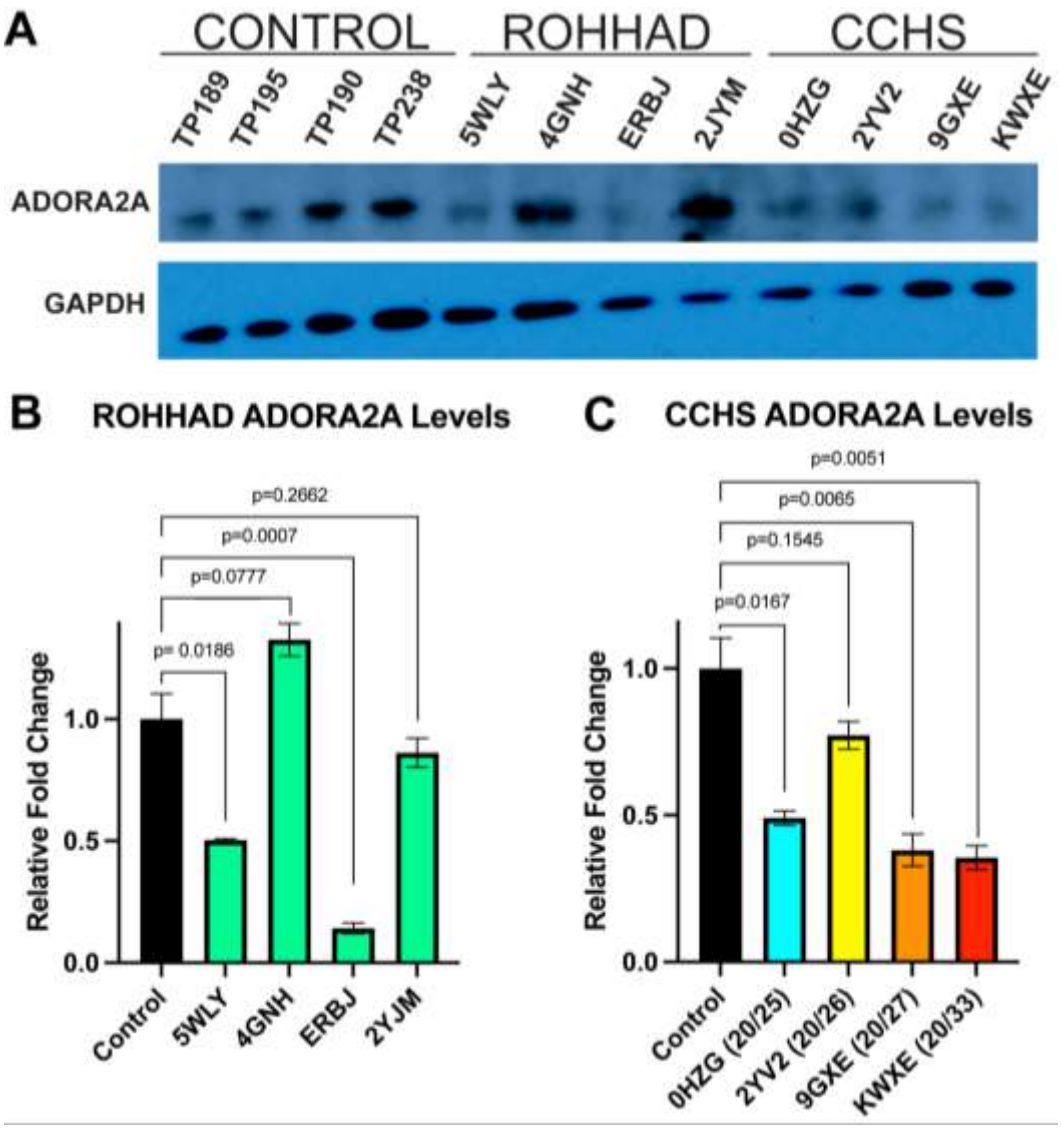

Figure 5-4. Western blot analysis of ADORA2A reveals differential expression in ROHHAD and CCHS neurons.

(A) ECL western blot of ADORA2A in Control, ROHHAD, and CCHS groups. An average of all four controls was used for normalization and comparison to each of the four individual ROHHAD and the four individual CCHS cell lines. The graphs were scaled differently for ROHHAD versus CCHS comparisons, but the same control samples and averages were used in B and C. **(B)** Quantification of ADORA2A protein in ROHHAD individuals. 5WLY and ERBJ show significant reduction, 4GNH with nonsignificant increase of protein level, and 2JYM is statistically unchanged. **(C)** ADORA2A quantification in CCHS individuals. 0HZG (20/25) shows a significant reduction, 2YV2 (20/26) exhibits a nonsignificant reduction, 9GXE (20/27) and KWXE (20/33) also show a significant reduction. Rapid-onset obesity with hypothalamic dysfunction, hypoventilation, and autonomic dysfunction (ROHHAD), Congenital Central Hypoventilation syndrome (CCHS).

PARM expansions in CCHS individuals. Further validation in a larger cohort of CCHS subjects with varying PARM mutations will be necessary to confirm PHOX2B-mediated regulation of ADORA2A.

Discussion

Uncovering the molecular commonalities and differences among these three syndromes is a crucial next step for identifying therapeutics and biomarkers specific to ROHHAD. Here, we used our unique model system, DPSC-derived neurons, to investigate molecular perturbations in these syndromes versus neurotypical children and identify unique and overlapping transcriptional signatures. Previously, we used DPSC neuronal cultures to investigate neurogenetic syndromes including Prader-Willi, Angelman, and Duplication 15q syndrome [26, 206, 287]. In this study, using RNAseq from individuals with ROHHAD, CCHS, and neurotypical children, we identified differentially expressed transcripts with shared expression between ROHHAD and CCHS. We then used previously published RNAseq data from PWS DPSC-derived neuronal cultures to compare these syndromes to PWS subjects [26]. We identified gene ontology enrichments in ROHHAD neurons, three transcripts that are differentially expressed in all three syndromes versus neurotypical control neurons and 58 transcripts that are differentially expressed in both ROHHAD and CCHS neurons.

For ROHHAD, CCHS, and PWS the three transcripts that are significantly different between all three syndromes versus control neurons were *FOXK1*, *FBH1*, and *ZNF18*. All three genes play roles in maintaining DNA integrity or transcriptional regulation. FOXK1 is crucial in regulating glucose metabolism and aerobic glycolysis [290, 291]. Compared to control neurons, ROHHAD, CCHS, and PWS neurons all had reduced expression of *FOXK1*. The reduction in expression in neurons from these three syndromes may pertain to a delay in neurogenesis, a feature shared among many developmental disorders. As stem cells develop into neurons, they switch their primary metabolic processes from glycolysis to mitochondrial respiration [292]. *FOXK1* plays a key role in this process [291]. Additionally, *FOXK1* has been associated with autism and delayed development in several studies [293, 294].FBH1 plays a role in responding to stalled or damaged replication forks. In response to DNA damage, FBH1 causes DNA double-stranded breaks and induces cell death [295-297]. ROHHAD, CCHS, and PWS have increased *FBH1* expression compared to control neurons. The increased expression of *FBH1* may be caused by or causative of increased DNA damage in disease neurons. Studies have shown that FBH1 is required for eliminating cells with excessive replicative stress [295]. Additionally, accumulation of damaged DNA has been directly linked to neuronal death in other syndromes, such as Alzheimer's disease [298, 299]. ZNF18 is involved in regulating transcription through RNA polymerase II. Although the function of this protein has not been well characterized, mutations in this gene have been associated with autism [300]. This association may explain the differing directionality in expression for ROHHAD and CCHS versus PWS, where the incidence of autism spectrum disorder is higher [132, 301]. Expression of *ZNF18* in PWS neurons is

significantly decreased versus control. In contrast, *ZNF18* expression is significantly increased in ROHHAD and CCHS neurons.

Enrichment analysis using the ranked list of differentially expressed transcripts between ROHHAD versus neurotypical control neurons identified significant enrichments in the phagocytic vesicle membrane compartment (GO:0045335), transmembrane transporter activity (GO:0042626), and acetylglucosaminyltransferase activity (GO:0008375). The four transcripts identified in the phagocytic vesicle membrane enrichment were *HLA-A*, *TAPBP*, *PIKFYVE* and *TCIRG1*. A phagocytic vesicle is an intracellular vesicle that arises due to phagocytosis, a key cellular process for eliminating cellular waste and maintaining cellular homeostasis [302]. In neurons, dysfunctional phagocytosis, either excessive or not enough, is detrimental to neuronal development and health [303]. Excessive microglial phagocytosis of live neurons and synapses has been implicated in various neurodegenerative disorders including Alzheimer's and Parkinson's disease [304, 305].

In ROHHAD neurons, there was an increased expression in the *HLA-A* and *PIKFYVE* transcripts and decreased expression of the *TAPBP* and *TCIRG1* genes. *HLA-A* encodes the antigen-presenting major histocompatibility complex class I, A. This molecule plays a critical role in the immune system by presenting peptides for recognition to cytotoxic T cells [230]. Inhibition of PIKFYVE, an endosomal kinase, was shown to reduce excitotoxicity and restore lysosomal maturation, in a cell model of Amyotrophic Lateral Sclerosis [306]. Most transcripts identified in the acetylglucosaminyltransferase activity enrichment (*MGAT1*, *GCNT3*, *LFNG* and *B3GALNT1)* were decreased in the ROHHAD neurons. Acetylglucosaminyltransferase activity is crucial for glycosylation, an important and complex post translational modification crucial for regulation of neuronal intercellular signaling. In *Drosophila melanogaster*, *Mgat1* null mutants were found to have disrupted synaptogenesis and signaling [307]. Interestingly, *MGAT1* variants are associated with susceptibility to obesity [308]. Decreased glycosylation activity is associated with neuronal death and neurodegenerative disease [309]. All transcripts identified in the transmembrane transporter activity category were decreased in the ROHHAD neurons. Several of the protein products of these transcripts localize to lysosomes. Neuronal lysosomes are crucial for degrading cellular debris and maintaining neuronal integrity. All the enrichment data taken together may allude to a dysfunction in clearing cellular debris and leading to decreased neuronal health in affected neurons or an immune mediated process related to ROHHAD and the propensity for ROHHAD neural crest cells to migrate and develop neural crest tumors in the body as DPSC are of neural crest origin.

We identified three transcripts that were uniquely significantly different between ROHHAD and PWS versus control (*ID1*, *CNN3*, and *OAZ3*). Although one of the primary commonalities between these syndromes is childhood obesity, these three genes do not appear to be related to obesity and two of these genes appear to have opposing expression patterns versus control neurons. Our molecular findings indicate that while both ROHHAD and PWS subjects present with childhood obesity, it is likely that the pathways responsible for obesity in these disorders arise from distinct molecular and

perhaps even behavioral defects. Lending support to this theory, PWS subjects are profoundly hyperphagic which is not routinely an underlying cause of obesity in ROHHAD patients [258].

The strongest finding in our RNAseq dataset was the large number of genes that are significantly different in both ROHHAD and CCHS versus control neurons. We identified 58 significantly differentially expressed transcripts versus neurotypical controls in common between these syndromes, all following similar expression patterns (i.e., both syndromes show either increased or decreased expression for the same gene versus control (see **Figure 5-3B**)). Within the 58 genes, we did not find any significant gene ontology enrichments, however, we did identify transcripts that correlate with neuronal processes and the phenotypes observed in both ROHHAD and CCHS, including *ASCC1*, *COL13A1*, *TANGO2*, and *PHACTR1*. *ASCC1*, a gene encoding for a transcriptional regulator, was found to be significantly increased in ROHHAD and CCHS neurons. This transcript has been associated with several congenital neuromuscular diseases including spinal muscular atrophy [310-312]. *COL13A1*, which encodes an extracellular synaptic protein that is required for neuromuscular junction synapse function, was significantly decreased in ROHHAD and CCHS neurons. Mutations in this gene are associated with a spectrum of myasthenic diseases that result in breathing difficulties and apneas [313-315]. *TANGO2* mutations and deficiency are associated with a variety of symptoms including hypothyroidism, metabolic and cardiac dysfunction, and rhabdomyolysis [316-319]. This gene was found to be significantly decreased in our dataset for both ROHHAD and CCHS versus control neurons. *PHACTR1* encodes a phosphatase and actin regulatory protein that plays a role in neuronal migration and dendritic arborization. Although we did see a reduction in PHACTR1 protein by western blot in several of the ROHHAD and CCHS subjects (**Figure A-6**) in accordance with our RNAseq data, this result was variable from individual to individual.

An adenosine receptor gene, *ADORA2A*, was also found to be significantly decreased in the ROHHAD and CCHS neurons versus neurotypical controls. *ADORA2A* encodes a member of a G-protein coupled receptor family that functions by increasing cAMP levels using adenosine as its primary agonist and is associated with Parkinson's disease [320, 321]. Physiologically, ADORA2A aides in regulation of cardiac rhythm and circulation, cerebral and renal blood flow, immune function, pain regulation and sleep. In *Adora2a*$^{-/-}$ mice, Adora2a specifically modulates the antiadrenergic effects of the Adora1 receptor [322]. Treatment with isoproterenol, a β-adrenergic molecule agonist, in WT and *Adora2a*$^{-/-}$ mice both showed antiadrenergic responses, with *Adora2a*$^{-/-}$ mice exhibiting a ~40% increase in antiadrenergic response. These findings supplement prior work showing decreased heart rate (HR) in *Adora2a*$^{-/-}$ mice and an increase in HR for *Adora1*$^{-/-}$ mice [323]. Previous clinical studies on ROHHAD patients show that some cases may present with bradycardia, a low resting heart rate [324]. The observed reduction of ADORA2A protein levels in two ROHHAD individuals may be able to explain this clinical feature. ADORA2A is thought to provide a protective effect against the development of pulmonary hypertension [325], another clinical phenotype that presents in some ROHHAD individuals consequent to recurrent low oxygen due to inadequately managed hypoventilation [260, 326]. Our findings that CCHS individuals have

decreasing ADORA2A protein expression with increasing *PHOX2B* PARM number suggests that ADORA2A regulation may be dependent on proper PHOX2B activity. In fact, two *PHOX2B* transcription factor binding sites can be found in or near the promoter of the *ADORA2A* gene (**Figure A-7**). The variance seen in the ROHHAD subjects for ADORA2A protein expression, as well as PHACTR1, is likely due to the spectrum of ROHHAD symptomology that unfolds across time and with varying severity. Further studies will be needed to establish that PHOX2B can directly regulate *ADORA2A* gene expression levels, which could be an important finding in both ROHHAD and CCHS.

The results presented here represent the first study using primary ROHHAD and CCHS neurons and showing molecular correlation between CCHS and ROHHAD pathogenesis. Although groundbreaking, there are some limitations to the interpretation of the data. As this is a rare syndrome, we were limited in the amount of specimen used for both RNAseq and western blot analysis. Further validation of these results in larger cohorts of ROHHAD and CCHS subjects will be necessary to confirm the results presented here. The PWS RNAseq data used for comparison here came from a separate experiment and, as such, batch effects may make comparing to the current study problematic. Additionally, these are developmentally young cortical-like neurons. However, the early neurodevelopmental timeframe that this model represents provides evidence of perturbed pathways seen even in immature neurons and provides insight into disease pathogenesis that is present from early neurodevelopment and may have significant downstream effects on later developmental phenotypes.

Conclusion

ROHHAD is a complex ANS disorder with an unknown genetic etiology. Although molecular, genetic, and clinical studies have been performed on ROHHAD and CCHS patients before, this is the first gene expression study on neurons derived from these individuals. In addition, no molecular or cellular pathways had previously been identified that reveal the underlying disease etiology. Here we uncovered an enrichment in differentially expressed transcripts related to phagocytic vesicle and receptor-mediated processes in ROHHAD neurons and an overlapping molecular signature between both ROHHAD and CCHS, a related ANS hypoventilation disorder. This overlap includes transcripts that control neurodevelopmental processes and molecular pathways that may be perturbed leading to ROHHAD pathology. We then validated the expression of a down-regulated transcript, *ADORA2A*, at the protein level and found significant reduction in ADORA2A protein for CCHS neurons and several ROHHAD subjects, although expression appears to vary more in the ROHHAD cohort. This variability in ROHHAD subjects likely reflects the broad spectrum of ROHHAD symptoms, the unfolding of the phenotype over time, and the unknown etiology of the disease. Continuing molecular studies and correlation with clinical phenotypes will be essential to uncovering the molecular pathways behind the various ROHHAD symptoms and identifying biomarkers that can be used to diagnose and treat ROHHAD early in the disease process**.**

CHAPTER 6. DISCUSSION AND FUTURE DIRECTIONS

Dental Pulp Stem Cells as a Tool to Study Neurogenetic Syndromes

In all chapters of my thesis, dental pulp stem cells (DPSC) were used to study the molecular etiology of Prader-Willi syndrome (PWS). In addition to the findings explicitly laid out in Chapters 2-5, this work is a proof of concept that DPSC are an excellent model system to study PWS and other rare neurogenetic syndromes. Using neuronal differentiation protocols that we have optimized, we studied gene expression and cellular phenotypes in actual PWS patient neurons. Our DPSC system allows us to collect large numbers of unique individual cell lines to study neurodevelopmental syndromes in the context of heterogenous genetic backgrounds. The ease of collection and non-invasive procedure to obtain DPSC makes it an excellent system for obtaining patient samples from children with neurodevelopmental syndromes remotely [136]. Chapters 2 and 4 show that once differentiated into neurons we observed expected gene expression for key imprinted genes in PWS, confirming that molecular methods used on our DPSC-neurons (RNAseq and SPLiT-Seq) are able to recapitulate the genetic signature of both PWS and neurotypical controls. We have published several papers recapitulating various disease state phenotypes using DPSC neurons [62, 219, 287]. Mouse models of PWS have failed to recapitulate all of the PWS phenotypes using single gene deletion, but rather many different models display some of the PWS characteristics [56], perhaps because multiple genes in the PWACR must be deleted at once to reveal all PWS characteristics. While induced pluripotent stem cells (iPSCs) have allowed researchers to study specific PWS genes and deletions in a single homogenous genetic background, with DPSC derived neuronal lines we are able to look at the interactions among different genetic backgrounds. The chapters laid out in this thesis provide a template for the study of other neurodevelopmental syndromes using patient neurons.

Moving forward, we plan to use the findings presented in this manuscript to perform rescue experiments and drug screens to find therapeutic avenues for alleviating PWS symptomology. Additionally, functional experiments to determine the electrophysiology of the neurons in these cultures will add to the utility of this model. In collaboration with another group at UTHSC, we have already established functionality of mechanosensitive PIEZO2 channels in DPSC-derived neurons and shown a difference in excitability of these channels in neurotypical control and Angelman syndrome neurons [327]. Other groups have determined that the DPSC-derived neuronal models show action potentials and calcium currents [93, 140, 141, 328], although the varying differentiation methods used across the literature, including both neurosphere and non-neurosphere methods, confound these results. Establishing the electrophysiological difference between neurotypical control and PWS neurons in our model will aid in determining the functional significance of the phenotypes described in Chapters 2-5 on the developing neurons. The delicate nature of these neurons makes electrophysiological recordings difficult. However, the advent of new electrophysiology techniques allows for greater ease of performing functional assays in the DPSC-derived neurons. Using Multi-Electrode Array (MEA) technology, cells can be grown and differentiated on an electrical

grid that measures neural activity across differentiation. The ability to monitor electrical characteristics of the developing cultures throughout differentiation and maturation would not only allow for the visualization of differences in the functional characteristics of PWS and control neurons but also identify at what point during development these cultures establish electrical characteristics of neurons. Establishment of these parameters will provide insight into the model system described here and the function of PWS neurons. Optimizing an MEA assay for these cultures would allow us to create a high throughput drug screening method for the PWS-specific electrophysiological phenotype uncovered.

Transcriptional Signatures of Prader-Willi Syndrome Neurons

The studies presented here represent a unique opportunity to investigate primary neurons from patients with PWS. Most of the work done on the neural components of PWS have used mouse neurons and iPSC derived neurons. Although both systems provide useful information, they are not able to capture the full PWS phenotype in the context of a large population of genetically variable PWS individuals. In Chapter 2, we looked at the transcriptional signatures of each of the PWS subtypes (deletion vs UPD) and identified a transcriptional signature common to PWS regardless of genetic subtype (**Figure 2-3**). Importantly, several genes within this overlap correlate with other cellular phenotypes laid out in the proceeding chapters including circadian and mitochondrial dysfunction in PWS neurons. *ATP7A*, a transmembrane copper transporter, is expressed in the SCN and displays circadian expression [329]. Copper homeostasis may act as a cue for circadian regulation within the SCN [329]. Mutations in *PEX10*, a peroxisome biogenesis factor, lead to Zellweger syndrome [330]. Patients with Zellweger syndrome also present with severe mitochondrial dysfunction in addition to hypotonia and developmental delay [331]. Further study of the other genes within this overlap will aid in genotype-phenotype correlation studies using PWS neurons.

While the differences between the UPD and deletion subtypes have been clinically defined, little work has been done to delineate these genetic subtypes at a cellular and transcriptional level in neurons. Although the classical PWS symptoms such as developmental delay, obesity, and hypotonia present in both subtypes, there are notable differences in important neuropsychiatric components such as the increased incidence of both ASD and cycloid psychosis in the UPD class [29, 135, 332]. These differences warrant a closer look at the transcriptional alterations and molecular mechanisms in deletion versus UPD neurons. Aside from the mitochondrial phenotype we found in the UPD+ASD neurons in Chapter 2, we uncovered important transcripts that may be involved in the increased neuropsychiatric symptoms within the UPD class that warrant further investigation. We found 37 transcripts that were differentially expressed versus control in the UPD group (both with and without ASD) but not the deletion group (**Figure 2-3A**). **Table A-6** lists these transcripts and their function. Within these 37 genes is a gene that is associated with bipolar disorder, *DGKH* [333-335]. Along with cycloid psychosis, bipolar disorder is prevalent at a much higher incidence in the PW-UPD group than the deletion group [336]. In fact, one case study found that 20% of

the UPD patients evaluated were diagnosed with bipolar disorder versus 2% of the deletion patients [332]. In our dataset this gene is expressed higher in PW-UPD neurons than in control or deletion neurons (**Figure 6-1**). Following up on this gene and the others identified in this dataset will aid in identifying underlying dysfunctional pathways present in PW-UPD neurons versus PW-del neurons that may lead to a predisposition for psychiatric disorders. Using our DPSC-neuron model presented here, we are the first group identifying both a cellular phenotype and a transcriptional signature in PW-UPD neurons that may lend PW-UPD patients to an increased incidence of neuropsychiatric disorders.

In Chapter 2 and Chapter 4, sequencing data using PW-del neurons is presented. Although two different techniques were used (RNAseq versus scRNA-seq), 14 transcripts were identified in both datasets as differentially expressed between PW-del neurons and neurotypical control neurons (**Figure 6-2**). **Table A-7** lists these transcripts and their functions. *UBE3A, HERC2* and *SNRPN,* genes within the PWACR, were identified in both datasets further confirming the validity of our novel model system. Within the 11 genes identified outside of the PWACR, eight are involved in the development of the nervous system (*RASGRF2*, *PHF10*, *TNR*, *FOXO1*, *SYNPO*, *FOXK1*, *NOTCH2*, and *CTNNA2*) [291, 337-343]. The overlap of these neurodevelopmental transcripts adds increasing evidence to our hypothesis that there is a developmental delay in the PWS neurons. Interestingly, in Chapter 5 we show that *FOXK1* expression is also significantly decreased in the ROHHAD and CCHS neurons (**Figure 5-1B**). FOXK1 is involved in the metabolic switch that occurs during the development from stem cell to neuron. With the decreased expression in this transcript seen across three different developmental disorders, it is a possible marker for delayed neural development in DPSC-derived neurons from individuals with neurogenetic conditions. Although we did not find a transcriptional link to the overlapping obesity phenotype in PWS and ROHHAD presented in Chapter 5, we may have found a biomarker of delayed neurogenesis (*FOXK1*) that should be further characterized in the context of neurodevelopmental syndromes. The identification of aberrant *FOXK1* expression across three neuro-developmental syndromes indicates the need to further characterize differences in developmental stage between control and neurodevelopmentally affected neurons. We may also need to modify our current protocol to normalize for the possible delay in neurodevelopmentally affected neurons such as an extended maturation period for the disease neurons.

A larger scale scRNA-seq experiment using additional PWS and control lines will enable us to tease out not only transcriptional differences between PWS and control neuronal populations but also the cellular subtype differences such as percentage of GABAergic versus glutamatergic neurons. In addition to identifying subpopulation percentage differences in PWS vs control, this large scale scRNA-seq experiment allows us to delve deeper into the transcriptomic signatures within these subpopulations to determine if certain neuronal subtypes are more affected than others in PWS. Once we obtain the scRNA-seq signatures of PWS and control neurons, we can use various rescues, both pharmacological and genetic, to tease out the monogenic effects of the various genes in the PWACR.

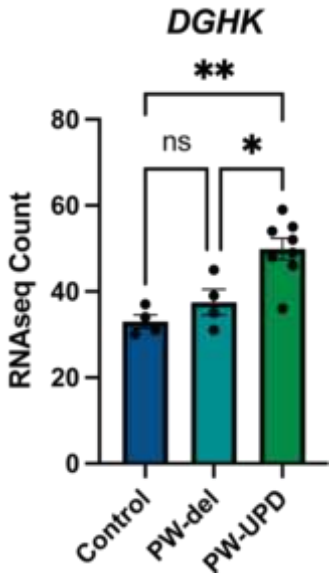

Figure 6-1. DGHK expression is significantly increased in PW-UPD neurons.
Bar graphs represent the mean RNAseq count for each group. Significance determined by One-way ANOVA. * = p-value ≤ 0.05, ** = p-value ≤ 0.01. Prader-Willi syndrome uniparental disomy subtype (PW-UPD).

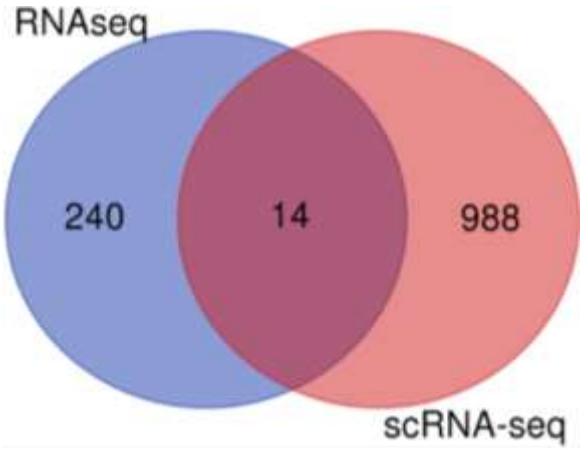

Figure 6-2. Significantly differentially expressed transcripts between PW-del and neurotypical control neurons identified by RNAseq and scRNA-seq.
Venn diagram created using the list of differentially expressed transcripts (p-value ≤ 0.05, FDR ≤ 0.05) between neurotypical control and PW-del neurons identified in RNAseq and scRNA-seq. 14 transcripts were identified by both sequencing technologies. Venn diagram created using http://bioinformatics.psb.ugent.be/webtools/Venn/. Prader-Willi syndrome deletion subtype (PW-del).

For genetic rescue experiments, individual lentiviral constructs containing key genes in the PWACR, such as *NDN*, *MAGEL2*, and *SNORD116*, can be used to restore expression of these genes in PWS and then the effect of this restoration on scRNA-seq transcriptional signatures and subpopulation differences can be determined. Additionally, further characterization of the DPSC prior to differentiation would provide insights into the neuronal propensity of these stem cells and identify surface markers that may allow us to sort for specific subpopulations of DPSC to determine whether some subpopulations have a higher neurogenic potential or whether specific surface markers identify stem cells more likely to become glial, glutamatergic, dopaminergic, etc. cell types. Identifying these surface markers will allow us to sort DPSC prior to differentiation, giving us better control of the homogeneity of the final neuronal cultures.

Mitochondrial Dysfunction in PWS

In Chapter 2, we found that in PW-UPD, which has an increased incidence of ASD and cycloid psychosis, there is a mitochondrial defect. In addition to the global decrease in mitochondrial transcripts, we found an abnormal aggregation of mitochondria in the ASD neurons. In these neurons, the mitochondria cluster in aggregates both in the perinuclear area and out into the projections. Mitochondria are critical in neuronal function, providing energy to the most energy-intensive organ in the body, the brain [173]. Additionally, mitochondria maintain calcium homeostasis at the synapse, which is essential for neurotransmitter release and communication in neural networks [173]. Identifying the functional consequences of this abnormal aggregation and decreased mitochondrial transcript expression is vital to determining whether this is causing ASD or a consequence of ASD in PWS. Assaying mitochondrial function in these neurons will provide insight into whether these mitochondria are functionally normal and are just mis-localized or if this is a compounding mitochondrial defect of both mis-localization and decreased bioenergetic function. The assay described in Chapter 2 provides an excellent model to test small molecules for rescue of this phenotype.

We recently created a TOMM20-GFP lentiviral construct to be transduced into the DPSC prior to neuronal differentiation. This TOMM20-GFP construct will allow us to visualize the mitochondria within the neurons as differentiation proceeds to determine when the mitochondrial aggregation phenotype begins. Once we determine where in the developmental process the mitochondria begin aggregating, we can attempt small molecule rescue not only on the mature neurons but at the developmental time point specific to the onset of this aggregate phenotype. Additionally, there are other mitochondrial properties that need to be studied in PWS ASD neurons including mitochondrial mass, membrane potential, biogenesis, and mitophagy. Various assays exist to assess these components of mitochondrial network dynamics. To determine mitochondrial mass and mitochondrial membrane potential (MMP). MitoTracker dyes can be used. Isolated mitochondria can be labeled with MitoTracker Green and then abundance can be determined using flow cytometry [344, 345]. This would provide insight into the differences in mitochondrial abundance in the ASD vs non-ASD neurons. Compared to MitoTracker Green, MitoTracker Deep Red FM accumulates in

mitochondria according to MMP. Using this fluorescent marker, an assessment of the difference in MMP between control and ASD neurons can uncovered. MitoTimer is a fluorescent reporter protein that can be transduced into DPSC, localized to the mitochondrial matrix, to determine mitochondrial biogenesis and health [346, 347]. This protein shifts its fluorescence spectrum as mitochondria age allowing for the quantification of both mitochondrial biogenesis and turnover. Quantification of these components of mitochondrial function will be key to determining what small molecules should be tested to correct the phenotype described in Chapter 2. There are other neurodevelopmental syndromes that include autism as a primary phenotype including Tuberous Sclerosis, Smith-Magenis, Angelman, and others for which we have collected DPSC. Assaying mitochondrial function and network dynamics in the neurons of subjects with these syndromes will likely reveal new ASD-associated disorders where mitochondrial defects are the major underlying cause of ASD.

Although the findings in Chapter 2 pertain to the UPD +ASD subtype of PWS, there is evidence for mitochondrial dysfunction in PWS regardless of genetic subtype. Indeed, mitochondrial function can be both affected by and can cause severe obesity, one of the primary phenotypes of PWS [348]. Butler *et al.* found that fibroblasts from PWS individuals had disturbed mitochondrial bioenergetics compared to control individuals. These defects included significantly reduced basal respiration, ATP-linked respiration and maximal respiratory capacity [166]. In a PWS imprinting center deletion mouse, researchers found that in both muscle and brain tissue mitochondrial transcript expression was significantly different from wildtype littermate controls [349]. Interestingly, CoQ10, an essential enzyme for mitochondrial function, is often given to PWS patients and has been shown to have positive effects on psychomotor development [350, 351]. **Figure 2-4C** shown here also shows differential expression of mitochondrial transcripts between PW-del neurons and the neurotypical control neurons. To confirm a mitochondrial dysfunction in PWS neurons regardless of ASD status, it will be important to assess the bioenergetics of PWS neuronal mitochondria using a functional assay such as the Seahorse XF Analyzer as well as the assays described in the preceding paragraph to determine mitochondrial mass, membrane potential, and biogenesis.

Chapter 4 details the delayed neurogenesis we found in PW-del neurons. Mitochondrial dysfunction may also play a role in this phenotype. Mitochondrial dynamics are critical for the process of neurogenesis and cellular bioenergetics have undergo important changes during the switch from self-renewing multipotent precursors to terminally differentiated neurons [352]. The two primary ATP-generating processes are glycolysis, occurring in the cytoplasm, and oxidative phosphorylation (OXPHOS), which occurs within mitochondria. Highly proliferative cells such as neural progenitors rely on glycolysis while cells with high energy demands such as neurons rely on OXPHOS [353, 354]. In fact, it has been shown that the glycolysis to OXPHOS switch is likely a cause of cell differentiation and not just an effect of cell fate determination [352, 355]. Interestingly, one group found that in Leigh syndrome, a severe mitochondrial disorder, neural progenitor cells maintained a glycolytic metabolic profile through differentiation resulting in defective neuronal maturation and morphogenesis [356]. Given the importance of this metabolic switch in the neuronal differentiation process, it is

likely that any aberrant mitochondrial process such as mitochondrial mass, localization or membrane potential would affect neurogenesis. It is possible that the phenotype described in Chapter 2 may cause the PW-UPD neurons to be even more developmentally delayed than the PW-del neurons described in Chapter 4. In Chapter 5, we discovered three transcripts that were differentially expressed versus control in all three syndromes (PWS, CCHS, and ROHHAD). One of those transcripts, *FOXK1*, is a transcription factor that regulates aerobic glycolysis which may be an important intermediary step in the glycolysis-OHXPOS switch [290, 291]. *FOXK1* may prove to be a marker of syndromic delayed neurodevelopment. It is possible that mitochondrial dysfunction in PWS is caused by the neural delay that we show in Chapter 4. For the UPD subtype, there are additional factors leading to increased mitochondrial dysfunction that, in turn, increase the likelihood of developing ASD, such as the increased dosage of *UBE3A*, which has been implicated in both ASD and mitochondrial function [357-359]. Dissecting the role of neuronal mitochondria in the context PWS pathogenesis will be vital not only for developing targeted therapeutics, but also for understanding the interplay between mitochondrial bioenergetics and cognitive phenotypes.

Circadian Rhythm Defects in PWS Pathogenesis

In Chapter 4, we describe circadian rhythm cycling defects found in PWS and in a related syndrome, SYS, which results from a truncating mutation in *MAGEL2*. We found that in PWS, there are two distinct circadian period phenotypes, short and long, differing from neurotypical control neurons by one hour. For the short period, cycles from different PWS individuals did not overlap. We also observed complete discordance in the cycling of SYS individuals and even in the replicates from the same individual. We hypothesize that *MAGEL2* is likely a candidate gene for the disrupted circadian cycling. MAGEL2 interacts with USP7, a stabilizer of CRY1, and acts as a rheostat in controlling circadian gene/protein expression. **Figure 4-5** shows the relationship of MAGEL2 within the transcriptional-translation feedback loop of the circadian pathway. The bioluminescent assay that we used here provides an excellent tool for assessing circadian rhythms in rare syndromes and will be quite useful for rescue experiments in the future. Our goal moving forward is to use small molecules shown to affect period length, shorter or longer, to correct these phenotypes and to restore *MAGEL2* in the PWS and SYS lines.

We plan to use known circadian rhythm small molecule modulators in our initial rescue experiments. These molecules target different portions of the circadian rhythm transcription translation feedback loop described in Chapter 3 to either lengthen or shorten the circadian period through post-translational modifications of CRY and PER proteins [360, 361]. We will also restore *MAGEL2* in both PWS and SYS to determine the effect of MAGEL2 on the circadian phenotypes we have uncovered. Finally, we will look at transcriptional and epigenetic differences between PWS and neurotypical control neurons at various circadian timepoints after initial circadian clock syncing (30, 42, 54, and 66 hours). Given the importance of the transcription factors, *PER1/2* and *CRY1/2*, on metabolism and the expression of other circadian transcripts, determining the transcriptional differences at various timepoints between control and PWS neurons will

provide additional molecular pathways that are perturbed at both the circadian and metabolic level.

Circadian rhythms are critical for cellular function. Almost all cell types have cell autonomous circadian rhythms that coordinate gene expression, protein degradation/stabilization, and epigenetic mechanisms. The central pacemaker in the brain is the suprachiasmatic nucleus (SCN) in the hypothalamus, which receives photic input to establish the phase of clock gene expression and then transmits this information to other neurons and peripheral tissues [362]. Any dysregulation of this process can have significant effects on biological functions including cognition, metabolism, and hormone production [362]. As PWS is a hypothalamic deficiency disorder and exhibits defects in many of these processes, it is possible that circadian rhythm dysfunction is the underlying cause for several phenotypes found in PWS. Importantly, circadian rhythm defects may play a role in both the mitochondrial defects and neural delay described in Chapters 2 and 4, as well as the onset of obesity [363-368].

Circadian function is crucial for mitochondrial dynamics. It has been shown that disturbing the molecular clock in animals affects mitochondrial rhythmicity, reactive oxygen species production and respiration [369]. PGC1α is a master regulator of mitochondrial biogenesis and we found it to be significantly decreased in PW-UPD +ASD neurons versus PW-UPD -ASD neurons (**Figure A-2**). Numerous studies indicate that PGC1α affects the transcription of *CLOCK* and *BMAL1* and ultimately plays a role in behavioral rhythms [369]. A PGC1α knockout mouse model was found to have disrupted diurnal rhythms, metabolism, and body temperature [370]. Additionally, several of the rhythmic genes in the mouse SCN encode for mitochondrial components [371]. In the *MAGEL2* null mouse model, in addition to circadian rhythm defects, metabolic issues were identified including hyperleptinemia [60, 372]. The work presented in Chapter 4 was done using PW-del neurons. It will be interesting to repeat those experiments in neurons derived from individuals with PW-UPD +ASD to determine if the circadian rhythms are further abolished in neurons with decreased PGC1α expression. Correcting the mitochondrial defects found in the UPD neurons may influence the circadian rhythms that we find in these neurons. Treating these neurons with the mitochondrial small molecular modulators used to restore the phenotype found in Chapter 2, may have effects on the circadian rhythms of these neurons as well as improving energy metabolism.

We established in Chapter 3 that DPSC do not display rhythmic circadian oscillations until they have been differentiated into neurons. This illustrates the importance of circadian rhythms in the neuronal differentiation process. Malik *et al*. found that in neurospheres from *Bmal1* knockout mice, terminal differentiation was altered and that these cultures displayed significantly increased numbers of glial cells [373]. Additionally, it has been shown that circadian genes affect neurogenesis in hippocampal neurons [374]. Interestingly, melatonin, whose production is highly coupled with circadian rhythms, has been found to facilitate neural stem cell differentiation and suppress proliferation [375, 376]. Although plasma melatonin levels between PWS and control individuals has not been found to be significantly different, melatonin levels

between deletion and UPD subgroups have shown significant differences with high inter-individual variability seen in all PWS subjects [377]. Determining whether PWS neurons "catch-up" to control neurons later in neural maturation and then, if they catch up, whether this effects the circadian cycling defect described in Chapter 3 will be essential to determine whether these two phenotypes are coupled or fixed independently. In the experiments presented in Chapter 3, the average circadian period length of the control neurons was ~27.1 hours. This differs by several hours from the expected circadian rhythms seen in human cells of 24 hours. It is possible that this difference is due to the developmental immaturity of these cultures. In fact, in the first weeks of life, newborns do not display rhythmic sleep patterns until 5-weeks of age when they establish circadian rhythm of ~25 hours [378]. The observance that the DPSC do not display rhythmic circadian rhythms, but that the 4-week mature neurons do, lends to the hypothesis that at some point during the differentiation period, circadian cycling begins and could change as the neurons mature. Repeating these cycling experiments at time points during the differentiation and at later maturity stages will be important to answer this question.

In summary, we show that DPSC are an excellent model for the study of neurogenetic syndromes and we created several assays to assess PWS cellular phenotypes that can be translated to other neurodevelopmental syndromes. Using patient neurons derived from DPSC, the work presented here fills a gap in the current PWS literature which is primarily comprised of research done in mouse models, fibroblasts, and iPSC lines. In addition to characterizing transcriptional signatures of PWS subtypes, we discovered a mitochondrial aggregation phenotype in PWS-UPD +ASD neurons and confirmed significantly different mitochondrial localization in ASD neurons versus neurotypical control, PW-del, and PW-UPD -ASD neurons. We used a bioluminescent assay to visualize circadian rhythms in PWS and SYS neurons and confirmed a cycling defect in both syndromes. Using a new approach to scRNA-seq (SPLiT-seq), we identified a delay in neurogenesis in PWS neurons and found several markers correlated to other PWS phenotypes. Finally, we used our DPSC-neuron system to compare the transcriptomes of PWS with similar syndromes, ROHHAD and CCHS. It is likely that several of these findings may be connected. Mitochondrial dysfunction may be affecting both circadian rhythms and neurodevelopment or the opposite could be true and delayed neurodevelopment is affecting mitochondrial dynamics and circadian function. Understanding the cause/effect dynamics of the phenotypes presented here is fundamental to understanding the disease pathogenesis and developing treatment strategies. Leveraging the findings outlined here, we hope to expand upon the phenotypes discovered to perform drug screens with the goal of finding therapeutic mechanisms to treat the cognitive symptoms of PWS.

LIST OF REFERENCES

1. Holm, V.A., S.B. Cassidy, M.G. Butler, J.M. Hanchett, L.R. Greenswag, B.Y. Whitman, and F. Greenberg, *Prader-Willi syndrome: consensus diagnostic criteria.* Pediatrics, 1993. **91**(2): p. 398-402.
2. Prader, A., A. Labhart, and H. Willi, *Ein Syndrom von Adipositas, Kleinwuchs, Kryptochismus und Oligophrenie nach myotoniertgem Zustand im Neugeborenalter.* Schweiz Med Wochenschr, 1956. **86**: p. 1260-61.
3. Ward, O.C., *Down's 1864 case of Prader-Willi syndrome: a follow-up report.* J R Soc Med, 1997. **90**(12): p. 694-6. 10.1177/014107689709001221.
4. Ledbetter, D.H., V.M. Riccardi, S.D. Airhart, R.J. Strobel, B.S. Keenan, and J.D. Crawford, *Deletions of chromosome 15 as a cause of the Prader-Willi syndrome.* N Engl J Med, 1981. **304**(6): p. 325-9. 10.1056/nejm198102053040604.
5. Butler, M.G., F.J. Meaney, and C.G. Palmer, *Clinical and cytogenetic survey of 39 individuals with Prader-Labhart-Willi syndrome.* Am J Med Genet, 1986. **23**(3): p. 793-809. 10.1002/ajmg.1320230307.
6. Ishikawa, T., M. Kanayama, and Y. Wada, *Prader-Willi syndrome in two siblings: one with normal karyotype, one with a terminal deletion of distal Xq.* Clin Genet, 1987. **32**(5): p. 295-9. 10.1111/j.1399-0004.1987.tb03293.x.
7. Smith, A., L. Robson, A. Neumann, M. Mulcahy, V. Chabros, et al., *Fluorescence in-situ hybridisation and molecular studies used in the characterisation of a Robertsonian translocation (13q15q) in Prader-Willi syndrome.* Clin Genet, 1993. **43**(1): p. 5-8. 10.1111/j.1399-0004.1993.tb04416.x.
8. Pettigrew, A.L., S.M. Gollin, F. Greenberg, V.M. Riccardi, and D.H. Ledbetter, *Duplication of proximal 15q as a cause of Prader-Willi syndrome.* Am J Med Genet, 1987. **28**(4): p. 791-802. 10.1002/ajmg.1320280403.
9. Nicholls, R.D., J.H. Knoll, M.G. Butler, S. Karam, and M. Lalande, *Genetic imprinting suggested by maternal heterodisomy in nondeletion Prader-Willi syndrome.* Nature, 1989. **342**(6247): p. 281-5. 10.1038/342281a0.
10. Manzardo, A.M., N. Weisensel, S. Ayala, W. Hossain, and M.G. Butler, *Prader-Willi syndrome genetic subtypes and clinical neuropsychiatric diagnoses in residential care adults.* Clin Genet, 2018. **93**(3): p. 622-631. 10.1111/cge.13142.
11. Ohta, T., T.A. Gray, P.K. Rogan, K. Buiting, J.M. Gabriel, et al., *Imprinting-mutation mechanisms in Prader-Willi syndrome.* Am J Hum Genet, 1999. **64**(2): p. 397-413. 10.1086/302233.
12. Buiting, K., B. Dittrich, S. Gross, C. Lich, C. Färber, et al., *Sporadic imprinting defects in Prader-Willi syndrome and Angelman syndrome: implications for imprint-switch models, genetic counseling, and prenatal diagnosis.* Am J Hum Genet, 1998. **63**(1): p. 170-80. 10.1086/301935.
13. Butler, M.G., D.C. Bittel, N. Kibiryeva, Z. Talebizadeh, and T. Thompson, *Behavioral differences among subjects with Prader-Willi syndrome and type I or type II deletion and maternal disomy.* Pediatrics, 2004. **113**(3 Pt 1): p. 565-73. 10.1542/peds.113.3.565.
14. Varela, M.C., F. Kok, N. Setian, C.A. Kim, and C.P. Koiffmann, *Impact of molecular mechanisms, including deletion size, on Prader-Willi syndrome*

phenotype: study of 75 patients. Clin Genet, 2005. **67**(1): p. 47-52. 10.1111/j.1399-0004.2005.00377.x.
15. Burnside, R.D., R. Pasion, F.M. Mikhail, A.J. Carroll, N.H. Robin, et al., *Microdeletion/microduplication of proximal 15q11.2 between BP1 and BP2: a susceptibility region for neurological dysfunction including developmental and language delay.* Hum Genet, 2011. **130**(4): p. 517-28. 10.1007/s00439-011-0970-4.
16. Butler, M.G., *Clinical and genetic aspects of the 15q11.2 BP1-BP2 microdeletion disorder.* J Intellect Disabil Res, 2017. **61**(6): p. 568-579. 10.1111/jir.12382.
17. McNamara, G.I. and A.R. Isles, *Dosage-sensitivity of imprinted genes expressed in the brain: 15q11-q13 and neuropsychiatric illness.* Biochem Soc Trans, 2013. **41**(3): p. 721-6. 10.1042/bst20130008.
18. Smith, S.E., Y.D. Zhou, G. Zhang, Z. Jin, D.C. Stoppel, and M.P. Anderson, *Increased gene dosage of Ube3a results in autism traits and decreased glutamate synaptic transmission in mice.* Sci Transl Med, 2011. **3**(103): p. 103ra97. 10.1126/scitranslmed.3002627.
19. Glenn, C.C., D.J. Driscoll, T.P. Yang, and R.D. Nicholls, *Genomic imprinting: potential function and mechanisms revealed by the Prader-Willi and Angelman syndromes.* Mol Hum Reprod, 1997. **3**(4): p. 321-32. 10.1093/molehr/3.4.321.
20. Xu, X., C. Li, X. Gao, K. Xia, H. Guo, et al., *Excessive UBE3A dosage impairs retinoic acid signaling and synaptic plasticity in autism spectrum disorders.* Cell Res, 2018. **28**(1): p. 48-68. 10.1038/cr.2017.132.
21. Noor, A., L. Dupuis, K. Mittal, A.C. Lionel, C.R. Marshall, et al., *15q11.2 Duplication Encompassing Only the UBE3A Gene Is Associated with Developmental Delay and Neuropsychiatric Phenotypes.* Hum Mutat, 2015. **36**(7): p. 689-93. 10.1002/humu.22800.
22. Salminen, I., S. Read, P. Hurd, and B. Crespi, *Genetic variation of UBE3A is associated with schizotypy in a population of typical individuals.* Psychiatry Res, 2019. **275**: p. 94-99. 10.1016/j.psychres.2019.03.019.
23. Bennett, J.A., S. Hodgetts, M.L. Mackenzie, A.M. Haqq, and L. Zwaigenbaum, *Investigating Autism-Related Symptoms in Children with Prader-Willi Syndrome: A Case Study.* Int J Mol Sci, 2017. **18**(3). 10.3390/ijms18030517.
24. Baker, E.K., D.E. Godler, M. Bui, C. Hickerton, C. Rogers, et al., *Exploring autism symptoms in an Australian cohort of patients with Prader-Willi and Angelman syndromes.* J Neurodev Disord, 2018. **10**(1): p. 24. 10.1186/s11689-018-9242-0.
25. Dimitropoulos, A., O. Zyga, and S.W. Russ, *Early Social Cognitive Ability in Preschoolers with Prader-Willi Syndrome and Autism Spectrum Disorder.* J Autism Dev Disord, 2019. **49**(11): p. 4441-4454. 10.1007/s10803-019-04152-4.
26. Victor, A.K., M. Donaldson, D. Johnson, W. Miller, and L.T. Reiter, *Molecular Changes in Prader-Willi Syndrome Neurons Reveals Clues About Increased Autism Susceptibility.* Front Mol Neurosci, 2021. **14**: p. 747855. 10.3389/fnmol.2021.747855.
27. Aman, L.C.S., K.E. Manning, J.E. Whittington, and A.J. Holland, *Mechanistic insights into the genetics of affective psychosis from Prader-Willi syndrome.* Lancet Psychiatry, 2018. **5**(4): p. 370-378. 10.1016/s2215-0366(18)30009-9.

28. Krefft, M., D. Frydecka, T. Adamowski, and B. Misiak, *From Prader-Willi syndrome to psychosis: translating parent-of-origin effects into schizophrenia research.* Epigenomics, 2014. **6**(6): p. 677-88. 10.2217/epi.14.52.
29. Singh, D., A. Sasson, V. Rusciano, Y. Wakimoto, A. Pinkhasov, and M. Angulo, *Cycloid Psychosis Comorbid with Prader-Willi Syndrome: A Case Series.* Am J Med Genet A, 2019. **179**(7): p. 1241-1245. 10.1002/ajmg.a.61181.
30. Stauder, J.E., H. Boer, R.H. Gerits, A. Tummers, J. Whittington, and L.M. Curfs, *Differences in behavioural phenotype between parental deletion and maternal uniparental disomy in Prader-Willi syndrome: an ERP study.* Clin Neurophysiol, 2005. **116**(6): p. 1464-70. 10.1016/j.clinph.2005.02.019.
31. Cassidy, S.B., M. Forsythe, S. Heeger, R.D. Nicholls, N. Schork, P. Benn, and S. Schwartz, *Comparison of phenotype between patients with Prader-Willi syndrome due to deletion 15q and uniparental disomy 15.* Am J Med Genet, 1997. **68**(4): p. 433-40.
32. Oldzej, J., J. Manazir, J.A. Gold, R. Mahmoud, K. Osann, et al., *Molecular subtype and growth hormone effects on dysmorphology in Prader-Willi syndrome.* Am J Med Genet A, 2020. **182**(1): p. 169-175. 10.1002/ajmg.a.61408.
33. Gunay-Aygun, M., S. Heeger, S. Schwartz, and S.B. Cassidy, *Delayed diagnosis in patients with Prader-Willi syndrome due to maternal uniparental disomy 15.* Am J Med Genet, 1997. **71**(1): p. 106-10.
34. Roof, E., W. Stone, W. MacLean, I.D. Feurer, T. Thompson, and M.G. Butler, *Intellectual characteristics of Prader-Willi syndrome: comparison of genetic subtypes.* J Intellect Disabil Res, 2000. **44 (Pt 1)**(Pt 1): p. 25-30. 10.1046/j.1365-2788.2000.00250.x.
35. Shepherd, D.A., N. Vos, S.M. Reid, D.E. Godler, A. Guzys, M. Moreno-Betancur, and D.J. Amor, *Growth Trajectories in Genetic Subtypes of Prader-Willi Syndrome.* Genes (Basel), 2020. **11**(7). 10.3390/genes11070736.
36. Matsubara, K., N. Murakami, M. Fukami, M. Kagami, T. Nagai, and T. Ogata, *Risk assessment of medically assisted reproduction and advanced maternal ages in the development of Prader-Willi syndrome due to UPD(15)mat.* Clin Genet, 2016. **89**(5): p. 614-9. 10.1111/cge.12691.
37. Singh, P., R. Mahmoud, J.A. Gold, J.L. Miller, E. Roof, et al., *Multicentre study of maternal and neonatal outcomes in individuals with Prader-Willi syndrome.* J Med Genet, 2018. **55**(9): p. 594-598. 10.1136/jmedgenet-2017-105118.
38. Matsubara, K., N. Murakami, T. Nagai, and T. Ogata, *Maternal age effect on the development of Prader-Willi syndrome resulting from upd(15)mat through meiosis 1 errors.* J Hum Genet, 2011. **56**(8): p. 566-71. 10.1038/jhg.2011.59.
39. Cassidy, S.B., S. Schwartz, J.L. Miller, and D.J. Driscoll, *Prader-Willi syndrome.* Genetics in Medicine, 2012. **14**(1): p. 10-26. https://doi.org/10.1038/gim.0b013e31822bead0.
40. Driscoll, D.J., J.L. Miller, S. Schwartz, and S.B. Cassidy, *Prader-Willi Syndrome*, in *GeneReviews(®)*, M.P. Adam, et al., Editors. 1993, University of Washington, Seattle. Copyright © 1993-2022, University of Washington, Seattle. GeneReviews is a registered trademark of the University of Washington, Seattle. All rights reserved.: Seattle (WA).

41. Whittington, J., A. Holland, T. Webb, J. Butler, D. Clarke, and H. Boer, *Academic underachievement by people with Prader–Willi syndrome.* Journal of Intellectual Disability Research, 2004. **48**(2): p. 188-200. https://doi.org/10.1111/j.1365-2788.2004.00473.x.
42. Tan, Q., C.E. Orsso, E.C. Deehan, L. Triador, C.J. Field, et al., *Current and emerging therapies for managing hyperphagia and obesity in Prader-Willi syndrome: A narrative review.* Obes Rev, 2020. **21**(5): p. e12992. 10.1111/obr.12992.
43. Butler, M.G., A.K. Victor, and L.T. Reiter, *Autonomic nervous system dysfunction in Prader-Willi syndrome.* Clin Auton Res, 2022. 10.1007/s10286-022-00909-7.
44. Tauber, M. and C. Hoybye, *Endocrine disorders in Prader-Willi syndrome: a model to understand and treat hypothalamic dysfunction.* Lancet Diabetes Endocrinol, 2021. **9**(4): p. 235-246. 10.1016/s2213-8587(21)00002-4.
45. Noordam, C., C. Höybye, and U. Eiholzer, *Prader-Willi Syndrome and Hypogonadism: A Review Article.* Int J Mol Sci, 2021. **22**(5). 10.3390/ijms22052705.
46. Radicioni, A.F., G. Di Giorgio, G. Grugni, M. Cuttini, V. Losacco, et al., *Multiple forms of hypogonadism of central, peripheral or combined origin in males with Prader-Willi syndrome.* Clin Endocrinol (Oxf), 2012. **76**(1): p. 72-7. 10.1111/j.1365-2265.2011.04161.x.
47. Cataldi, M., D. Arnaldi, V. Tucci, F. De Carli, G. Patti, et al., *Sleep disorders in Prader-Willi syndrome, evidence from animal models and humans.* Sleep Med Rev, 2021. **57**: p. 101432. 10.1016/j.smrv.2021.101432.
48. Pavone, M., V. Caldarelli, S. Khirani, M. Colella, A. Ramirez, et al., *Sleep disordered breathing in patients with Prader-Willi syndrome: A multicenter study.* Pediatr Pulmonol, 2015. **50**(12): p. 1354-9. 10.1002/ppul.23177.
49. Nixon, G.M. and R.T. Brouillette, *Sleep and breathing in Prader-Willi syndrome.* Pediatr Pulmonol, 2002. **34**(3): p. 209-17. 10.1002/ppul.10152.
50. Sedky, K., D.S. Bennett, and A. Pumariega, *Prader Willi syndrome and obstructive sleep apnea: co-occurrence in the pediatric population.* J Clin Sleep Med, 2014. **10**(4): p. 403-9. 10.5664/jcsm.3616.
51. Gillett, E.S. and I.A. Perez, *Disorders of Sleep and Ventilatory Control in Prader-Willi Syndrome.* Diseases, 2016. **4**(3). 10.3390/diseases4030023.
52. Arens, R., D. Gozal, K.J. Omlin, F.R. Livingston, J. Liu, T.G. Keens, and S.L. Ward, *Hypoxic and hypercapnic ventilatory responses in Prader-Willi syndrome.* J Appl Physiol (1985), 1994. **77**(5): p. 2224-30. 10.1152/jappl.1994.77.5.2224.
53. Camfferman, D., R.D. McEvoy, F. O'Donoghue, and K. Lushington, *Prader Willi Syndrome and excessive daytime sleepiness.* Sleep Med Rev, 2008. **12**(1): p. 65-75. 10.1016/j.smrv.2007.08.005.
54. Cotton, S. and A. Richdale, *Brief report: parental descriptions of sleep problems in children with autism, Down syndrome, and Prader-Willi syndrome.* Res Dev Disabil, 2006. **27**(2): p. 151-61. 10.1016/j.ridd.2004.12.003.
55. Rosenwasser, A.M. and F.W. Turek, *Neurobiology of Circadian Rhythm Regulation.* Sleep Med Clin, 2015. **10**(4): p. 403-12. 10.1016/j.jsmc.2015.08.003.
56. Kummerfeld, D.M., C.A. Raabe, J. Brosius, D. Mo, B.V. Skryabin, and T.S. Rozhdestvensky, *A Comprehensive Review of Genetically Engineered Mouse*

Models for Prader-Willi Syndrome Research. Int J Mol Sci, 2021. **22**(7). 10.3390/ijms22073613.
57. Cattanach, B.M., J.A. Barr, E.P. Evans, M. Burtenshaw, C.V. Beechey, et al., *A candidate mouse model for Prader-Willi syndrome which shows an absence of Snrpn expression.* Nat Genet, 1992. **2**(4): p. 270-4. 10.1038/ng1292-270.
58. Gabriel, J.M., M. Merchant, T. Ohta, Y. Ji, R.G. Caldwell, et al., *A transgene insertion creating a heritable chromosome deletion mouse model of Prader-Willi and angelman syndromes.* Proc Natl Acad Sci U S A, 1999. **96**(16): p. 9258-63. 10.1073/pnas.96.16.9258.
59. Li, C., W. Lu, L. Yang, Z. Li, X. Zhou, et al., *MKRN3 regulates the epigenetic switch of mammalian puberty via ubiquitination of MBD3.* Natl Sci Rev, 2020. **7**(3): p. 671-685. 10.1093/nsr/nwaa023.
60. Bischof, J.M., C.L. Stewart, and R. Wevrick, *Inactivation of the mouse Magel2 gene results in growth abnormalities similar to Prader-Willi syndrome.* Hum Mol Genet, 2007. **16**(22): p. 2713-9. 10.1093/hmg/ddm225.
61. Kozlov, S.V., J.W. Bogenpohl, M.P. Howell, R. Wevrick, S. Panda, et al., *The imprinted gene Magel2 regulates normal circadian output.* Nat Genet, 2007. **39**(10): p. 1266-72. 10.1038/ng2114.
62. Chen, H., A.K. Victor, J. Klein, K.F. Tacer, D.J.C. Tai, et al., *Loss of MAGEL2 in Prader-Willi syndrome leads to decreased secretory granule and neuropeptide production.* JCI Insight, 2020. **5**(17). 10.1172/jci.insight.138576.
63. Mercer, R.E. and R. Wevrick, *Loss of magel2, a candidate gene for features of Prader-Willi syndrome, impairs reproductive function in mice.* PLoS One, 2009. **4**(1): p. e4291. 10.1371/journal.pone.0004291.
64. Muscatelli, F., D.N. Abrous, A. Massacrier, I. Boccaccio, M. Le Moal, P. Cau, and H. Cremer, *Disruption of the mouse Necdin gene results in hypothalamic and behavioral alterations reminiscent of the human Prader-Willi syndrome.* Hum Mol Genet, 2000. **9**(20): p. 3101-10. 10.1093/hmg/9.20.3101.
65. Ren, J., S. Lee, S. Pagliardini, M. Gérard, C.L. Stewart, J.J. Greer, and R. Wevrick, *Absence of Ndn, encoding the Prader-Willi syndrome-deleted gene necdin, results in congenital deficiency of central respiratory drive in neonatal mice.* J Neurosci, 2003. **23**(5): p. 1569-73. 10.1523/jneurosci.23-05-01569.2003.
66. Zanella, S., F. Watrin, S. Mebarek, F. Marly, M. Roussel, et al., *Necdin plays a role in the serotonergic modulation of the mouse respiratory network: implication for Prader-Willi syndrome.* J Neurosci, 2008. **28**(7): p. 1745-55. 10.1523/jneurosci.4334-07.2008.
67. Lu, R., Y. Dong, and J.D. Li, *Necdin regulates BMAL1 stability and circadian clock through SGT1-HSP90 chaperone machinery.* Nucleic Acids Res, 2020. **48**(14): p. 7944-7957. 10.1093/nar/gkaa601.
68. Tsai, T.F., Y.H. Jiang, J. Bressler, D. Armstrong, and A.L. Beaudet, *Paternal deletion from Snrpn to Ube3a in the mouse causes hypotonia, growth retardation and partial lethality and provides evidence for a gene contributing to Prader-Willi syndrome.* Hum Mol Genet, 1999. **8**(8): p. 1357-64. 10.1093/hmg/8.8.1357.
69. Ding, F., H.H. Li, S. Zhang, N.M. Solomon, S.A. Camper, P. Cohen, and U. Francke, *SnoRNA Snord116 (Pwcr1/MBII-85) deletion causes growth deficiency*

and hyperphagia in mice. PLoS One, 2008. **3**(3): p. e1709. 10.1371/journal.pone.0001709.
70. Skryabin, B.V., L.V. Gubar, B. Seeger, J. Pfeiffer, S. Handel, et al., *Deletion of the MBII-85 snoRNA gene cluster in mice results in postnatal growth retardation.* PLoS Genet, 2007. **3**(12): p. e235. 10.1371/journal.pgen.0030235.
71. Pace, M., M. Falappa, A. Freschi, E. Balzani, C. Berteotti, et al., *Loss of Snord116 impacts lateral hypothalamus, sleep, and food-related behaviors.* JCI Insight, 2020. **5**(12). 10.1172/jci.insight.137495.
72. Adhikari, A., N.A. Copping, B. Onaga, M.C. Pride, R.L. Coulson, et al., *Cognitive deficits in the Snord116 deletion mouse model for Prader-Willi syndrome.* Neurobiol Learn Mem, 2019. **165**: p. 106874. 10.1016/j.nlm.2018.05.011.
73. Coulson, R.L., D.H. Yasui, K.W. Dunaway, B.I. Laufer, A. Vogel Ciernia, et al., *Snord116-dependent diurnal rhythm of DNA methylation in mouse cortex.* Nat Commun, 2018. **9**(1): p. 1616. 10.1038/s41467-018-03676-0.
74. Hebras, J., V. Marty, J. Personnaz, P. Mercier, N. Krogh, et al., *Reassessment of the involvement of Snord115 in the serotonin 2c receptor pathway in a genetically relevant mouse model.* Elife, 2020. **9**. 10.7554/eLife.60862.
75. Liu, Q., S.C. Spusta, R. Mi, R.N.T. Lassiter, M.R. Stark, et al., *Human Neural Crest Stem Cells Derived from Human ESCs and Induced Pluripotent Stem Cells: Induction, Maintenance, and Differentiation into Functional Schwann Cells.* Stem Cells Translational Medicine, 2012. **2012**(1): p. 266-278.
76. Chen, X., Q. Gu, X. Wang, Q. Ma, H. Tang, et al., *Directed neuronal differentiation of mouse embryonic and induced pluripotent stem cells and their gene expression profiles.* International Journal of Molecular Medicine, 2013. **32**(1).
77. Badja, C., G. Maleeva, C. El-Yazidi, E. Barruet, M. Lasserre, et al., *Efficient and cost-effective generation of mature neurons from human induced pluripotent stem cells.* Stem Cells Translational Medicine, 2014. **3**(12): p. 1467-1472.
78. Yan, Y., S. Shin, B. Jha, Q. Liu, J. Sheng, et al., *Efficient and rapid derivation of primitive neural stem cells and generation of brain subtype neurons from human pluripotent stem cells.* Stem Cells Translational Medicine, 2013. **2**(11): p. 862-870.
79. K. Kim, A. Doi, B. Wen, K. Ng, R. Zhao, et al., *Epigenetic memory in induced pluiripotent stem cells.* Nature, 2010. **467**(7313).
80. Yoshihara, M., Y. Hayashizaki, and Y. Murakawa, *Genomic Instability of iPSCs: Challenges Towards Their Clinical Applications.* Stem Cell Reviews, 2017. **13**(1): p. 7-16. 10.1007/s12015-016-9680-6.
81. Liu, Z., Y. Tang, S. Lu, J. Zhou, Z. Du, et al., *The tumourigenicity of iPS cells and their differentiated derivatives.* Journal of Cellular and Molecular Medicine, 2013. **17**(6): p. 782-791.
82. Gore, A., Z. Li, H.-L. Fung, J. Young, S. Agarwal, et al., *Somatic coding mutations in human induced pluripotent stem cells.* Nature, 2011. **471**(7336).
83. Gronthos, S., M. Mankani, J. Brahim, P. Gehron Robey, and S. Shi, *Postnatal human dental pulp stem cells (DPSCs) in vitro and in vivo.* PNAS, 2000. **97**(25): p. 13625 - 13630.

84. Gronthos, S., J. Brahim, W. Li, L.W. Fisher, N. Cherman, et al., *Stem Cell Properties of Human Dental Pulp Stem Cells.* J Dent Res, 2002. **81**(8): p. 531-535.
85. Wilson, R., N. Urraca, C. Skobowiat, K.A. Hope, L. Miravalle, et al., *Assesment of the tumorigenic potential of spontaneously immortalized and hTERT immortalized cultured dental pulp stem cells.* Stem Cells Translational Medicine, 2015(4): p. 905-912.
86. Dunaway, K., S. Goorha, L. Matelski, N. Urraca, P. Lein, et al., *Dental pulp stem cells model early life and imprinted DNA methylation patterns.* Stem Cells, 2017.
87. Goorha, S. and L. Reiter, *Culturing and Neuronal Differentiation of Human Dental Pulp Stem Cells.* Curr Protoc Hum Genet., 2017. **92**(21).
88. Ohnuki, M. and K. Takahashi, *Present and future challenges of induced pluripotent stem cells.* Philosophical Transactions of the Royal Society B: Biological Sciences, 2015. **370**(1680): p. 20140367. 10.1098/rstb.2014.0367.
89. Cao, S., K. Loh, Y. Pei, W. Zhang, and J. Han, *Overcoming barriers to the clinical utilization of iPSCs: reprogramming efficiency, safety and quality.* Protein & Cell, 2012. **3**(11): p. 834-845. 10.1007/s13238-012-2078-6.
90. Kálmán, S., E. Hathy, and J.M. Réthelyi, *A Dishful of a Troubled Mind: Induced Pluripotent Stem Cells in Psychiatric Research.* Stem Cells International, 2016. **2016**: p. 7909176. 10.1155/2016/7909176.
91. Nosrat, I.V., C.A. Smith, P. Mullally, L. Olson, and C.A. Nosrat, *Dental pulp cells proved neurotrophic support for dopaminergic neurons and differentiate into neurons in vitro; implications for tissue engineering and repair in the nervous system.* European Journal of Neuroscience, 2004. **19**: p. 2388-2398.
92. Arthur, A., G. Rychkov, S. Shi, S.A. Koblar, and S. Gronthos, *Adult Human Dental Pulp Stem Cells Differentiate Toward Functionally Active Neurons Under Appropriate Environmental Cues.* Stem Cells, 2008. **2008**(26): p. 1787-1795.
93. Kiraly, M., B. Porcsalmy, A. Pataki, K. Kadar, M. Jelitai, et al., *Simultaneous PKC and cAMP activation induces differentiation of human dental pulp stem cells into functionally active neurons.* Neurochemistry International, 2009. **55**: p. 323-332.
94. Wang, J., X. Wang, Z. Sun, X. Wang, H. Yang, S. Shi, and S. Wang, *Stem cells from human-exfoliated deciduous teeth can differentiate into dopaminergic neuron-like cells.* Stem Cells and Development, 2010. **19**(9): p. 1375-1383.
95. Chang, C.-C., K.-C. Chang, S.-J. Tsai, H.-H. Chang, and C.-P. Lin, *Neurogenic differentiation of dental pulp stem cells to neuron-like cells in dopaminergic and motor neuronal inductive media.* Journal of the Formosan Medical Association, 2014. **2014**(113): p. 956-965.
96. Kanafi, M., D. Majumdar, R. Bhonde, P. Gupta, and I. Datta, *Midbrain cues dictate differentiation of human dental pulp stem cells towards functional dopaminergic neurons.* Journal of Cellular Physiology, 2014(229): p. 1369-1377.
97. Cho, Y.-A., D.-S. Kim, M. Song, W.-J. Bae, S. Lee, and E.-C. Kim, *Protein Interacting with Never in Mitosis A-1 Induces Glutamatergic and GABAergic Neuronal Differentiation in Human Dental Pulp Stem Cells.* Journal of Endodontics, 2016. **42**(7): p. 1055-1061.

98. Martens, W., K. Sanen, M. Georgiou, T. Struys, A. Bronckaers, et al., *Human dental pulp stem cells can differentiate into Schwann cells and promote and guide neurite outgrowth in an aligned tissue-engineered collagen construct in vitro.* FASEB J, 2014. **28**: p. 1634-1643.
99. Young, F.I., V. Telezhkin, S.J. Youde, M.S. Langley, M. Stack, et al., *Clonal Heterogeneity in the Neuronal and Glial Differentiation of Dental Pulp Stem/Progenitor Cells.* Stem Cells International, 2016. **2016**.
100. Kiraly, M., K. Kadar, D.B. Horvathy, P. Nardai, G.Z. Racz, et al., *Integration of neuronally predifferentiated human dental pulp stem cells into rat brain in vivo.* Neurochem. Int., 2011.
101. Fujii, H., K. Matsubara, K. Sakai, M. Ito, K. Ohno, M. Ueda, and A. Yamamoto, *Dopaminergic differentiation of stem cells from human deciduous teeth and their therapeutic benefits for Pakinsonian rats.* Brain Research, 2015. **1613**: p. 59-72.
102. Nuti, N., C. Corallo, B.M.F. Chan, M. Ferrari, and B. Gerami-Naini, *Multipotent differentiation of human dental pulp stem cells: a literature review.* Stem Cell Rev and Rep, 2016. **2016**(12): p. 511-523.
103. Bobis, S., D. Jarocha, and M. Majka, *Mesenchymal stem cells: characteristics and clinical applications.* Folia Histochem Cytobiol, 2006. **44**(4): p. 215-30.
104. Miura, M., S. Gronthos, M. Zhao, B. Lu, L.W. Fisher, P.G. Robey, and S. Shi, *SHED: Stem cells from human exfoliated deciduous teeth.* PNAS, 2003. **100**(10): p. 5807-5812.
105. Kerkis, I. and A.I. Caplan, *Stem Cells in Dental Pulp of Deciduous Teeth.* Tissue Engineering. Part B, Reviews, 2012. **18**(2): p. 129-138. 10.1089/ten.teb.2011.0327.
106. Karaoz, E., P.C. Demircan, O. Saglam, A. Aksoy, F. Kaymaz, and G. Duruksu, *Human dental pulp stem cells demonstrate better neural and epithelial stem cell properties than bone marrow-derived mesenchymal stem cells.* Histochem Cell Biol, 2011. **2011**(136).
107. Ren, H., Y. Sang, F. Zhang, Z. Liu, N. Qi, and Y. Chen, *Comparative analysis of human mesenchymal stem cells from umbilical cord, dental pulp, and menstrual blood as sources for cell therapy.* Stem Cells International, 2016. **2016**.
108. Kang, C.-M., H. Kim, J.S. Song, B.-J. Choi, S.-O. Kim, et al., *Genetic comparison of stemness of human umbilical cord and dental pulp.* Stem Cells International, 2016. **2016**.
109. Isobe, Y., N. Koyama, K. Nakao, K. Osawa, M. Ikeno, et al., *Comparison of human mesenchymal stem cells derived from bone marrow, synovial fluid, adult dental pulp, and exfoliated deciduous tooth pulp.* International Journal of Oral & Maxillofacial Surgery, 2016. **45**: p. 124-131.
110. Aghajani, F., T. Hiishmand, M. Khanmohammadi, S. Khanjani, H. Edalatkhah, S. Kazemnejad, and A.H. Zarnani, *Comparative Immunophenotypic Characteristics, Proliferative Features, and Osteogenic Differentiation of Stem Cells Isolated from Human Permanent and Deciduous Teeth with Bone Marrow.* Molecular Biotechnology, 2016. **58**(6): p. 415-427.
111. Chang, Y.-C., W.-C. Li, N.-F. Twu, H.-Y. Li, W.-L. Lo, et al., *Induction of dental pulp-derived induced pluripotent stem cells in the absence of c-Myc for*

differentiation into neuron-like cells. Journal of the Chinese Medical Association, 2014. **77**: p. 618-625.
112. Tamaoki, N., K. Takahashi, T. Tanaka, T. Ichisaka, H. Aoki, et al., *Dental Pulp Cells for Induced Pluripotent Stem Cell Banking.* Journal of Dental Research, 2010. **89**(8): p. 773-778. 10.1177/0022034510366846.
113. Yan, X., H. Qin, C. Qu, R.S. Tuan, S. Shi, and G.T. Huang, *iPS cells reprogrammed from human mesenchymal-like stem/progenitor cells of dental tissue origin.* Stem Cells Dev, 2010. **19**(4): p. 469-80. 10.1089/scd.2009.0314.
114. Kawano, E., T. Toriumi, S. Iguchi, D. Suzuki, S. Sato, and M. Honda, *Induction of neural crest cells from human dental pulp-derived induced pluripotent stem cells.* Biomed Res, 2017. **38**(2): p. 135-147. 10.2220/biomedres.38.135.
115. Chen, J., M. Lin, J.J. Foxe, E. Pedrosa, A. Hrabovsky, et al., *Transcriptome Comparison of Human Neurons Generated Using Induced Pluripotent Stem Cells Derived from Dental Pulp and Skin Fibroblasts.* PLoS ONE, 2013. **8**(10): p. e75682. 10.1371/journal.pone.0075682.
116. Lee, H.J., S.S. Choi, S.-R. Lee, and K.-T. Chang, *Stem Cell Therapy in Neurological and Neurodegenerative Disease*, in *Neurological Regeneration*, P.V. Pham, Editor. 2017, Springer International Publishing: Cham. p. 1-12.
117. Yoo, J., H.-S. Kim, and D.-Y. Hwang, *Stem cells as promising therapeutic options for neurological disorders.* Journal of Cellular Biochemistry, 2013. **114**(4): p. 743-753. 10.1002/jcb.24427.
118. Ben-David, U. and N. Benvenisty, *The tumorigenicity of human embryonic and induced pluripotent stem cells.* Nat Rev Cancer, 2011. **11**(4): p. 268-77. 10.1038/nrc3034.
119. Liang, Y., H. Zhang, Q.S. Feng, M.B. Cai, W. Deng, et al., *The propensity for tumorigenesis in human induced pluripotent stem cells is related with genomic instability.* Chin J Cancer, 2013. **32**(4): p. 205-12. 10.5732/cjc.012.10065.
120. Wang, Y., Z. Zhang, Y. Chi, Q. Zhang, F. Xu, et al., *Long-term cultured mesenchymal stem cells frequently develop genomic mutations but do not undergo malignant transformation.* Cell Death & Disease, 2013. **4**(12): p. e950. 10.1038/cddis.2013.480.
121. Mayo, V., Y. Sawatari, C.-Y.C. Huang, and F. Garcia-Godoy, *Neural crest-derived dental stem cells--Where we are and where we are going.* Journal of Dentistry, 2014. **42**: p. 1043-1051.
122. Urraca, N., R. Memon, I. El-Iyachi, S. Goorha, C. Valdez, et al., *Characterization of neurons from immortalized dental pulp stem cells for the study of neurogenetic disorders.* Stem Cell Research, 2015. **15**: p. 722-730.
123. Majumdar, D., M. Kanafi, R. Bhonde, P. Gupta, and I. Datta, *Differential neuronal plasticity of dental pulp stem cells from exfoliated deciduous and permanent teeth towards dopaminergic neurons.* Journal of Cellular Physiology, 2016. **231**: p. 2048-2063.
124. Terzi, M.Y., M. Izmirli, and B. Gogebakan, *The cell fate: senescence or quiescence.* Molecular Biology Reports, 2016. **43**(11): p. 1213-1220. 10.1007/s11033-016-4065-0.
125. Turinetto, V., E. Vitale, and C. Giachino, *Senescence in Human Mesenchymal Stem Cells: Functional Changes and Implications in Stem Cell-Based Therapy.*

International Journal of Molecular Sciences, 2016. **17**(7): p. 1164. 10.3390/ijms17071164.
126. Yi, Q., O. Liu, F. Yan, X. Lin, S. Diao, et al., *Analysis of Senescence-Related Differentiation Potentials and Gene Expression Profiles in Human Dental Pulp Stem Cells.* Cells Tissues Organs, 2016. **2016**.
127. Piper, S.L., M. Wang, A. Yamamoto, F. Malek, A. Luu, A.C. Kuo, and H.T. Kim, *Inducible immortality in hTERT-human mesenchymal stem cells.* Journal of Orthopaedic Research, 2012. **30**: p. 1879-1885.
128. Cassidy, S.B., S. Schwartz, J.L. Miller, and D.J. Driscoll, *Prader-Willi syndrome.* Genet Med, 2012. **14**(1): p. 10-26. 10.1038/gim.0b013e31822bead0.
129. Cheon, C.K., *Genetics of Prader-Willi syndrome and Prader-Will-Like syndrome.* Annals of pediatric endocrinology & metabolism, 2016. **21**(3): p. 126-135. 10.6065/apem.2016.21.3.126.
130. Angulo, M.A., M.G. Butler, and M.E. Cataletto, *Prader-Willi syndrome: a review of clinical, genetic, and endocrine findings.* J Endocrinol Invest, 2015. **38**(12): p. 1249-63. 10.1007/s40618-015-0312-9.
131. Bennett, J.A., T. Germani, A.M. Haqq, and L. Zwaigenbaum, *Autism spectrum disorder in Prader-Willi syndrome: A systematic review.* American Journal of Medical Genetics, 2015(167A): p. 2936-2944.
132. Dykens, E.M., E. Roof, H. Hunt-Hawkins, N. Dankner, E.B. Lee, et al., *Diagnoses and characteristics of autism spectrum disorders in children with Prader-Willi syndrome.* J Neurodev Disord, 2017. **9**: p. 18. 10.1186/s11689-017-9200-2.
133. Whittington, J. and A. Holland, *Neurobehavioral phenotype in Prader-Willi syndrome.* Am J Med Genet C Semin Med Genet, 2010. **154c**(4): p. 438-47. 10.1002/ajmg.c.30283.
134. Baker, E.K., D.E. Godler, M. Bui, C. Hickerton, C. Rogers, et al., *Exploring autism symptoms in an Australian cohort of patients with Prader-Willi and Angelman syndromes.* Journal of neurodevelopmental disorders, 2018. **10**(1): p. 24-24. 10.1186/s11689-018-9242-0.
135. Verhoeven, W.M., S. Tuinier, and L.M. Curfs, *Prader-Willi syndrome: cycloid psychosis in a genetic subtype?* Acta Neuropsychiatr, 2003. **15**(1): p. 32-7. 10.1034/j.1601-5215.2003.00006.x.
136. Goorha, S. and L.T. Reiter, *Culturing and Neuronal Differentiation of Human Dental Pulp Stem Cells.* Curr Protoc Hum Genet, 2017. **92**(21): p. 21 6 1-21 6 10. 10.1002/cphg.28.
137. Victor, A.K. and L.T. Reiter, *Dental pulp stem cells for the study of neurogenetic disorders.* Hum Mol Genet, 2017. **26**(R2): p. R166-R171. 10.1093/hmg/ddx208.
138. Ikbale, E.-A., S. Goorha, L.T. Reiter, and G.A. Miranda-Carboni, *Effects of hTERT immortalization on osteogenic and adipogenic differentiation of dental pulp stem cells.* Data in brief, 2016. **6**: p. 696-699. 10.1016/j.dib.2016.01.009.
139. Nuti, N., C. Corallo, B.M.F. Chan, M. Ferrari, and B. Gerami-Naini, *Multipotent Differentiation of Human Dental Pulp Stem Cells: a Literature Review.* Stem Cell Reviews and Reports, 2016. **12**(5): p. 511-523. 10.1007/s12015-016-9661-9.
140. Li, D., X.Y. Zou, I. El-Ayachi, L.O. Romero, Z. Yu, et al., *Human Dental Pulp Stem Cells and Gingival Mesenchymal Stem Cells Display Action Potential*

Capacity In Vitro after Neuronogenic Differentiation. Stem Cell Rev, 2019. **15**(1): p. 67-81. 10.1007/s12015-018-9854-5.
141. Gervois, P., T. Struys, P. Hilkens, A. Bronckaers, J. Ratajczak, et al., *Neurogenic maturation of human dental pulp stem cells following neurosphere generation induces morphological and electrophysiological characteristics of functional neurons.* Stem Cells and Development, 2015. **24**(2015): p. 296-311.
142. Urraca, N., K. Hope, A.K. Victor, T.G. Belgard, R. Memon, et al., *Significant transcriptional changes in 15q duplication by not Angelman syndrome deletion stem cell-derived neurons.* Molecular Autism, 2018. **6**(9).
143. Widmann, J., J. Stombaugh, D. McDonald, J. Chocholousova, P. Gardner, et al., *RNASTAR: an RNA STructural Alignment Repository that provides insight into the evolution of natural and artificial RNAs.* Rna, 2012. **18**(7): p. 1319-27. 10.1261/rna.032052.111.
144. Metsalu, T. and J. Vilo, *ClustVis: a web tool for visualizing clustering of multivariate data using Principal Component Analysis and heatmap.* Nucleic Acids Research, 2015. **43**(W1): p. W566-W570. 10.1093/nar/gkv468.
145. Huang da, W., B.T. Sherman, and R.A. Lempicki, *Systematic and integrative analysis of large gene lists using DAVID bioinformatics resources.* Nat Protoc, 2009. **4**(1): p. 44-57. 10.1038/nprot.2008.211.
146. Bennett, J.A., T. Germani, A.M. Haqq, and L. Zwaigenbaum, *Autism spectrum disorder in Prader-Willi syndrome: A systematic review.* Am J Med Genet A, 2015. **167a**(12): p. 2936-44. 10.1002/ajmg.a.37286.
147. Mouti, A., R. Dryer, and M. Kohn, *Differentiating Autism Spectrum Disorder From ADHD Using the Social Communication Questionnaire.* J Atten Disord, 2019. **23**(8): p. 828-837. 10.1177/1087054718781945.
148. Hutchins, P., K. Williams, N. Silove, and C. Allen, *Validity of the social communication questionnaire in assessing risk of autism in preschool children with developmental problems.* J Autism Dev Disord., 2007. **37**(7): p. 1272-8.
149. Chesnut, S.R., T. Wei, L. Barnard-Brak, and D.M. Richman, *A meta-analysis of the social communication questionnaire: Screening for autism spectrum disorder.* Autism, 2017. **21**(8): p. 920-928. 10.1177/1362361316660065.
150. Barnard-Brak, L., D.M. Richman, S.R. Chesnut, and T.D. Little, *Social Communication Questionnaire scoring procedures for autism spectrum disorder and the prevalence of potential social communication disorder in ASD.* Sch Psychol Q, 2016. **31**(4): p. 522-533. 10.1037/spq0000144.
151. Sappok, T., A. Diefenbacher, I. Gaul, and S. Bolte, *Validity of the social communication questionnaire in adults with intellectual disabilities and suspected autism spectrum disorder.* Am J Intellect Dev Disabil, 2015. **120**(3): p. 203-14. 10.1352/1944-7558-120.3.203.
152. Hulsen, T., J. de Vlieg, and W. Alkema, *BioVenn – a web application for the comparison and visualization of biological lists using area-proportional Venn diagrams.* BMC Genomics, 2008. **9**(1): p. 488. 10.1186/1471-2164-9-488.
153. Huang da, W., B.T. Sherman, and R.A. Lempicki, *Bioinformatics enrichment tools: paths toward the comprehensive functional analysis of large gene lists.* Nucleic Acids Res, 2009. **37**(1): p. 1-13. 10.1093/nar/gkn923.

154. Nguyen, H.T.N., H. Kato, K. Masuda, H. Yamaza, Y. Hirofuji, et al., *Impaired neurite development associated with mitochondrial dysfunction in dopaminergic neurons differentiated from exfoliated deciduous tooth-derived pulp stem cells of children with autism spectrum disorder.* Biochem Biophys Rep, 2018. **16**: p. 24-31. 10.1016/j.bbrep.2018.09.004.
155. Lavie, J., R. Serrat, N. Bellance, G. Courtand, J.W. Dupuy, et al., *Mitochondrial morphology and cellular distribution are altered in SPG31 patients and are linked to DRP1 hyperphosphorylation.* Hum Mol Genet, 2017. **26**(4): p. 674-685. 10.1093/hmg/ddw425.
156. Barone, R., R. Rizzo, G. Tabbì, M. Malaguarnera, R.E. Frye, and J. Bastin, *Nuclear Peroxisome Proliferator-Activated Receptors (PPARs) as Therapeutic Targets of Resveratrol for Autism Spectrum Disorder.* Int J Mol Sci, 2019. **20**(8). 10.3390/ijms20081878.
157. Wang, L., K. Zhou, Z. Fu, D. Yu, H. Huang, X. Zang, and X. Mo, *Brain Development and Akt Signaling: the Crossroads of Signaling Pathway and Neurodevelopmental Diseases.* J Mol Neurosci, 2017. **61**(3): p. 379-384. 10.1007/s12031-016-0872-y.
158. Niciu, M.J., X.M. Ma, R. El Meskini, G.V. Ronnett, R.E. Mains, and B.A. Eipper, *Developmental changes in the expression of ATP7A during a critical period in postnatal neurodevelopment.* Neuroscience, 2006. **139**(3): p. 947-64. 10.1016/j.neuroscience.2006.01.044.
159. Burnett, L.C., C.A. LeDuc, C.R. Sulsona, D. Paull, R. Rausch, et al., *Deficiency in prohormone convertase PC1 impairs prohormone processing in Prader-Willi syndrome.* J Clin Invest, 2017. **127**(1): p. 293-305. 10.1172/jci88648.
160. Suckale, J. and M. Solimena, *The insulin secretory granule as a signaling hub.* Trends Endocrinol Metab, 2010. **21**(10): p. 599-609. 10.1016/j.tem.2010.06.003.
161. D'Ambrosi, N. and L. Rossi, *Copper at synapse: Release, binding and modulation of neurotransmission.* Neurochem Int, 2015. **90**: p. 36-45. 10.1016/j.neuint.2015.07.006.
162. Kaler, S.G., *ATP7A-Related Copper Transport Disorders*, in *GeneReviews*, M.P. Adam, et al., Editors. 1993, University of Washington, Seattle: Seattle (WA).
163. Schanding, G.T.J., K.P. Nowell, and R.P. Goin-Kochel, *Utility of the Social Communication Questionnaire-Current and Social Responsiveness Scale as Teacher-Report Screening Tools for Autism Spectrum Disorders.* J Autism Dev Disord, 2012. **42**.
164. Guo, R., J. Gu, S. Zong, M. Wu, and M. Yang, *Structure and mechanism of mitochondrial electron transport chain.* Biomed J, 2018. **41**(1): p. 9-20. 10.1016/j.bj.2017.12.001.
165. Cogliati, S., I. Lorenzi, G. Rigoni, F. Caicci, and M.E. Soriano, *Regulation of Mitochondrial Electron Transport Chain Assembly.* J Mol Biol, 2018. **430**(24): p. 4849-4873. 10.1016/j.jmb.2018.09.016.
166. Butler, M.G., W.A. Hossain, R. Tessman, and P.C. Krishnamurthy, *Preliminary observations of mitochondrial dysfunction in Prader-Willi syndrome.* Am J Med Genet A, 2018. **176**(12): p. 2587-2594. 10.1002/ajmg.a.40526.

167. Weissman, J.R., R.I. Kelley, M.L. Bauman, B.H. Cohen, K.F. Murray, et al., *Mitochondrial disease in autism spectrum disorder patients: a cohort analysis.* PLoS One, 2008. **3**(11): p. e3815. 10.1371/journal.pone.0003815.
168. Abbeduto, L., A.J. Thurman, A. McDuffie, J. Klusek, R.T. Feigles, et al., *ASD Comorbidity in Fragile X Syndrome: Symptom Profile and Predictors of Symptom Severity in Adolescent and Young Adult Males.* Journal of Autism and Developmental Disorders, 2019. **49**(3): p. 960-977. 10.1007/s10803-018-3796-2.
169. Izzo, A., N. Mollo, M. Nitti, S. Paladino, G. Calì, et al., *Mitochondrial dysfunction in down syndrome: molecular mechanisms and therapeutic targets.* Mol Med, 2018. **24**(1): p. 2. 10.1186/s10020-018-0004-y.
170. Hirofuji, S., Y. Hirofuji, H. Kato, K. Masuda, H. Yamaza, et al., *Mitochondrial dysfunction in dopaminergic neurons differentiated from exfoliated deciduous tooth-derived pulp stem cells of a child with Rett syndrome.* Biochem Biophys Res Commun, 2018. **498**(4): p. 898-904. 10.1016/j.bbrc.2018.03.077.
171. Ebrahimi-Fakhari, D., A. Saffari, L. Wahlster, A. Di Nardo, D. Turner, et al., *Impaired Mitochondrial Dynamics and Mitophagy in Neuronal Models of Tuberous Sclerosis Complex.* Cell Rep, 2016. **17**(4): p. 1053-1070. 10.1016/j.celrep.2016.09.054.
172. Rose, S., D.M. Niyazov, D.A. Rossignol, M. Goldenthal, S.G. Kahler, and R.E. Frye, *Clinical and molecular characteristics of mitochondrial dysfunction in Autism Spectrum disorder.* Molecular Diagnosis & Therapy, 2019. **2018**(22): p. 517-593.
173. Kann, O. and R. Kovacs, *Mitochondria and neuronal activity.* Am J Physiol Cell Physiol, 2007. **292**(2): p. C641-57. 10.1152/ajpcell.00222.2006.
174. Li, Z., K. Okamoto, Y. Hayashi, and M. Sheng, *The importance of dendritic mitochondria in the morphogenesis and plasticity of spines and synapses.* Cell, 2004. **119**(6): p. 873-87. 10.1016/j.cell.2004.11.003.
175. Princz, A., K. Kounakis, and N. Tavernarakis, *Mitochondrial contributions to neuronal development and function.* Biol Chem, 2018. **399**(7): p. 723-739. 10.1515/hsz-2017-0333.
176. Rose, S., D.M. Niyazov, D.A. Rossignol, M. Goldenthal, S.G. Kahler, and R.E. Frye, *Clinical and Molecular Characteristics of Mitochondrial Dysfunction in Autism Spectrum Disorder.* Mol Diagn Ther, 2018. **22**(5): p. 571-593. 10.1007/s40291-018-0352-x.
177. Rojas-Charry, L., L. Nardi, A. Methner, and M.J. Schmeisser, *Abnormalities of synaptic mitochondria in autism spectrum disorder and related neurodevelopmental disorders.* J Mol Med (Berl), 2021. **99**(2): p. 161-178. 10.1007/s00109-020-02018-2.
178. Burté, F., V. Carelli, P.F. Chinnery, and P. Yu-Wai-Man, *Disturbed mitochondrial dynamics and neurodegenerative disorders.* Nat Rev Neurol, 2015. **11**(1): p. 11-24. 10.1038/nrneurol.2014.228.
179. Lin, M.T. and M.F. Beal, *Mitochondrial dysfunction and oxidative stress in neurodegenerative diseases.* Nature, 2006. **443**(7113): p. 787-95. 10.1038/nature05292.
180. Johnson, J., E. Mercado-Ayon, Y. Mercado-Ayon, Y.N. Dong, S. Halawani, L. Ngaba, and D.R. Lynch, *Mitochondrial dysfunction in the development and*

progression of neurodegenerative diseases. Arch Biochem Biophys, 2021. **702**: p. 108698. 10.1016/j.abb.2020.108698.
181. Rossignol, D. and R. Frye, *Mitochondrial dysfunction in autism spectrum disorders: a systematic review and meta-analysis.* Molecular Psychiatry, 2012. **2012**(17): p. 290-314.
182. Lin, M.Y. and Z.H. Sheng, *Regulation of mitochondrial transport in neurons.* Exp Cell Res, 2015. **334**(1): p. 35-44. 10.1016/j.yexcr.2015.01.004.
183. Shoffner, J., L. Hyams, G.N. Langley, S. Cossette, L. Mylacraine, et al., *Fever plus mitochondrial disease could be risk factors for autistic regression.* J Child Neurol, 2010. **25**(4): p. 429-34. 10.1177/0883073809342128.
184. Poling, J.S., R.E. Frye, J. Shoffner, and A.W. Zimmerman, *Developmental regression and mitochondrial dysfunction in a child with autism.* J Child Neurol, 2006. **21**(2): p. 170-2. 10.1177/08830738060210021401.
185. Khemakhem, A.M., R.E. Frye, A. El-Ansary, L. Al-Ayadhi, and A.B. Bacha, *Novel biomarkers of metabolic dysfunction is autism spectrum disorder: potential for biological diagnostic markers.* Metab Brain Dis, 2017. **32**(6): p. 1983-1997. 10.1007/s11011-017-0085-2.
186. Laszlo, A., E. Horvath, E. Eck, and M. Fekete, *Serum serotonin, lactate and pyruvate levels in infantile autistic children.* Clin Chim Acta, 1994. **229**(1-2): p. 205-7.
187. Essa, M.M., G.J. Guillemin, M.I. Waly, M.M. Al-Sharbati, Y.M. Al-Farsi, et al., *Increased markers of oxidative stress in autistic children of the Sultanate of Oman.* Biol Trace Elem Res, 2012. **147**(1-3): p. 25-7. 10.1007/s12011-011-9280-x.
188. Gu, F., V. Chauhan, K. Kaur, W.T. Brown, G. LaFauci, J. Wegiel, and A. Chauhan, *Alterations in mitochondrial DNA copy number and the activities of electron transport chain complexes and pyruvate dehydrogenase in the frontal cortex from subjects with autism.* Transl Psychiatry, 2013. **3**: p. e299. 10.1038/tp.2013.68.
189. Anitha, A., K. Nakamura, I. Thanseem, K. Yamada, Y. Iwayama, et al., *Brain region-specific altered expression and association of mitochondria-related genes in autism.* Mol Autism, 2012. **3**(1): p. 12. 10.1186/2040-2392-3-12.
190. Anitha, A., K. Nakamura, I. Thanseem, H. Matsuzaki, T. Miyachi, et al., *Downregulation of the expression of mitochondrial electron transport complex genes in autism brains.* Brain Pathol, 2013. **23**(3): p. 294-302. 10.1111/bpa.12002.
191. Ginsberg, M.R., R.A. Rubin, T. Falcone, A.H. Ting, and M.R. Natowicz, *Brain transcriptional and epigenetic associations with autism.* PLoS One, 2012. **7**(9): p. e44736. 10.1371/journal.pone.0044736.
192. Scarpulla, R.C., *Metabolic control of mitochondrial biogenesis through the PGC-1 family regulatory network.* Biochim Biophys Acta, 2011. **1813**(7): p. 1269-78. 10.1016/j.bbamcr.2010.09.019.
193. Jornayvaz, F.R. and G.I. Shulman, *Regulation of mitochondrial biogenesis.* Essays Biochem, 2010. **47**: p. 69-84. 10.1042/bse0470069.

194. Ventura-Clapier, R., A. Garnier, and V. Veksler, *Transcriptional control of mitochondrial biogenesis: the central role of PGC-1alpha.* Cardiovasc Res, 2008. **79**(2): p. 208-17. 10.1093/cvr/cvn098.
195. Xu, Y., J.A. Kabba, W. Ruan, Y. Wang, S. Zhao, et al., *The PGC-1alpha Activator ZLN005 Ameliorates Ischemia-Induced Neuronal Injury In Vitro and In Vivo.* Cell Mol Neurobiol, 2018. **38**(4): p. 929-939. 10.1007/s10571-017-0567-0.
196. Zhang, L.N., H.Y. Zhou, Y.Y. Fu, Y.Y. Li, F. Wu, et al., *Novel small-molecule PGC-1alpha transcriptional regulator with beneficial effects on diabetic db/db mice.* Diabetes, 2013. **62**(4): p. 1297-307. 10.2337/db12-0703.
197. Manni, R., L. Politini, L. Nobili, F. Ferrillo, C. Livieri, et al., *Hypersomnia in the Prader Willi syndrome: clinical-electrophysiological features and underlying factors.* Clin Neurophysiol, 2001. **112**(5): p. 800-5. 10.1016/s1388-2457(01)00483-7.
198. Hiroe, Y., Y. Inoue, S. Higami, Y. Suto, and R. Kawahara, *Relationship between hypersomnia and respiratory disorder during sleep in Prader-Willi syndrome.* Psychiatry Clin Neurosci, 2000. **54**(3): p. 323-5. 10.1046/j.1440-1819.2000.00697.x.
199. Smith, I.E., M.A. King, P.W. Siklos, and J.M. Shneerson, *Treatment of ventilatory failure in the Prader-Willi syndrome.* Eur Respir J, 1998. **11**(5): p. 1150-2. 10.1183/09031936.98.11051150.
200. Lassi, G., L. Priano, S. Maggi, C. Garcia-Garcia, E. Balzani, et al., *Deletion of the Snord116/SNORD116 Alters Sleep in Mice and Patients with Prader-Willi Syndrome.* Sleep, 2016. **39**(3): p. 637-44. 10.5665/sleep.5542.
201. Devos, J., S.V. Weselake, and R. Wevrick, *Magel2, a Prader-Willi syndrome candidate gene, modulates the activities of circadian rhythm proteins in cultured cells.* J Circadian Rhythms, 2011. **9**(1): p. 12. 10.1186/1740-3391-9-12.
202. Carias, K.V., M. Zoeteman, A. Seewald, M.R. Sanderson, J.M. Bischof, and R. Wevrick, *A MAGEL2-deubiquitinase complex modulates the ubiquitination of circadian rhythm protein CRY1.* PLoS One, 2020. **15**(4): p. e0230874. 10.1371/journal.pone.0230874.
203. Schaaf, C.P. and F. Marbach, *Schaaf-Yang Syndrome*, in *GeneReviews(®)*, M.P. Adam, et al., Editors. 1993, University of Washington, Seattle. Copyright © 1993-2022, University of Washington, Seattle. GeneReviews is a registered trademark of the University of Washington, Seattle. All rights reserved.: Seattle (WA).
204. Powell, W.T., C.P. Schaaf, M.E. Rech, and J. Wrede, *Polysomnographic characteristics and sleep-disordered breathing in Schaaf-Yang syndrome.* Pediatr Pulmonol, 2020. **55**(11): p. 3162-3167. 10.1002/ppul.25056.
205. Marbach, F., M. Elgizouli, M. Rech, J. Beygo, F. Erger, et al., *The adult phenotype of Schaaf-Yang syndrome.* Orphanet J Rare Dis, 2020. **15**(1): p. 294. 10.1186/s13023-020-01557-8.
206. Chen, H., A.K. Victor, J. Klein, K.F. Tacer, D.J. Tai, et al., *Loss of MAGEL2 in Prader-Willi syndrome leads to decreased secretory granule and neuropeptide production.* JCI Insight, 2020. **5**(17). 10.1172/jci.insight.138576.

207. Ramanathan, C. and A.C. Liu, *Developing Mammalian Cellular Clock Models Using Firefly Luciferase Reporter.* Methods Mol Biol, 2018. **1755**: p. 49-64. 10.1007/978-1-4939-7724-6_4.
208. O'Neill, J.S., E.S. Maywood, J.E. Chesham, J.S. Takahashi, and M.H. Hastings, *cAMP-dependent signaling as a core component of the mammalian circadian pacemaker.* Science, 2008. **320**(5878): p. 949-53. 10.1126/science.1152506.
209. Yagita, K. and H. Okamura, *Forskolin induces circadian gene expression of rPer1, rPer2 and dbp in mammalian rat-1 fibroblasts.* FEBS Lett, 2000. **465**(1): p. 79-82. 10.1016/s0014-5793(99)01724-x.
210. Kaneko, H., T. Kaitsuka, and K. Tomizawa *Response to Stimulations Inducing Circadian Rhythm in Human Induced Pluripotent Stem Cells*. Cells, 2020. **9**, DOI: 10.3390/cells9030620.
211. Dierickx, P., M.W. Vermunt, M.J. Muraro, M.P. Creyghton, P.A. Doevendans, et al., *Circadian networks in human embryonic stem cell-derived cardiomyocytes.* EMBO reports, 2017. **18**(7): p. 1199-1212. https://doi.org/10.15252/embr.201743897.
212. Mohawk, J.A., C.B. Green, and J.S. Takahashi, *Central and peripheral circadian clocks in mammals.* Annu Rev Neurosci, 2012. **35**: p. 445-62. 10.1146/annurev-neuro-060909-153128.
213. Srikanta, S.B. and N. Cermakian, *To Ub or not to Ub: Regulation of circadian clocks by ubiquitination and deubiquitination.* J Neurochem, 2021. **157**(1): p. 11-30. 10.1111/jnc.15132.
214. Wijesuriya, T.M., L. De Ceuninck, D. Masschaele, M.R. Sanderson, K.V. Carias, J. Tavernier, and R. Wevrick, *The Prader-Willi syndrome proteins MAGEL2 and necdin regulate leptin receptor cell surface abundance through ubiquitination pathways.* Hum Mol Genet, 2017. **26**(21): p. 4215-4230. 10.1093/hmg/ddx311.
215. Serin, Y. and N. Acar Tek, *Effect of Circadian Rhythm on Metabolic Processes and the Regulation of Energy Balance.* Annals of Nutrition and Metabolism, 2019. **74**(4): p. 322-330. 10.1159/000500071.
216. Reinke, H. and G. Asher, *Crosstalk between metabolism and circadian clocks.* Nature Reviews Molecular Cell Biology, 2019. **20**(4): p. 227-241. 10.1038/s41580-018-0096-9.
217. Tacer, K.F. and P.R. Potts, *Cellular and disease functions of the Prader-Willi Syndrome gene MAGEL2.* Biochem J, 2017. **474**(13): p. 2177-2190. 10.1042/bcj20160616.
218. Kalsner, L. and S.J. Chamberlain, *Prader-Willi, Angelman, and 15q11-q13 Duplication Syndromes.* Pediatric clinics of North America, 2015. **62**(3): p. 587-606. 10.1016/j.pcl.2015.03.004.
219. Dunaway, K., S. Goorha, L. Matelski, N. Urraca, P.J. Lein, et al., *Dental Pulp Stem Cells Model Early Life and Imprinted DNA Methylation Patterns.* Stem Cells, 2017. **35**(4): p. 981-988. 10.1002/stem.2563.
220. Li, D., X.Y. Zou, I. El-Ayachi, L.O. Romero, Z. Yu, et al., *Human Dental Pulp Stem Cells and Gingival Mesenchymal Stem Cells Display Action Potential Capacity In Vitro after Neuronogenic Differentiation.* Stem Cell Rev Rep, 2019. **15**(1): p. 67-81. 10.1007/s12015-018-9854-5.

221. Rosenberg, A.B., C.M. Roco, R.A. Muscat, A. Kuchina, P. Sample, et al., *Single-cell profiling of the developing mouse brain and spinal cord with split-pool barcoding.* Science, 2018. **360**(6385): p. 176-182. 10.1126/science.aam8999.
222. Dobin, A., C.A. Davis, F. Schlesinger, J. Drenkow, C. Zaleski, et al., *STAR: ultrafast universal RNA-seq aligner.* Bioinformatics, 2013. **29**(1): p. 15-21. 10.1093/bioinformatics/bts635.
223. Garmire, D.G., X. Zhu, A. Mantravadi, Q. Huang, B. Yunits, et al., *GranatumX: A Community-engaging, Modularized, and Flexible Webtool for Single-cell Data Analysis.* Genomics Proteomics Bioinformatics, 2021. **19**(3): p. 452-460. 10.1016/j.gpb.2021.07.005.
224. Zhu, X., T.K. Wolfgruber, A. Tasato, C. Arisdakessian, D.G. Garmire, and L.X. Garmire, *Granatum: a graphical single-cell RNA-Seq analysis pipeline for genomics scientists.* Genome Med, 2017. **9**(1): p. 108. 10.1186/s13073-017-0492-3.
225. Zhu, X., T.K. Wolfgruber, A. Tasato, C. Arisdakessian, D.G. Garmire, and L.X. Garmire, *Granatum: a graphical single-cell RNA-Seq analysis pipeline for genomics scientists.* Genome Medicine, 2017. **9**(1): p. 108. 10.1186/s13073-017-0492-3.
226. Tsang, S.M., E. Oliemuller, and B.A. Howard, *Regulatory roles for SOX11 in development, stem cells and cancer.* Semin Cancer Biol, 2020. **67**(Pt 1): p. 3-11. 10.1016/j.semcancer.2020.06.015.
227. Rengaraj, D., B.R. Lee, K.J. Park, S.I. Lee, K.S. Kang, et al., *The distribution of neuron-specific gene family member 1 in brain and germ cells: Implications for the regulation of germ-line development by brain.* Dev Dyn, 2011. **240**(4): p. 850-61. 10.1002/dvdy.22575.
228. Koiliari, E., P. Roussos, E. Pasparakis, T. Lencz, A. Malhotra, et al., *The CSMD1 genome-wide associated schizophrenia risk variant rs10503253 affects general cognitive ability and executive function in healthy males.* Schizophr Res, 2014. **154**(1-3): p. 42-7. 10.1016/j.schres.2014.02.017.
229. Stelzer, G., N. Rosen, I. Plaschkes, S. Zimmerman, M. Twik, et al., *The GeneCards Suite: From Gene Data Mining to Disease Genome Sequence Analyses.* Current Protocols in Bioinformatics, 2016. **54**(1): p. 1.30.1-1.30.33. https://doi.org/10.1002/cpbi.5.
230. Safran, M., N. Rosen, M. Twik, R. BarShir, T.I. Stein, et al., *The GeneCards Suite*, in *Practical Guide to Life Science Databases*, I. Abugessaisa and T. Kasukawa, Editors. 2021, Springer Nature Singapore: Singapore. p. 27-56.
231. Co, M., A.G. Anderson, and G. Konopka, *FOXP transcription factors in vertebrate brain development, function, and disorders.* WIREs Developmental Biology, 2020. **9**(5): p. e375. https://doi.org/10.1002/wdev.375.
232. Harkin, L.F., S.J. Lindsay, Y. Xu, A. Alzu'bi, A. Ferrara, et al., *Neurexins 1-3 Each Have a Distinct Pattern of Expression in the Early Developing Human Cerebral Cortex.* Cereb Cortex, 2017. **27**(1): p. 216-232. 10.1093/cercor/bhw394.
233. Yap, C.C., L. Digilio, L. McMahon, and B. Winckler, *The endosomal neuronal proteins Nsg1/NEEP21 and Nsg2/P19 are itinerant, not resident proteins of dendritic endosomes.* Sci Rep, 2017. **7**(1): p. 10481. 10.1038/s41598-017-07667-x.

234. Debaigt, C., H. Hirling, P. Steiner, J.P. Vincent, and J. Mazella, *Crucial role of neuron-enriched endosomal protein of 21 kDa in sorting between degradation and recycling of internalized G-protein-coupled receptors.* J Biol Chem, 2004. **279**(34): p. 35687-91. 10.1074/jbc.M402751200.
235. Miraoui, H., A.A. Dwyer, G.P. Sykiotis, L. Plummer, W. Chung, et al., *Mutations in FGF17, IL17RD, DUSP6, SPRY4, and FLRT3 are identified in individuals with congenital hypogonadotropic hypogonadism.* Am J Hum Genet, 2013. **92**(5): p. 725-43. 10.1016/j.ajhg.2013.04.008.
236. Men, M., X. Wang, J. Wu, W. Zeng, F. Jiang, R. Zheng, and J.D. Li, *Prevalence and associated phenotypes of DUSP6, IL17RD and SPRY4 variants in a large Chinese cohort with isolated hypogonadotropic hypogonadism.* J Med Genet, 2021. **58**(1): p. 66-72. 10.1136/jmedgenet-2019-106786.
237. Barroso, P.S., A.A.L. Jorge, A.M. Lerario, L.R. Montenegro, G.A. Vasques, et al., *Clinical and Genetic Characterization of a Constitutional Delay of Growth and Puberty Cohort.* Neuroendocrinology, 2020. **110**(11-12): p. 959-966. 10.1159/000504783.
238. Mojsilović, S., A. Jauković, J.F. Santibañez, and D. Bugarski, *Interleukin-17 and its implication in the regulation of differentiation and function of hematopoietic and mesenchymal stem cells.* Mediators Inflamm, 2015. **2015**: p. 470458. 10.1155/2015/470458.
239. Athanasiu, L., S. Giddaluru, C. Fernandes, A. Christoforou, I. Reinvang, et al., *A genetic association study of CSMD1 and CSMD2 with cognitive function.* Brain Behav Immun, 2017. **61**: p. 209-216. 10.1016/j.bbi.2016.11.026.
240. Steen, V.M., C. Nepal, K.M. Ersland, R. Holdhus, M. Nævdal, et al., *Neuropsychological deficits in mice depleted of the schizophrenia susceptibility gene CSMD1.* PLoS One, 2013. **8**(11): p. e79501. 10.1371/journal.pone.0079501.
241. Ruiz-Martínez, J., L.J. Azcona, A. Bergareche, J.F. Martí-Massó, and C. Paisán-Ruiz, *Whole-exome sequencing associates novel CSMD1 gene mutations with familial Parkinson disease.* Neurol Genet, 2017. **3**(5): p. e177. 10.1212/nxg.0000000000000177.
242. Hetman, M. and L.P. Slomnicki, *Ribosomal biogenesis as an emerging target of neurodevelopmental pathologies.* J Neurochem, 2019. **148**(3): p. 325-347. 10.1111/jnc.14576.
243. Slomnicki, L.P., M. Pietrzak, A. Vashishta, J. Jones, N. Lynch, et al., *Requirement of Neuronal Ribosome Synthesis for Growth and Maintenance of the Dendritic Tree.* J Biol Chem, 2016. **291**(11): p. 5721-5739. 10.1074/jbc.M115.682161.
244. Lisabeth, E.M., G. Falivelli, and E.B. Pasquale, *Eph receptor signaling and ephrins.* Cold Spring Harb Perspect Biol, 2013. **5**(9). 10.1101/cshperspect.a009159.
245. Liu, D.Z., B.P. Ander, Y. Tian, B. Stamova, G.C. Jickling, R.R. Davis, and F.R. Sharp, *Integrated analysis of mRNA and microRNA expression in mature neurons, neural progenitor cells and neuroblastoma cells.* Gene, 2012. **495**(2): p. 120-7. 10.1016/j.gene.2011.12.041.

246. Henkemeyer, M., O.S. Itkis, M. Ngo, P.W. Hickmott, and I.M. Ethell, *Multiple EphB receptor tyrosine kinases shape dendritic spines in the hippocampus.* J Cell Biol, 2003. **163**(6): p. 1313-26. 10.1083/jcb.200306033.
247. Khodosevich, K., Y. Watanabe, and H. Monyer, *EphA4 preserves postnatal and adult neural stem cells in an undifferentiated state in vivo.* J Cell Sci, 2011. **124**(Pt 8): p. 1268-79. 10.1242/jcs.076059.
248. Bartkowska, K., A. Paquin, A.S. Gauthier, D.R. Kaplan, and F.D. Miller, *Trk signaling regulates neural precursor cell proliferation and differentiation during cortical development.* Development, 2007. **134**(24): p. 4369-80. 10.1242/dev.008227.
249. Hoshiba, Y., T. Toda, H. Ebisu, M. Wakimoto, S. Yanagi, and H. Kawasaki, *Sox11 Balances Dendritic Morphogenesis with Neuronal Migration in the Developing Cerebral Cortex.* J Neurosci, 2016. **36**(21): p. 5775-84. 10.1523/jneurosci.3250-15.2016.
250. Bergsland, M., M. Werme, M. Malewicz, T. Perlmann, and J. Muhr, *The establishment of neuronal properties is controlled by Sox4 and Sox11.* Genes Dev, 2006. **20**(24): p. 3475-86. 10.1101/gad.403406.
251. Co, M., A.G. Anderson, and G. Konopka, *FOXP transcription factors in vertebrate brain development, function, and disorders.* Wiley Interdiscip Rev Dev Biol, 2020. **9**(5): p. e375. 10.1002/wdev.375.
252. Vernes, S.C., P.L. Oliver, E. Spiteri, H.E. Lockstone, R. Puliyadi, et al., *Foxp2 regulates gene networks implicated in neurite outgrowth in the developing brain.* PLoS Genet, 2011. **7**(7): p. e1002145. 10.1371/journal.pgen.1002145.
253. Pook, C., J.M. Ahrens, and M. Clagett-Dame, *Expression pattern of Nav2 in the murine CNS with development.* Gene Expr Patterns, 2020. **35**: p. 119099. 10.1016/j.gep.2020.119099.
254. Accogli, A., S. Lu, I. Musante, P. Scudieri, J.A. Rosenfeld, et al., *Loss of Neuron Navigator 2 Impairs Brain and Cerebellar Development.* Cerebellum, 2022. 10.1007/s12311-022-01379-3.
255. Gomez, A.M., L. Traunmüller, and P. Scheiffele, *Neurexins: molecular codes for shaping neuronal synapses.* Nat Rev Neurosci, 2021. **22**(3): p. 137-151. 10.1038/s41583-020-00415-7.
256. Carroll, M.S., P.P. Patwari, A.S. Kenny, C.D. Brogadir, T.M. Stewart, and D.E. Weese-Mayer, *Rapid-onset obesity with hypothalamic dysfunction, hypoventilation, and autonomic dysregulation (ROHHAD): Response to ventilatory challenges.* Pediatr Pulmonol, 2015. **50**(12): p. 1336-45. 10.1002/ppul.23164.
257. Ize-Ludlow, D., J.A. Gray, M.A. Sperling, E.M. Berry-Kravis, J.M. Milunsky, et al., *Rapid-onset obesity with hypothalamic dysfunction, hypoventilation, and autonomic dysregulation presenting in childhood.* Pediatrics, 2007. **120**(1): p. e179-88. 10.1542/peds.2006-3324.
258. Ceccherini, I., K.C. Kurek, and D.E. Weese-Mayer, *Developmental disorders affecting the respiratory system: CCHS and ROHHAD.* Handb Clin Neurol, 2022. **189**: p. 53-91. 10.1016/b978-0-323-91532-8.00005-7.
259. Barclay, S.F., C.M. Rand, L.A. Borch, L. Nguyen, P.A. Gray, et al., *Rapid-Onset Obesity with Hypothalamic Dysfunction, Hypoventilation, and Autonomic*

Dysregulation (ROHHAD): exome sequencing of trios, monozygotic twins and tumours. Orphanet J Rare Dis, 2015. **10**: p. 103. 10.1186/s13023-015-0314-x.
260. Patwari, P.P., C.M. Rand, E.M. Berry-Kravis, D. Ize-Ludlow, and D.E. Weese-Mayer, *Monozygotic twins discordant for ROHHAD phenotype.* Pediatrics, 2011. **128**(3): p. e711-5. 10.1542/peds.2011-0155.
261. Giacomozzi, C., F. Guaraldi, P. Cambiaso, M. Niceta, E. Verrillo, M. Tartaglia, and R. Cutrera, *Anti-Hypothalamus and Anti-Pituitary Auto-antibodies in ROHHAD Syndrome: Additional Evidence Supporting an Autoimmune Etiopathogenesis.* Horm Res Paediatr, 2019. **92**(2): p. 124-132. 10.1159/000499163.
262. Rand, C.M., P.P. Patwari, E.A. Rodikova, L. Zhou, E.M. Berry-Kravis, et al., *Rapid-onset obesity with hypothalamic dysfunction, hypoventilation, and autonomic dysregulation: analysis of hypothalamic and autonomic candidate genes.* Pediatr Res, 2011. **70**(4): p. 375-8. 10.1203/PDR.0b013e318229474d.
263. De Pontual, L., D. Trochet, S. Caillat-Zucman, O.A. Abou Shenab, P. Bougneres, et al., *Delineation of late onset hypoventilation associated with hypothalamic dysfunction syndrome.* Pediatric Research, 2008. **64**(6): p. 689-694. 10.1203/PDR.0b013e318187dd0e.
264. Sartori, S., E. Priante, A. Pettenazzo, P. Marson, A. Suppiej, et al., *Intrathecal synthesis of oligoclonal bands in rapid-onset obesity with hypothalamic dysfunction, hypoventilation, and autonomic dysregulation syndrome: new evidence supporting immunological pathogenesis.* J Child Neurol, 2014. **29**(3): p. 421-5. 10.1177/0883073812469050.
265. Hawton, K.A.C., R. Doffinger, A.V. Ramanan, S.C. Langton Hewer, H.J. Evans, D. Giri, and J.P. Hamilton Shield, *Rituximab therapy in ROHHAD(NET) syndrome.* J Pediatr Endocrinol Metab, 2022. **35**(8): p. 1102-1106. 10.1515/jpem-2022-0085.
266. Zhou, A., C.M. Rand, S.M. Hockney, G. Niewijk, P. Reineke, et al., *Paired-like homeobox gene (PHOX2B) nonpolyalanine repeat expansion mutations (NPARMs): genotype-phenotype correlation in congenital central hypoventilation syndrome (CCHS).* Genet Med, 2021. **23**(9): p. 1656-1663. 10.1038/s41436-021-01178-x.
267. Weese-Mayer, D.E., C.M. Rand, I. Khaytin, S.M. Slattery, K.L. Yap, M.L. Marazita, and E.M. Berry-Kravis, *Congenital Central Hypoventilation Syndrome*, in *GeneReviews(®)*, M.P. Adam, et al., Editors. 2021, University of Washington, Seattle: Seattle (WA).
268. Weese-Mayer, D.E., E.M. Berry-Kravis, I. Ceccherini, T.G. Keens, D.A. Loghmanee, and H. Trang, *An official ATS clinical policy statement: Congenital central hypoventilation syndrome: genetic basis, diagnosis, and management.* Am J Respir Crit Care Med, 2010. **181**(6): p. 626-44. 10.1164/rccm.200807-1069ST.
269. Barclay, S.F., C.M. Rand, L. Nguyen, R.J.A. Wilson, R. Wevrick, et al., *ROHHAD and Prader-Willi syndrome (PWS): clinical and genetic comparison.* Orphanet J Rare Dis, 2018. **13**(1): p. 124. 10.1186/s13023-018-0860-0.
270. Cassidy, S.B. and D.J. Driscoll, *Prader-Willi syndrome.* Eur J Hum Genet, 2009. **17**(1): p. 3-13. 10.1038/ejhg.2008.165.

271. Gronthos, S., J. Brahim, W. Li, L.W. Fisher, N. Cherman, et al., *Stem cell properties of human dental pulp stem cells.* J Dent Res, 2002. **81**(8): p. 531-5. 10.1177/154405910208100806.
272. Miura, M., S. Gronthos, M. Zhao, B. Lu, L.W. Fisher, P.G. Robey, and S. Shi, *SHED: stem cells from human exfoliated deciduous teeth.* Proc Natl Acad Sci U S A, 2003. **100**(10): p. 5807-12. 10.1073/pnas.0937635100.
273. Ferro, F., R. Spelat, and C.S. Baheney, *Dental pulp stem cell (DPSC) isolation, characterization, and differentiation.* Methods Mol Biol, 2014. **1210**: p. 91-115. 10.1007/978-1-4939-1435-7_8.
274. Rafiee, F., Z. Pourteymourfard-Tabrizi, M.R. Mahmoudian-Sani, A. Mehri-Ghahfarrokhi, A. Soltani, M. Hashemzadeh-Chaleshtori, and M.S. Jami, *Differentiation of dental pulp stem cells into neuron-like cells.* Int J Neurosci, 2020. **130**(2): p. 107-116. 10.1080/00207454.2019.1664518.
275. Geng, Y.W., Z. Zhang, M.Y. Liu, and W.P. Hu, *Differentiation of human dental pulp stem cells into neuronal by resveratrol.* Cell Biol Int, 2017. **41**(12): p. 1391-1398. 10.1002/cbin.10835.
276. Gonmanee, T., T. Arayapisit, K. Vongsavan, C. Phruksaniyom, and H. Sritanaudomchai, *Optimal culture conditions for neurosphere formation and neuronal differentiation from human dental pulp stem cells.* J Appl Oral Sci, 2021. **29**: p. e20210296. 10.1590/1678-7757-2021-0296.
277. Kogo, Y., C. Seto, Y. Totani, M. Mochizuki, T. Nakahara, et al., *Rapid differentiation of human dental pulp stem cells to neuron-like cells by high K(+) stimulation.* Biophys Physicobiol, 2020. **17**: p. 132-139. 10.2142/biophysico.BSJ-2020023.
278. Zainal Ariffin, S.H., S. Kermani, I.Z. Zainol Abidin, R. Megat Abdul Wahab, Z. Yamamoto, et al., *Differentiation of dental pulp stem cells into neuron-like cells in serum-free medium.* Stem Cells Int, 2013. **2013**: p. 250740. 10.1155/2013/250740.
279. Al-Maswary, A.A., M. O'Reilly, A.P. Holmes, A.D. Walmsley, P.R. Cooper, and B.A. Scheven, *Exploring the neurogenic differentiation of human dental pulp stem cells.* PLoS One, 2022. **17**(11): p. e0277134. 10.1371/journal.pone.0277134.
280. Chun, S.Y., S. Soker, Y.J. Jang, T.G. Kwon, and E.S. Yoo, *Differentiation of Human Dental Pulp Stem Cells into Dopaminergic Neuron-like Cells in Vitro.* J Korean Med Sci, 2016. **31**(2): p. 171-7. 10.3346/jkms.2016.31.2.171.
281. Osathanon, T., C. Sawangmake, N. Nowwarote, and P. Pavasant, *Neurogenic differentiation of human dental pulp stem cells using different induction protocols.* Oral Dis, 2014. **20**(4): p. 352-8. 10.1111/odi.12119.
282. Young, F.I., V. Telezhkin, S.J. Youde, M.S. Langley, M. Stack, et al., *Clonal Heterogeneity in the Neuronal and Glial Differentiation of Dental Pulp Stem/Progenitor Cells.* Stem Cells Int, 2016. **2016**: p. 1290561. 10.1155/2016/1290561.
283. Solis-Castro, O.O., F.M. Boissonade, and M.N. Rivolta, *Establishment and neural differentiation of neural crest-derived stem cells from human dental pulp in serum-free conditions.* Stem Cells Transl Med, 2020. **9**(11): p. 1462-1476. 10.1002/sctm.20-0037.

284. Kanafi, M., D. Majumdar, R. Bhonde, P. Gupta, and I. Datta, *Midbrain cues dictate differentiation of human dental pulp stem cells towards functional dopaminergic neurons.* J Cell Physiol, 2014. **229**(10): p. 1369-77. 10.1002/jcp.24570.
285. Urraca, N., R. Memon, I. El-Iyachi, S. Goorha, C. Valdez, et al., *Characterization of neurons from immortalized dental pulp stem cells for the study of neurogenetic disorders.* Stem Cell Res, 2015. **15**(3): p. 722-730. 10.1016/j.scr.2015.11.004.
286. Pham, T.T.M., H. Kato, H. Yamaza, K. Masuda, Y. Hirofuji, et al., *Altered development of dopaminergic neurons differentiated from stem cells from human exfoliated deciduous teeth of a patient with Down syndrome.* BMC Neurol, 2018. **18**(1): p. 132. 10.1186/s12883-018-1140-2.
287. Urraca, N., K. Hope, A.K. Victor, T.G. Belgard, R. Memon, et al., *Significant transcriptional changes in 15q duplication but not Angelman syndrome deletion stem cell-derived neurons.* Mol Autism, 2018. **9**: p. 6. 10.1186/s13229-018-0191-y.
288. Phipson, B., S. Lee, I.J. Majewski, W.S. Alexander, and G.K. Smyth, *ROBUST HYPERPARAMETER ESTIMATION PROTECTS AGAINST HYPERVARIABLE GENES AND IMPROVES POWER TO DETECT DIFFERENTIAL EXPRESSION.* Ann Appl Stat, 2016. **10**(2): p. 946-963. 10.1214/16-aoas920.
289. Eden, E., R. Navon, I. Steinfeld, D. Lipson, and Z. Yakhini, *GOrilla: a tool for discovery and visualization of enriched GO terms in ranked gene lists.* BMC Bioinformatics, 2009. **10**(1): p. 48. 10.1186/1471-2105-10-48.
290. Sakaguchi, M., W. Cai, C.H. Wang, C.T. Cederquist, M. Damasio, et al., *FoxK1 and FoxK2 in insulin regulation of cellular and mitochondrial metabolism.* Nat Commun, 2019. **10**(1): p. 1582. 10.1038/s41467-019-09418-0.
291. Sukonina, V., H. Ma, W. Zhang, S. Bartesaghi, S. Subhash, et al., *FOXK1 and FOXK2 regulate aerobic glycolysis.* Nature, 2019. **566**(7743): p. 279-283. 10.1038/s41586-019-0900-5.
292. Hu, C., L. Fan, P. Cen, E. Chen, Z. Jiang, and L. Li, *Energy Metabolism Plays a Critical Role in Stem Cell Maintenance and Differentiation.* Int J Mol Sci, 2016. **17**(2): p. 253. 10.3390/ijms17020253.
293. Narita, A., M. Nagai, S. Mizuno, S. Ogishima, G. Tamiya, et al., *Clustering by phenotype and genome-wide association study in autism.* Transl Psychiatry, 2020. **10**(1): p. 290. 10.1038/s41398-020-00951-x.
294. Atsem, S., J. Reichenbach, R. Potabattula, M. Dittrich, C. Nava, et al., *Paternal age effects on sperm FOXK1 and KCNA7 methylation and transmission into the next generation.* Hum Mol Genet, 2016. **25**(22): p. 4996-5005. 10.1093/hmg/ddw328.
295. Fugger, K., W.K. Chu, P. Haahr, A.N. Kousholt, H. Beck, et al., *FBH1 co-operates with MUS81 in inducing DNA double-strand breaks and cell death following replication stress.* Nat Commun, 2013. **4**: p. 1423. 10.1038/ncomms2395.
296. Jeong, Y.T., M. Rossi, L. Cermak, A. Saraf, L. Florens, et al., *FBH1 promotes DNA double-strand breakage and apoptosis in response to DNA replication stress.* J Cell Biol, 2013. **200**(2): p. 141-9. 10.1083/jcb.201209002.

297. Potenski, C.J. and H.L. Klein, *Death becomes her: FBH1, DNA damage and apoptosis.* Cell Cycle, 2013. **12**(9): p. 1336-7. 10.4161/cc.24668.
298. Kieroń, M., C. Żekanowski, A. Falk, and M. Wężyk, *Oxidative DNA Damage Signalling in Neural Stem Cells in Alzheimer's Disease.* Oxid Med Cell Longev, 2019. **2019**: p. 2149812. 10.1155/2019/2149812.
299. Lin, X., A. Kapoor, Y. Gu, M.J. Chow, J. Peng, K. Zhao, and D. Tang, *Contributions of DNA Damage to Alzheimer's Disease.* Int J Mol Sci, 2020. **21**(5). 10.3390/ijms21051666.
300. Chahrour, M.H., T.W. Yu, E.T. Lim, B. Ataman, M.E. Coulter, et al., *Whole-exome sequencing and homozygosity analysis implicate depolarization-regulated neuronal genes in autism.* PLoS Genet, 2012. **8**(4): p. e1002635. 10.1371/journal.pgen.1002635.
301. Butler, M.G., S.N. Hartin, W.A. Hossain, A.M. Manzardo, V. Kimonis, et al., *Molecular genetic classification in Prader-Willi syndrome: a multisite cohort study.* J Med Genet, 2019. **56**(3): p. 149-153. 10.1136/jmedgenet-2018-105301.
302. Uribe-Querol, E. and C. Rosales, *Phagocytosis: Our Current Understanding of a Universal Biological Process.* Front Immunol, 2020. **11**: p. 1066. 10.3389/fimmu.2020.01066.
303. Stavoe, A.K.H. and E.L.F. Holzbaur, *Autophagy in Neurons.* Annu Rev Cell Dev Biol, 2019. **35**: p. 477-500. 10.1146/annurev-cellbio-100818-125242.
304. Butler, C.A., A.S. Popescu, E.J.A. Kitchener, D.H. Allendorf, M. Puigdellívol, and G.C. Brown, *Microglial phagocytosis of neurons in neurodegeneration, and its regulation.* J Neurochem, 2021. **158**(3): p. 621-639. 10.1111/jnc.15327.
305. Fu, R., Q. Shen, P. Xu, J.J. Luo, and Y. Tang, *Phagocytosis of microglia in the central nervous system diseases.* Mol Neurobiol, 2014. **49**(3): p. 1422-34. 10.1007/s12035-013-8620-6.
306. Shi, Y., S. Lin, K.A. Staats, Y. Li, W.-H. Chang, et al., *Haploinsufficiency leads to neurodegeneration in C9ORF72 ALS/FTD human induced motor neurons.* Nature Medicine, 2018. **24**(3): p. 313-325. 10.1038/nm.4490.
307. Parkinson, W., M.L. Dear, E. Rushton, and K. Broadie, *N-glycosylation requirements in neuromuscular synaptogenesis.* Development, 2013. **140**(24): p. 4970-81. 10.1242/dev.099192.
308. Jacobsson, J.A., M. Rask-Andersen, U. Risérus, G. Moschonis, A. Koumpitski, et al., *Genetic variants near the MGAT1 gene are associated with body weight, BMI and fatty acid metabolism among adults and children.* Int J Obes (Lond), 2012. **36**(1): p. 119-29. 10.1038/ijo.2011.11.
309. Wang, A.C., E.H. Jensen, J.E. Rexach, H.V. Vinters, and L.C. Hsieh-Wilson, *Loss of O-GlcNAc glycosylation in forebrain excitatory neurons induces neurodegeneration.* Proc Natl Acad Sci U S A, 2016. **113**(52): p. 15120-15125. 10.1073/pnas.1606899113.
310. Böhm, J., E. Malfatti, E. Oates, K. Jones, G. Brochier, et al., *Novel ASCC1 mutations causing prenatal-onset muscle weakness with arthrogryposis and congenital bone fractures.* J Med Genet, 2019. **56**(9): p. 617-621. 10.1136/jmedgenet-2018-105390.

311. Meunier, J., R.N. Villar-Quiles, I. Duband-Goulet, and A. Ferreiro, *Inherited Defects of the ASC-1 Complex in Congenital Neuromuscular Diseases.* Int J Mol Sci, 2021. **22**(11). 10.3390/ijms22116039.
312. Rosano, K.K., D.J. Wegner, M. Shinawi, D. Baldridge, R.C. Bucelli, et al., *Biallelic ASCC1 variants including a novel intronic variant result in expanded phenotypic spectrum of spinal muscular atrophy with congenital bone fractures 2 (SMABF2).* Am J Med Genet A, 2021. **185**(7): p. 2190-2197. 10.1002/ajmg.a.62219.
313. Dusl, M., T. Moreno, F. Munell, A. Macaya, M. Gratacòs, et al., *Congenital myasthenic syndrome caused by novel COL13A1 mutations.* J Neurol, 2019. **266**(5): p. 1107-1112. 10.1007/s00415-019-09239-7.
314. Kediha, M.I., M. Tazir, D. Sternberg, B. Eymard, and L. Alipacha, *Moderate phenotype of a congenital myasthenic syndrome type 19 caused by mutation of the COL13A1 gene: a case report.* J Med Case Rep, 2022. **16**(1): p. 134. 10.1186/s13256-022-03268-z.
315. Rodríguez Cruz, P.M., J. Cossins, E.P. Estephan, F. Munell, K. Selby, et al., *The clinical spectrum of the congenital myasthenic syndrome resulting from COL13A1 mutations.* Brain, 2019. **142**(6): p. 1547-1560. 10.1093/brain/awz107.
316. Dines, J.N., K. Golden-Grant, A. LaCroix, A.M. Muir, D.L. Cintrón, et al., *TANGO2: expanding the clinical phenotype and spectrum of pathogenic variants.* Genet Med, 2019. **21**(3): p. 601-607. 10.1038/s41436-018-0137-y.
317. Hoebeke, C., A. Cano, P. De Lonlay, and B. Chabrol, *Clinical phenotype associated with TANGO2 gene mutation.* Arch Pediatr, 2021. **28**(1): p. 80-86. 10.1016/j.arcped.2020.11.004.
318. Lalani, S.R., B. Graham, L. Burrage, Y.C. Lai, F. Scaglia, et al., *TANGO2-Related Metabolic Encephalopathy and Arrhythmias*, in *GeneReviews(®)*, M.P. Adam, et al., Editors. 2018, University of Washington, Seattle: Seattle (WA).
319. Schymick, J., P. Leahy, T. Cowan, M.R.Z. Ruzhnikov, R. Gates, et al., *Variable clinical severity in TANGO2 deficiency: Case series and literature review.* Am J Med Genet A, 2022. **188**(2): p. 473-487. 10.1002/ajmg.a.62543.
320. Siokas, V., A.M. Aloizou, Z. Tsouris, I. Liampas, P. Liakos, et al., *ADORA2A rs5760423 and CYP1A2 rs762551 Polymorphisms as Risk Factors for Parkinson's Disease.* J Clin Med, 2021. **10**(3). 10.3390/jcm10030381.
321. Merighi, S., E. Battistello, I. Casetta, D. Gragnaniello, T.E. Poloni, et al., *Upregulation of Cortical A2A Adenosine Receptors Is Reflected in Platelets of Patients with Alzheimer's Disease.* J Alzheimers Dis, 2021. **80**(3): p. 1105-1117. 10.3233/jad-201437.
322. Chandrasekera, P.C., V.J. McIntosh, F.X. Cao, and R.D. Lasley, *Differential effects of adenosine A2a and A2b receptors on cardiac contractility.* Am J Physiol Heart Circ Physiol, 2010. **299**(6): p. H2082-9. 10.1152/ajpheart.00511.2010.
323. Yang, J.N., J.F. Chen, and B.B. Fredholm, *Physiological roles of A1 and A2A adenosine receptors in regulating heart rate, body temperature, and locomotion as revealed using knockout mice and caffeine.* Am J Physiol Heart Circ Physiol, 2009. **296**(4): p. H1141-9. 10.1152/ajpheart.00754.2008.

324. Özcan, G., E. Özsu, Z. Şiklar, and N. Çobanoğlu, *A Rare Cause of Sleep-Disordered Breathing: ROHHAD Syndrome.* Front Pediatr, 2020. **8**: p. 573227. 10.3389/fped.2020.573227.
325. Cai, Z., L. Tu, C. Guignabert, D. Merkus, and Z. Zhou, *Purinergic Dysfunction in Pulmonary Arterial Hypertension.* J Am Heart Assoc, 2020. **9**(18): p. e017404. 10.1161/jaha.120.017404.
326. Stowe, R.C. and O. Afolabi-Brown, *Pulmonary hypertension and chronic hypoventilation in ROHHAD syndrome treated with average-volume assured pressure support.* Pediatr Investig, 2019. **3**(4): p. 253-256. 10.1002/ped4.12168.
327. Romero, L.O., R. Caires, A. Kaitlyn Victor, J. Ramirez, F.J. Sierra-Valdez, et al., *Linoleic acid improves PIEZO2 dysfunction in a mouse model of Angelman Syndrome.* Nat Commun, 2023. **14**(1): p. 1167. 10.1038/s41467-023-36818-0.
328. Arimura, Y., Y. Shindo, R. Yamanaka, M. Mochizuki, K. Hotta, et al., *Peripheral-neuron-like properties of differentiated human dental pulp stem cells (hDPSCs).* PLoS One, 2021. **16**(5): p. e0251356. 10.1371/journal.pone.0251356.
329. Yamada, Y. and R.A. Prosser, *Copper in the suprachiasmatic circadian clock: A possible link between multiple circadian oscillators.* Eur J Neurosci, 2020. **51**(1): p. 47-70. 10.1111/ejn.14181.
330. Okumoto, K., R. Itoh, N. Shimozawa, Y. Suzuki, S. Tamura, N. Kondo, and Y. Fujiki, *Mutations in PEX10 is the cause of Zellweger peroxisome deficiency syndrome of complementation group B.* Hum Mol Genet, 1998. **7**(9): p. 1399-405. 10.1093/hmg/7.9.1399.
331. Vögtle, F.N. and C. Meisinger, *Mitochondria as emergency landing for abandoned peroxins.* EMBO Rep, 2021. **22**(10): p. e53790. 10.15252/embr.202153790.
332. Sinnema, M., H. Boer, P. Collin, M.A. Maaskant, K.E. van Roozendaal, C.T. Schrander-Stumpel, and L.M. Curfs, *Psychiatric illness in a cohort of adults with Prader-Willi syndrome.* Res Dev Disabil, 2011. **32**(5): p. 1729-35. 10.1016/j.ridd.2011.02.027.
333. Kittel-Schneider, S., T. Wobrock, H. Scherk, T. Schneider-Axmann, S. Trost, et al., *Influence of DGKH variants on amygdala volume in patients with bipolar affective disorder and schizophrenia.* Eur Arch Psychiatry Clin Neurosci, 2015. **265**(2): p. 127-36. 10.1007/s00406-014-0513-9.
334. Matsumoto, Y., A. Suzuki, T. Shirata, N. Takahashi, K. Noto, K. Goto, and K. Otani, *Implication of the DGKH genotype in openness to experience, a premorbid personality trait of bipolar disorder.* J Affect Disord, 2018. **238**: p. 539-541. 10.1016/j.jad.2018.06.031.
335. Baum, A.E., N. Akula, M. Cabanero, I. Cardona, W. Corona, et al., *A genome-wide association study implicates diacylglycerol kinase eta (DGKH) and several other genes in the etiology of bipolar disorder.* Mol Psychiatry, 2008. **13**(2): p. 197-207. 10.1038/sj.mp.4002012.
336. Soni, S., J. Whittington, A.J. Holland, T. Webb, E.N. Maina, H. Boer, and D. Clarke, *The phenomenology and diagnosis of psychiatric illness in people with Prader-Willi syndrome.* Psychol Med, 2008. **38**(10): p. 1505-14. 10.1017/s0033291707002504.

337. Gómez, C., D. Jimeno, A. Fernández-Medarde, R. García-Navas, N. Calzada, and E. Santos, *Ras-GRF2 regulates nestin-positive stem cell density and onset of differentiation during adult neurogenesis in the mouse dentate gyrus.* Mol Cell Neurosci, 2017. **85**: p. 127-147. 10.1016/j.mcn.2017.09.006.
338. Azieva, A.M., A.A. Sheinov, F.A. Galkin, S.G. Georgieva, and N.V. Soshnikova, *Stability of Chromatin Remodeling Complex Subunits Is Determined by Their Phosphorylation Status.* Dokl Biochem Biophys, 2018. **479**(1): p. 66-68. 10.1134/s1607672918020035.
339. Anlar, B. and A. Gunel-Ozcan, *Tenascin-R: role in the central nervous system.* Int J Biochem Cell Biol, 2012. **44**(9): p. 1385-9. 10.1016/j.biocel.2012.05.009.
340. Kim, D.Y., I. Hwang, F.L. Muller, and J.H. Paik, *Functional regulation of FoxO1 in neural stem cell differentiation.* Cell Death Differ, 2015. **22**(12): p. 2034-45. 10.1038/cdd.2015.123.
341. Yap, K., A. Drakew, D. Smilovic, M. Rietsche, M.H. Paul, et al., *The actin-modulating protein synaptopodin mediates long-term survival of dendritic spines.* Elife, 2020. **9**. 10.7554/eLife.62944.
342. Higuchi, M., H. Kiyama, T. Hayakawa, Y. Hamada, and Y. Tsujimoto, *Differential expression of Notch1 and Notch2 in developing and adult mouse brain.* Brain Res Mol Brain Res, 1995. **29**(2): p. 263-72. 10.1016/0169-328x(94)00257-f.
343. Schaffer, A.E., M.W. Breuss, A.O. Caglayan, N. Al-Sanaa, H.Y. Al-Abdulwahed, et al., *Biallelic loss of human CTNNA2, encoding αN-catenin, leads to ARP2/3 complex overactivity and disordered cortical neuronal migration.* Nat Genet, 2018. **50**(8): p. 1093-1101. 10.1038/s41588-018-0166-0.
344. Doherty, E. and A. Perl, *Measurement of Mitochondrial Mass by Flow Cytometry during Oxidative Stress.* React Oxyg Species (Apex), 2017. **4**(10): p. 275-283. 10.20455/ros.2017.839.
345. Clutton, G., K. Mollan, M. Hudgens, and N. Goonetilleke, *A Reproducible, Objective Method Using MitoTracker® Fluorescent Dyes to Assess Mitochondrial Mass in T Cells by Flow Cytometry.* Cytometry Part A, 2019. **95**(4): p. 450-456. https://doi.org/10.1002/cyto.a.23705.
346. Laker, R.C., P. Xu, K.A. Ryall, A. Sujkowski, B.M. Kenwood, et al., *A novel MitoTimer reporter gene for mitochondrial content, structure, stress, and damage in vivo.* The Journal of biological chemistry, 2014. **289**(17): p. 12005-12015. 10.1074/jbc.M113.530527.
347. Gottlieb, R.A. and A. Stotland, *MitoTimer: a novel protein for monitoring mitochondrial turnover in the heart.* J Mol Med (Berl), 2015. **93**(3): p. 271-8. 10.1007/s00109-014-1230-6.
348. de Mello, A.H., A.B. Costa, J.D.G. Engel, and G.T. Rezin, *Mitochondrial dysfunction in obesity.* Life Sci, 2018. **192**: p. 26-32. 10.1016/j.lfs.2017.11.019.
349. Yazdi, P.G., H. Su, S. Ghimbovschi, W. Fan, P.E. Coskun, et al., *Differential gene expression reveals mitochondrial dysfunction in an imprinting center deletion mouse model of Prader-Willi syndrome.* Clin Transl Sci, 2013. **6**(5): p. 347-55. 10.1111/cts.12083.
350. Eiholzer, U., U. Meinhardt, V. Rousson, N. Petrovic, M. Schlumpf, and D. l'Allemand, *Developmental profiles in young children with Prader-Labhart-Willi*

syndrome: effects of weight and therapy with growth hormone or coenzyme Q10. Am J Med Genet A, 2008. **146a**(7): p. 873-80. 10.1002/ajmg.a.32137.
351. Butler, M.G., M. Dasouki, D. Bittel, S. Hunter, A. Naini, and S. DiMauro, *Coenzyme Q10 levels in Prader-Willi syndrome: comparison with obese and non-obese subjects.* Am J Med Genet A, 2003. **119a**(2): p. 168-71. 10.1002/ajmg.a.10055.
352. Iwata, R. and P. Vanderhaeghen, *Regulatory roles of mitochondria and metabolism in neurogenesis.* Curr Opin Neurobiol, 2021. **69**: p. 231-240. 10.1016/j.conb.2021.05.003.
353. Agostini, M., F. Romeo, S. Inoue, M.V. Niklison-Chirou, A.J. Elia, et al., *Metabolic reprogramming during neuronal differentiation.* Cell Death Differ, 2016. **23**(9): p. 1502-14. 10.1038/cdd.2016.36.
354. Khacho, M., A. Clark, D.S. Svoboda, J. Azzi, J.G. MacLaurin, et al., *Mitochondrial Dynamics Impacts Stem Cell Identity and Fate Decisions by Regulating a Nuclear Transcriptional Program.* Cell Stem Cell, 2016. **19**(2): p. 232-247. 10.1016/j.stem.2016.04.015.
355. Homem, C.C.F., V. Steinmann, T.R. Burkard, A. Jais, H. Esterbauer, and J.A. Knoblich, *Ecdysone and mediator change energy metabolism to terminate proliferation in Drosophila neural stem cells.* Cell, 2014. **158**(4): p. 874-888. 10.1016/j.cell.2014.06.024.
356. Inak, G., A. Rybak-Wolf, P. Lisowski, T.M. Pentimalli, R. Jüttner, et al., *Defective metabolic programming impairs early neuronal morphogenesis in neural cultures and an organoid model of Leigh syndrome.* Nat Commun, 2021. **12**(1): p. 1929. 10.1038/s41467-021-22117-z.
357. Panov, J., L. Simchi, Y. Feuermann, and H. Kaphzan, *Bioinformatics Analyses of the Transcriptome Reveal Ube3a-Dependent Effects on Mitochondrial-Related Pathways.* Int J Mol Sci, 2020. **21**(11). 10.3390/ijms21114156.
358. Simchi, L., J. Panov, O. Morsy, Y. Feuermann, and H. Kaphzan, *Novel Insights into the Role of UBE3A in Regulating Apoptosis and Proliferation.* J Clin Med, 2020. **9**(5). 10.3390/jcm9051573.
359. Vatsa, N. and N.R. Jana, *UBE3A and Its Link With Autism.* Front Mol Neurosci, 2018. **11**: p. 448. 10.3389/fnmol.2018.00448.
360. Rahman, S., K. Wittine, M. Sedić, and E.P. Markova-Car, *Small Molecules Targeting Biological Clock; A Novel Prospective for Anti-Cancer Drugs.* Molecules, 2020. **25**(21). 10.3390/molecules25214937.
361. Cha, H.K., S. Chung, H.Y. Lim, J.-W. Jung, and G.H. Son, *Small Molecule Modulators of the Circadian Molecular Clock With Implications for Neuropsychiatric Diseases.* Frontiers in Molecular Neuroscience, 2019. **11**. 10.3389/fnmol.2018.00496.
362. Dibner, C., U. Schibler, and U. Albrecht, *The mammalian circadian timing system: organization and coordination of central and peripheral clocks.* Annu Rev Physiol, 2010. **72**: p. 517-49. 10.1146/annurev-physiol-021909-135821.
363. Poole, J. and D. Ray, *The Role of Circadian Clock Genes in Critical Illness: The Potential Role of Translational Clock Gene Therapies for Targeting Inflammation, Mitochondrial Function, and Muscle Mass in Intensive Care.* J Biol Rhythms, 2022. **37**(4): p. 385-402. 10.1177/07487304221092727.

364. Mezhnina, V., O.P. Ebeigbe, A. Poe, and R.V. Kondratov, *Circadian Control of Mitochondria in Reactive Oxygen Species Homeostasis.* Antioxid Redox Signal, 2022. **37**(10-12): p. 647-663. 10.1089/ars.2021.0274.
365. Kenche, H., M. Singh, J. Smith, and K. Shen, *Neuronal mitochondrial dysfunction in a cellular model of circadian rhythm disruption is rescued by donepezil.* Biochem Biophys Res Commun, 2021. **567**: p. 56-62. 10.1016/j.bbrc.2021.06.029.
366. Rácz, B., M. Dušková, L. Stárka, V. Hainer, and M. Kunešová, *Links between the circadian rhythm, obesity and the microbiome.* Physiol Res, 2018. **67**(Suppl 3): p. S409-s420. 10.33549/physiolres.934020.
367. Engin, A., *Circadian Rhythms in Diet-Induced Obesity.* Adv Exp Med Biol, 2017. **960**: p. 19-52. 10.1007/978-3-319-48382-5_2.
368. Li, Y., J. Ma, K. Yao, W. Su, B. Tan, et al., *Circadian rhythms and obesity: Timekeeping governs lipid metabolism.* J Pineal Res, 2020. **69**(3): p. e12682. 10.1111/jpi.12682.
369. de Goede, P., J. Wefers, E.C. Brombacher, P. Schrauwen, and A. Kalsbeek, *Circadian rhythms in mitochondrial respiration.* J Mol Endocrinol, 2018. **60**(3): p. R115-r130. 10.1530/jme-17-0196.
370. Liu, C., S. Li, T. Liu, J. Borjigin, and J.D. Lin, *Transcriptional coactivator PGC-1alpha integrates the mammalian clock and energy metabolism.* Nature, 2007. **447**(7143): p. 477-81. 10.1038/nature05767.
371. Panda, S., M.P. Antoch, B.H. Miller, A.I. Su, A.B. Schook, et al., *Coordinated transcription of key pathways in the mouse by the circadian clock.* Cell, 2002. **109**(3): p. 307-20. 10.1016/s0092-8674(02)00722-5.
372. Mercer, R.E., S.D. Michaelson, M.J. Chee, T.A. Atallah, R. Wevrick, and W.F. Colmers, *Magel2 is required for leptin-mediated depolarization of POMC neurons in the hypothalamic arcuate nucleus in mice.* PLoS Genet, 2013. **9**(1): p. e1003207. 10.1371/journal.pgen.1003207.
373. Malik, A., R.V. Kondratov, R.J. Jamasbi, and M.E. Geusz, *Circadian Clock Genes Are Essential for Normal Adult Neurogenesis, Differentiation, and Fate Determination.* PLoS One, 2015. **10**(10): p. e0139655. 10.1371/journal.pone.0139655.
374. Bouchard-Cannon, P., L. Mendoza-Viveros, A. Yuen, M. Kærn, and H.-Ying M. Cheng, *The Circadian Molecular Clock Regulates Adult Hippocampal Neurogenesis by Controlling the Timing of Cell-Cycle Entry and Exit.* Cell Reports, 2013. **5**(4): p. 961-973. https://doi.org/10.1016/j.celrep.2013.10.037.
375. Moriya, T., N. Horie, M. Mitome, and K. Shinohara, *Melatonin influences the proliferative and differentiative activity of neural stem cells.* J Pineal Res, 2007. **42**(4): p. 411-8. 10.1111/j.1600-079X.2007.00435.x.
376. Chen, X., X. Li, Z. Du, W. Shi, Y. Yao, et al., *Melatonin promotes the acquisition of neural identity through extracellular-signal-regulated kinases 1/2 activation.* J Pineal Res, 2014. **57**(2): p. 168-76. 10.1111/jpi.12153.
377. Butler, M.G., D.T. Brandau, M.F. Theodoro, and U. Garg, *Morning melatonin levels in Prader-Willi syndrome.* Am J Med Genet A, 2009. **149a**(8): p. 1809-13. 10.1002/ajmg.a.33001.

378. Wong, S.D., K.P. Wright, Jr., R.L. Spencer, C. Vetter, L.M. Hicks, O.G. Jenni, and M.K. LeBourgeois, *Development of the circadian system in early life: maternal and environmental factors.* J Physiol Anthropol, 2022. **41**(1): p. 22. 10.1186/s40101-022-00294-0.
379. Blomqvist, M., K. Ahlberg, J. Lindgren, S. Ferdinandusse, and J. Asin-Cayuela, *Identification of a novel mutation in PEX10 in a patient with attenuated Zellweger spectrum disorder: a case report.* J Med Case Rep, 2017. **11**(1): p. 218. 10.1186/s13256-017-1365-5.
380. Le Rumeur, E., *Dystrophin and the two related genetic diseases, Duchenne and Becker muscular dystrophies.* Bosn J Basic Med Sci, 2015. **15**(3): p. 14-20. 10.17305/bjbms.2015.636.
381. Tzifi, F., R. Pons, C. Athanassaki, M. Poulou, and E. Kanavakis, *Congenital cataracts, facial dysmorphism, and neuropathy syndrome.* Pediatr Neurol, 2011. **45**(3): p. 206-8. 10.1016/j.pediatrneurol.2011.05.008.
382. Lipton, J.O. and M. Sahin, *The neurology of mTOR.* Neuron, 2014. **84**(2): p. 275-91. 10.1016/j.neuron.2014.09.034.
383. Tümer, Z. and L.B. Møller, *Menkes disease.* Eur J Hum Genet, 2010. **18**(5): p. 511-8. 10.1038/ejhg.2009.187.
384. Bridgman, P.C., *Myosin-dependent transport in neurons.* J Neurobiol, 2004. **58**(2): p. 164-74. 10.1002/neu.10320.
385. Castro-Mondragon, J.A., R. Riudavets-Puig, I. Rauluseviciute, R.B. Lemma, L. Turchi, et al., *JASPAR 2022: the 9th release of the open-access database of transcription factor binding profiles.* Nucleic Acids Res, 2022. **50**(D1): p. D165-d173. 10.1093/nar/gkab1113.

APPENDIX A. SUPPLEMENTARY FIGURES AND TABLES

Table A-1. Cell lines used for RNAseq and immunocytochemistry analysis.

Cell Line	Diagnosis	Sex	ASD Status
38*	N/A	F	Unknown
182*	N/A	F	Normal
189*	N/A	F	Unknown
238*	N/A	M	Normal
195	N/A	M	Normal
312	N/A	M	Normal
152*	PW-del	M	Normal
192*	PW-del	F	Normal
225*	PW-del	M	Normal
258*	PW-del	F	Normal
148	PW-del	M	Normal
307	PW-del	F	Normal
156*	PW-UPD	F	Normal
162*	PW-UPD	F	Normal
171*	PW-UPD	F	Normal
249*	PW-UPD	F	Normal
270	PW-UPD	F	Normal
191	PW-UPD	M	Normal
235	PW-UPD	M	Normal
197	PW-UPD	M	Normal
94*	PW-UPD	F	Possible ASD
228*	PW-UPD	M	Possible ASD
250*	PW-UPD	M	Possible ASD
268*	PW-UPD	F	Possible ASD
277	PW-UPD	F	Possible ASD
181	PW-UPD	M	Possible ASD

Asterisk (*) denotes subjects used in RNAseq experiment. Prader-Willi syndrome deletion subtype (PW-del), Prader-Willi syndrome uniparental disomy subtype (PW-UPD).

Table A-2. Core PWS transcripts outside of the 15q11.2-13 region that were significantly different versus control in all PWS subgroups.

Gene	Function	Link to PWS
PEX10	Peroxisomes breakdown toxins and synthesize lipids	Mutations lead to Zellweger syndrome. Primary phenotypes of Zellweger syndrome are hypotonia and neurodevelopmental delay [379]
SNTB2	Plays a role in regulation of secretory granules and localization of membrane proteins	Dystrophins are associated with muscular dystrophy [380]
CTDP1	Dephosphorylates a subunit of RNApol making it available for transcription	Mutations are associated with neuropathy, facial dysmorphism, and cataracts [381]
AKT1S1	Subunit of mTORC, which regulates cell growth in response to nutrients and hormonal signaling	Altered mTORC signaling has been linked to a variety of neurological disorders including autism, epilepsy, and neurodegenerative disorders [382]
ATP7A	Supplies copper to copper requiring proteins in the secretory pathway	Associated with Menkes disease [383]. Primary phenotypes are hypotonia, hypothermia, failure to thrive, and seizures.
MYL5	Component of ATPase cellular motor protein myosin	Myosin has many neuronal functions, particularly at the synapse [384]
MIPOL1	Function is not well characterized	Link to hand and feet abnormalities
TMEM92	Transmembrane protein with unknown function	Unknown
DHRS1	Functions as an oxidoreductase	Associated with speech/ language impairment

Prader-Will syndrome (PWS).

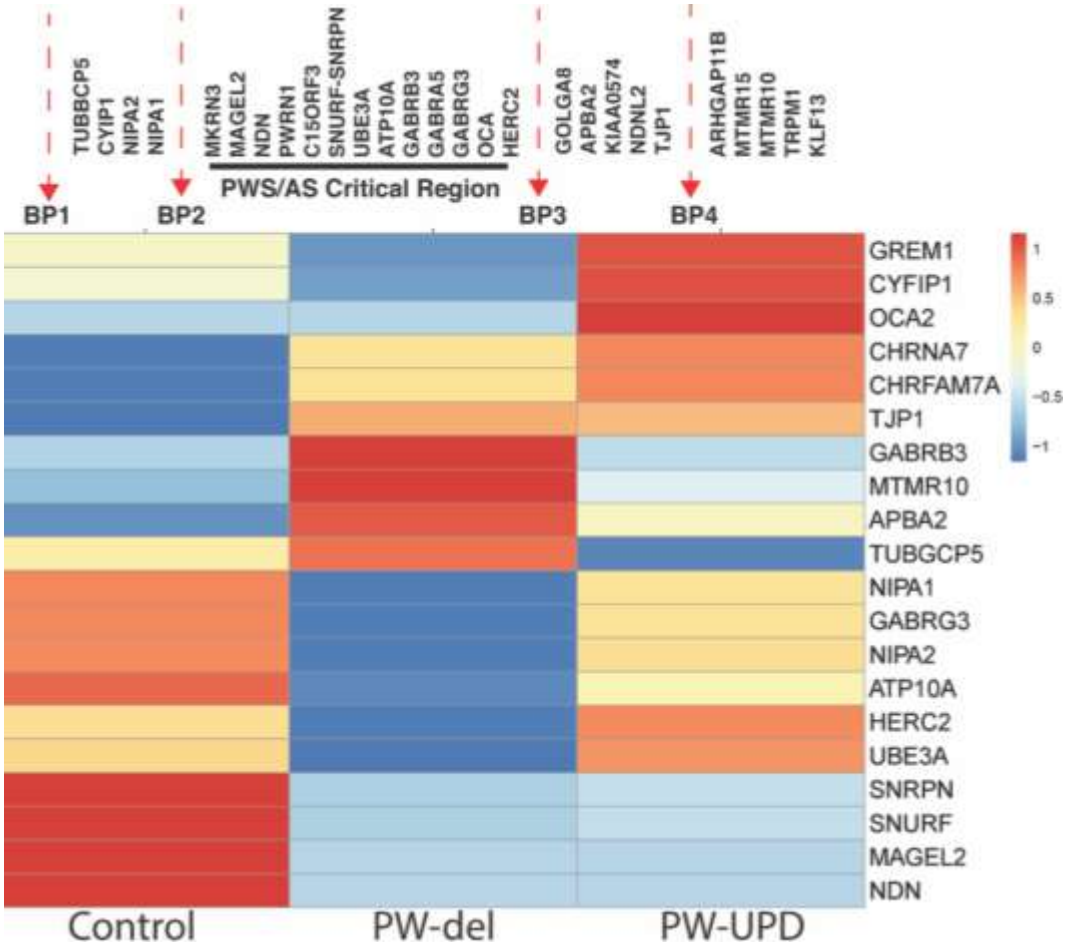

Figure A-1. Genes in the 15q11.2-q13 critical region shows expected PWS imprinted expression.

Across the PWS/AS critical region, maternally imprinted genes such as *MAGEL2*, *SNRPN*, and *SNURF* showed decreased expression in both PW-del and PW-UPD neurons. Angelman syndrome (AS), Prader-Willi syndrome (PWS), Prader-Willi syndrome deletion subtype (PW-del), Prader-Willi syndrome uniparental disomy subtype (PW-UPD).

Table A-3. List of genes identified in DAVID mitochondrial enrichment categories.

Gene	Full Name	Function
ACOT9	Acyl-CoA Thioesterase 9	Mitochondrial acyl-CoA thioesterase
AGPAT5	1-Acylglycerol-3-Phosphate O-Acyltransferase 5	Expressed in mitochondria
AIFM1	Apoptosis Inducing Factor Mitochondria Associated 1	NADH oxidoreductase found in the mitochondrial intermembrane space
BNIP1	BCL2 Interacting Protein 1	Involved in mitophagy
CLTC	Clathrin Heavy Chain	Expressed in mitochondria
CMC4	C-X9-C Motif Containing 4	Expressed in mitochondria
COX5B	Cytochrome C Oxidase Subunit 5B	Component of the electron transport chain
COX7B	Cytochrome C Oxidase Subunit 7B	Component of the electron transport chain
COX7C	Cytochrome C Oxidase Subunit 7C	Component of the electron transport chain
CS	Citrate Synthase	TCA cycle enzyme
CYB5A	Cytochrome B5 Type A	Electron carrier expressed in mitochondria
EHHADH	Enoyl-CoA Hydratase And 3-Hydroxyacyl CoA Dehydrogenase	Involved in mitochondrial fatty acid oxidation
FDXR	Ferredoxin Reductase	Mitochondrial flavoprotein involved in the electron transport chain
GFM1	G Elongation Factor Mitochondrial 1	Mitochondrial translation elongation factor
GHR	Growth Hormone Receptor	Expressed in mitochondria
GLUD1	Glutamate Dehydrogenase 1	Mitochondrial matrix enzyme
GPX1	Glutathione Peroxidase 1	Protects cells from oxidative stress
GSTP1	Glutathione S-Transferase Pi 1	Protects cells from oxidative stress
HAP1	Huntingtin Associated Protein 1	Expressed in mitochondria
MFN2	Mitofusin 2	Involved in mitochondrial fusion and maintenance of the mitochondial matrix
MINOS1	Mitochondrial Contact Site And Cristae Organizing System Subunit 10	Involved in the maintenance of mitochondrial architecture
MRPL4	Mitochondrial Ribosomal Protein L4	Component of the mitochondrial ribosomal 39S subunit
MRPL41	Mitochondrial Ribosomal Protein L41	Component of the mitochondrial ribosomal 39S subunit
MRPL47	Mitochondrial Ribosomal Protein L47	Component of the mitochondrial ribosomal 39S subunit
MRPS33	Mitochondrial Ribosomal Protein S33	Component of the mitochondrial ribosomal 28S subunit

Table A-3. Cont.

Gene	Full Name	Function
MRPS5	Mitochondrial Ribosomal Protein S5	Component of the mitochondrial ribosomal 28S subunit
MTIF2	Mitochondrial Translational Initiation Factor 2	Mitochondrial translation intitation factor
NAXE	NAD(P)HX Epimerase	Involved in mitochondrial metabolic processes
NDUFA1	NADH:Ubiquinone Oxidoreductase Subunit A1	Component of the electron transport chain
NDUFV2	NADH:Ubiquinone Oxidoreductase Core Subunit V2	Component of the electron transport chain
NFS1	Cysteine Desulfurase, Mitochondrial	Expressed in mitochondria
NT5M	5',3'-Nucleotidase, Mitochondrial	5' nucleotidase localized to the mitochondrial matrix
OAT	Ornithine Aminotransferase	Mitochondrial enzyme ornithine aminotransferase
OXLD1	Oxidoreductase Like Domain Containing 1	Expressed in mitochondria
PERP	P53 Apoptosis Effector Related To PMP22	Expressed in mitochondria
POR	Cytochrome P450 Oxidoreductase	Enzyme involved in electron transport
PRKAR2B	Protein Kinase CAMP-Dependent Type II Regulatory Subunit Beta	Plays a role in regulating energy balance
RMND1	Required For Meiotic Nuclear Division 1 Homolog	Involved in mitochondrial translation
SDHC	Succinate Dehydrogenase Complex Subunit C	Component of the electron transport chain
SDHD	Succinate Dehydrogenase Complex Subunit D	Component of the electron transport chain
SLC25A36	Solute Carrier Family 25 Member 36	Mitochondrial transport protein
SLC25A39	Solute Carrier Family 25 Member 39	Mitochondrial transport protein
SLC25A5	Solute Carrier Family 25 Member 5	Mitochondrial transport protein
SLC35F6	Solute Carrier Family 35 Member F6	Involved in the maintenance of mitochondrial membrane potential
SUCLG2	Succinate-CoA Ligase GDP-Forming Subunit Beta	TCA cycle enzyme
SYNE2	Spectrin Repeat Containing Nuclear Envelope Protein 2	Expressed in mitochondria
TIMM17A	Translocase Of Inner Mitochondrial Membrane 17A	Mitochondrial transport protein
TMEM160	Transmembrane Protein 160	Expressed in mitochondria

Table A-3. Cont.

TMTC1	Transmembrane O-Mannosyltransferase Targeting Cadherins 1	Expressed in mitochondria
TP63	Tumor Protein P63	Expressed in mitochondria
TUFM	Tu Translation Elongation Factor, Mitochondrial	Mitochondrial translation elongation factor
TXN	Thioredoxin	Involved in redox reactions
UQCR10	Ubiquinol-Cytochrome C Reductase, Complex III Subunit X	Component of the electron transport chain
UQCR11	Ubiquinol-Cytochrome C Reductase, Complex III Subunit XI	Component of the electron transport chain
UQCRC2	Ubiquinol-Cytochrome C Reductase Core Protein 2	Component of the electron transport chain
UQCRFS1	Ubiquinol-Cytochrome C Reductase, Rieske Iron-Sulfur Polypeptide 1	Component of the electron transport chain
UQCRH	Ubiquinol-Cytochrome C Reductase Hinge Protein	Component of the electron transport chain
USP30	Ubiquitin Specific Peptidase 30	Involved in mitophagy

Database for Annotation, Visualization and Integrated Discovery (DAVID).

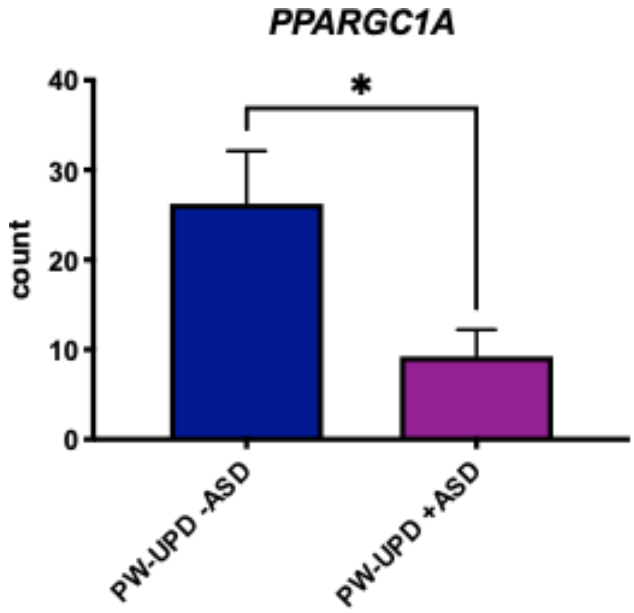

Figure A-2. Expression of mitochondrial biogenesis factor, *PPARGC1A*, is significantly decreased in PW-UPD +ASD neurons.
Mean RNAseq count for each group is shown in the graph. Significance was determined by an unpaired *t*-test. * = *p*-value $\leq$ 0.05. Prader-Willi syndrome uniparental disomy subtype (PW-UPD), autism spectrum disorder (ASD).

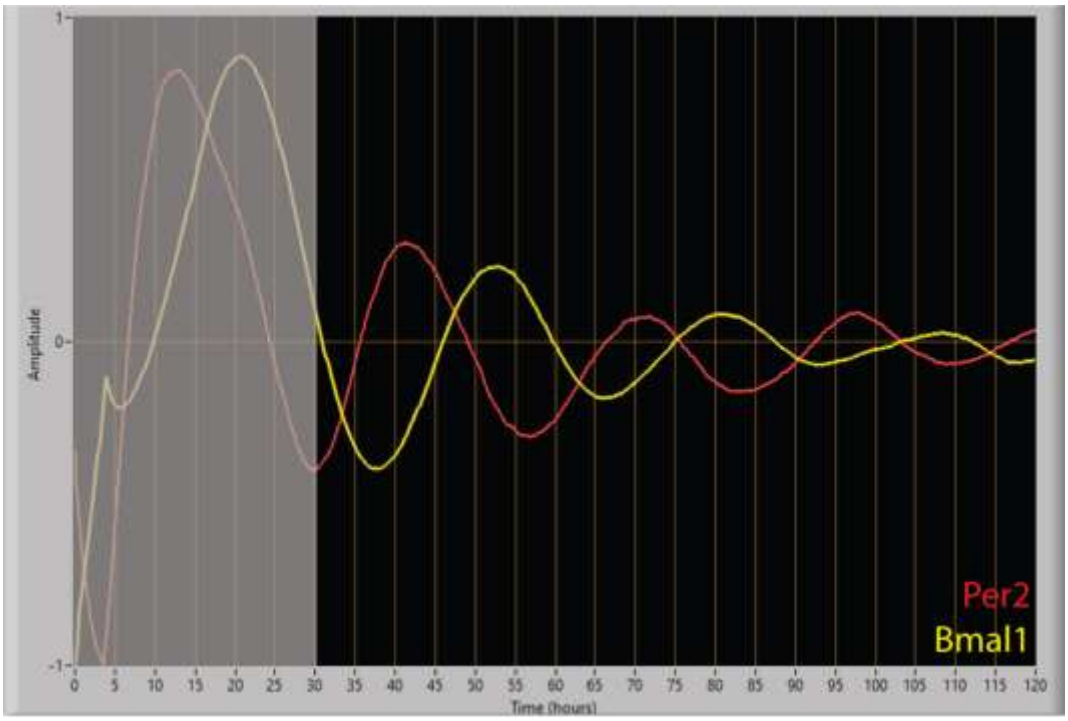

Figure A-3. *Bmal1* and *Per2* show anti-phasic expression across time in SYS neurons.
Per2:Luciferase (red trace) and Bmal1:Luciferase (yellow trace) are CLOCK-controlled genes that negatively regulate each other. *Per2* and *Bmal1* show the expected anti-phasic expression across time in SYS subjects. Schaaf-Yang syndrome (SYS).

Table A-4. Genes identified during enrichment analysis and their function.

Gene	Gene Summary	Enrichment Category
ABCB9	Encodes for ATP-dependent low-affinity peptide transporter which translocates a broad spectrum of peptides from the cytosol to the lysosomal lumen for degradation.	ATPase-coupled transmembrane transporter activity
ABCD4	Encodes for a lysosomal membrane protein that transports cobalamin (Vitamin B12) from the lysosomal lumen to the cytosol in an ATP-dependent manner.	ATPase-coupled transmembrane transporter activity
ATP6V1G2	Encodes for a a component of vacuolar ATPase (V-ATPase), a multisubunit enzyme that mediates acidification of intracellular compartments of eukaryotic cells.	ATPase-coupled transmembrane transporter activity
B3GALNT1	Encodes for a member of the beta-1,3-galactosyltransferase family. Plays a role in the preimplantation stage of embryonic development.	Acetylglucosaminyltransferase activity
GCNT3	Encodes for a Glycosyltransferase that can synthesize all known mucin beta 6 N-acetylglucosaminides.	Acetylglucosaminyltransferase activity
HLA-A	Encodes for Antigen-presenting major histocompatibility complex class I (MHCI) molecule. Class I molecules play a central role in the immune system by presenting peptides derived from the endoplasmic reticulum lumen so that they can be recognized by cytotoxic T cells.	Phagocytic vesicle membrane
LFNG	Encodes for a glycosyltransferase that initiates the elongation of O-linked fucose residues attached to EGF-like repeats in the extracellular domain of Notch molecules.	Acetylglucosaminyltransferase activity
MGAT1	Encodes for a glycosyltransferase that initiates complex N-linked carbohydrate formation.	Acetylglucosaminyltransferase activity
PIKFYVE	Encodes for Dual specificity kinase implicated in myriad essential cellular processes such as maintenance of endomembrane homeostasis, and endocytic-vacuolar pathway, lysosomal trafficking, nuclear transport, stress- or hormone-induced signaling and cell cycle progression.	Phagocytic vesicle membrane
TAPBP	Encodes a transmembrane glycoprotein which mediates interaction between newly assembled major histocompatibility complex (MHC) class I molecules and the transporter associated with antigen processing (TAP), which is required for the transport of antigenic peptides across the endoplasmic reticulum membrane.	Phagocytic vesicle membrane
TCIRG1	Encodes a subunit of a large protein complex known as a vacuolar H+-ATPase (V-ATPase). The protein complex acts as a pump to move protons across the membrane. This movement of protons helps regulate the pH of cells and their surrounding environment.	Phagocytic vesicle membrane and ATPase-coupled transmembrane transporter activity

Data Source: Safran, M., Rosen, N., Twik, M., BarShir, R., Stein, T. I., Dahary, D., Fishilevich, S., and Lancet, D. (2021) The GeneCards Suite. In *Practical Guide to Life*

Table A-4. Cont.

Science Databases (Abugessaisa, I., and Kasukawa, T., eds) pp. 27-56, Springer Nature Singapore, Singapore.

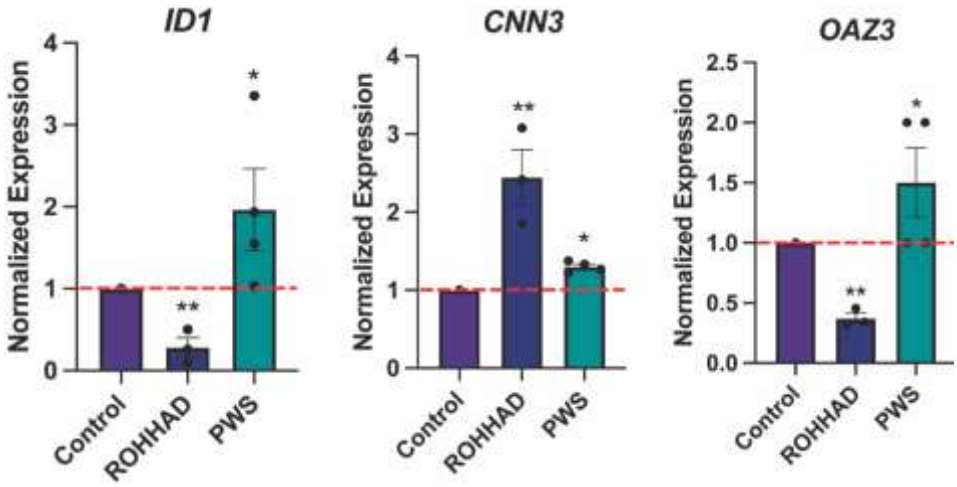

Figure A-4. Significantly differentially expressed genes in common for ROHHAD and PWS versus control subjects.

RNAseq data from the experiment presented here and our previously published RNAseq data for PWS versus control neurons [26] were analyzed for overlapping genes unique to ROHHAD and PWS versus control neurons (p-value $\leq$ 0.05, FDR $\leq$ 0.05, fold-change $\leq$0.5 or $\geq$1.5). Bar graphs represent average RNAseq expression for each group across the three 3 these genes. Expression was normalized to the average of the control expression in each study. The dashed red line indicates control expression level. None of these genes have an obvious role in the obesity phenotype shared by PWS and ROHHAD. Significance determined by a Wilcoxon's t-test for control versus ROHHAD and PWS. * = p-value $\leq$ 0.05, ** = p-value $\leq$ 0.01. Rapid-onset obesity with hypothalamic dysfunction, hypoventilation, and autonomic dysfunction (ROHHAD), Prader-Willi syndrome (PWS).

Table A-5. Differentially expressed genes versus control for ROHHAD and CCHS neurons.

Gene Name	Gene Summary
ADAM8	Encodes for an ADAM (a disintegrin and metalloprotease domain) family member, involved in cell adhesion during neurodegeneration and a target for allergic respiratory diseases.
ADIRF	Adipose Regulatory Factor protein encoding gene. Involved in PPARA gene expression and the development of the nervous system.
ADORA2A	Encodes for a guanine nucleotide-binding protein-coupled receptor (GPCR) family member. Utilizes adenosine as its endogenous agonist to increase intracellular cAMP levels. Maintains proper cardiac rhythm and circulation, cerebral and renal blood flow, immune function, pain regulation, and sleep.
ANKRD29	Gene encoding for the Ankyrin Repeat Domain-Containing Protein 29 (ANKRD29) and thought to be an integral membrane component.
ASCC1	Encodes for Activating Signal Cointegrator 1 Complex Subunit 1. ASC-1 plays a vital role in gene transactivation by multiple transcription factors. Mutations are associated with Barrett esophagus and esophageal adenocarcinoma.
ATP6V1G2	Encodes for ATPase H+ Transporting V1 Subunit G2. Multisubunit enzyme mediating acidification of intracellular compartments of eukaryotic cells. This process is needed for protein sorting, zymogen activation, receptor-mediated endocytosis, and synaptic vesicle proton gradient generation.
B3GALNT1	Encodes for a member of the beta-1,3-galactosyltransferase family. Plays a role in the preimplantation stage of embryonic development.
CAPN15	Encodes for Calpain 15, a protein that acts as a transcription factor, RNA-binding protein, and protein-protein interactions during development of the visual system.
CAPS	Encodes for the protein Calcyphosine, a calcium-binding protein involved in regulation of ion transport.
CD109	Encodes for the glycosyl phosphatidylinositol (GPI)-linked glycoprotein, CD109, acting as a negative regulator of TGF-β signaling.
CNKSR3	Encodes for Connector Enhancer of Kinase Suppressor of Ras 3. Involved in the negative regulation of the ERK1 and ERK2 cascade, peptidyl-serine phosphorylation, and the positive regulation of Na+ transport.
COL13A1	Encodes for the nonfibrillar collagen, Collagen Type XIII Alpha 1 Chain, and is found in all connective tissue-producing cells. It possesses a transmembrane domain and is documented to localize to the plasma membrane.
CRYBG1	Encodes for the Crystallin Beta-Gamma Domain Containing 1 protein and is associated with Melanoma.
DNASE1	Encodes for Deoxyribonuclease 1. Mutations are associated with Systemic Lupus Erthematosus.
DUOX1	Encodes for Dual Oxidase 1, a glycoprotein family member of the NADPH oxidase family.
EPS8L2	Encodes for EPS8 family member, EPS8 Like 2. Mutations are associated with deafness and is involved in the olfactory signaling pathway and sound sensory processing.
FBH1	Encodes for the F-Box DNA Helicase 1 protein.
FGR	Encodes for the FGR Proto-Oncogene, an Src Family Tyrosine Kinase. Functions as a negative regulator of cell migration and adhesion triggered by the beta-2 integrin signal transduction pathway.
FOXK1	Encodes for the Forkhead Box K1 protein that has DNA-binding transcription repressor activity, and involved in processes such as glucose metabolism, aerobic glycolysis, muscle cell differentiation and autophagy.

Table A-5. Cont.

Gene Name	Gene Summary
GSN	Encodes for Gelsolin, an actin-depolymerizing factor that binds to actin monomers and filaments to prevent monomer exchange. Associated with Amyloidosis and Amyloidosis, Finnish Type.
HEXIM2	Encodes for Hexamethylene Bis-Acetamide-Inducible Protein 2. Negatively regulates the kinase activity of the cyclin-dependent kinase P-TEFb.
HHIPL1	Encodes for the HHIP Like 1 protein that belongs to the glucose/sorbosone dehydrogenase family. Also contains a folate and reduced folic acid derivative binding domain.
IL12A	Encodes for Interleukin 12A, a cytokine subunit.
INPP5F	Encodes for the Inositol Polyphosphate-5-Phosphatase F. Activity is specific for phosphatidylinositol 4,5-bisphosphate and phosphatidylinositol 3,4,5-trisphosphate.
KAT6B	Encodes for the Lysine Acetyltransferase 6 B, a component of the MOZ/MORF complex. Required for RUNX2-dependent transcriptional activation and potentially involved in brain development. Mutations are associated with acute myeloid leukemias.
LAPTM5	Encodes for the Lysosomal-Associated Multitransmembrane Protein 5. May play a role in hematopoiesis.
LCOR	Encodes for the Ligand Dependent Nuclear Receptor Corepressor protein. Expressed in fetal and adult tissues. Associated with Breast Medullary Carcinoma and Uterus Carcinoma.
LYPD3	Encodes for LY6/PLAUR Domain Containing 3 protein that acts upstream or within cell-matrix adhesion.
MPV17L	Encodes for the Mitochondrial Inner Membrane Protein 17 Like protein, a negative regulator of the hydrogen peroxide biosynthetic process and mitochondrial outer membrane permeabilization involved in apoptotic signaling pathway.
MUC4	Encodes for Mucin 4, one of the major constituents of mucus, covering epithelial surfaces.
MYO18A	Encodes for the Myosin XVIIIA protein. Binds to GOLPH3, linking the Golgi to the cytoskeleton and influencing Golgi membrane trafficking, may also be required for cell migration.
NETO1	Encodes for the Neuropilin And Tolloid Like 1 protein. Thought to play a role in Hippocampal spatial learning and memory through regulation of synaptic N-methyl-D-aspartic acid receptor complexes.
NPIPB5	Encodes for the Nuclear Pore Complex Interacting Protein Family Member B5 protein.
OTUB2	Encodes for the OUT Deubiquitinase, Ubiquitin Aldehyde Binding 2 protein. Involved in protein metabolism.
PAIP2B	Encodes for Poly(A) Binding Protein Interacting Protein 2B. Enhances translation by circularizing mRNA through EIF4G1 translation initiation factor interaction.
PAK4	Encodes for P21 (RAC1) Activated Kinase 4 and acts as an effector to link Rho GTPases to the cytoskeleton during reorganization and nuclear signaling.
PHACTR1	Encodes for Phosphatase And Actin Regulator 1 protein. Functions by binding actin and regulating the actin cytoskeleton reorganization.
PML	Encodes for the PML Nuclear Body Scaffold protein, a member of the tripartite motif (TRIM) family. Functions as a transcription factor and tumor suppressor.
PPFIBP2	Encodes for PPFIA Binding Protein 2, member of the LAR protein-tyrosine phosphatase-interacting protein (Liprin) family. Plays part in axonal guidance and neuronal synapse development by LAR protein-tyrosine phosphatase plasma membrane recruitment.
PRR19	Encodes for Proline Rich 19 protein that promotes meiotic crossing over formation through CNTD1 interaction.

Table A-5. Cont.

Gene Name	Gene Summary
PTPRU	Encodes for Protein Tyrosine Phosphatase Receptor Type U, a protein tyrosine phosphatase (PTP) family member. PTPs are known to regulate cell growth, differentiation, mitotic cycle, and oncogenic transformation through signaling.
RELCH	Encodes for RAB11 Binding And LisH Domain, Coiled-Coil And Heat Repeat Containing protein. Involved in intracellular cholesterol transport.
RIN3	Encodes for Ras And Rab Interactor 3 protein and acts as a binding partner to RAB5 small GTPases.
RNF32	Encodes for Ring Finger Protein 32. RING finger motifs are observed in functionally different proteins involved in protein-DNA or protein-protein interactions. Expressed during spermatogenesis.
RPUSD1	Encodes for the RNA Pseudouridine Synthase Domain Containing 1 protein. Thought to be involved in enzyme-directed rRNA pseudouridine synthesis and enable pseudouridine synthase activity.
SLC26A11	Encodes for the Solute Carrier Family 26 Member 11 protein. Family members are crucial for cellular homeostasis and intracellular electrolyte balance.
SPDYE2	Encodes for Speedy/RINGO Cell Cycle Regulator Family Member E2. Thought to enable protein kinase binding activity.
SPDYE2B	Encodes for Speedy/RINGO Cell Cycle Regulator Family Member E2B. Thought to enable protein kinase binding activity.
SPDYE6	Encodes for Speedy/RINGO Cell Cycle Regulator Family Member E6. Plays a role in cell cycle progression through binding and activation of cylin-dependent kinases.
SYTL3	Encodes for the Synaptotagmin Like 3 protein. Functions by binding to phospholipids in the presence of Ca^{2+} ions.
TANGO2	Encodes for the Transport And Golgi Organization 2 Homolog protein. Thought to play a role in secretory protein loading in the endoplasmic reticulum.
TBC1D3C	Encodes for TBC1 Domain Family Member 3C. Thought to be involved in GTPase signaling and vesicle trafficking.
TBC1D3E	Encodes for TBC1 Domain Family Member 3E. Thought to be involved in the activation of GTPase activity and intracellular protein transport.
TFAP4	Encodes for the Transcription Factor AP-4 protein. Activated both viral and cellular genes by binding to symmetrical CAGCTG DNA sequences.
ZNF18	Encodes for Zinc Finger Protein 18. Has RNA polymerase II-specific and RNA polymerase II-cis regulatory region sequence-specific DNA binding activity. Thought to regulate transcription by RNA polymerase II.
ZNF148	Encodes for Zinc Finger Protein 148. Activates transcription of T-cell receptor and intestinal alkaline phosphatase genes. Mutations have been associated with global developmental delay, hypoplastic corpus callosum, and dysmorphic facies.
ZNF567	Encodes for Zinc Finger Protein 567. Thought to enable DNA-binding transcription factor activity and have RNA polymerase II-cis regulatory region sequence-specific DNA binding activity.
ZNF782	Encodes for Zinc Finger Protein 782. Thought to enable DNA-binding transcription factor activity, RNA polymerase II-specific and RNA polymerase II-cis regulatory region sequence-specific DNA binding activity.

Rapid-onset obesity with hypothalamic dysfunction, hypoventilation, and autonomic dysfunction (ROHHAD), Congenital Central Hypoventilation syndrome (CCHS). *Data Source*: Safran, M., Rosen, N., Twik, M., BarShir, R., Stein, T. I., Dahary, D., Fishilevich, S., and Lancet, D. (2021) The GeneCards Suite. In *Practical Guide to Life*

Table A-5. Cont.

Science Databases (Abugessaisa, I., and Kasukawa, T., eds) pp. 27-56, Springer Nature Singapore, Singapore.

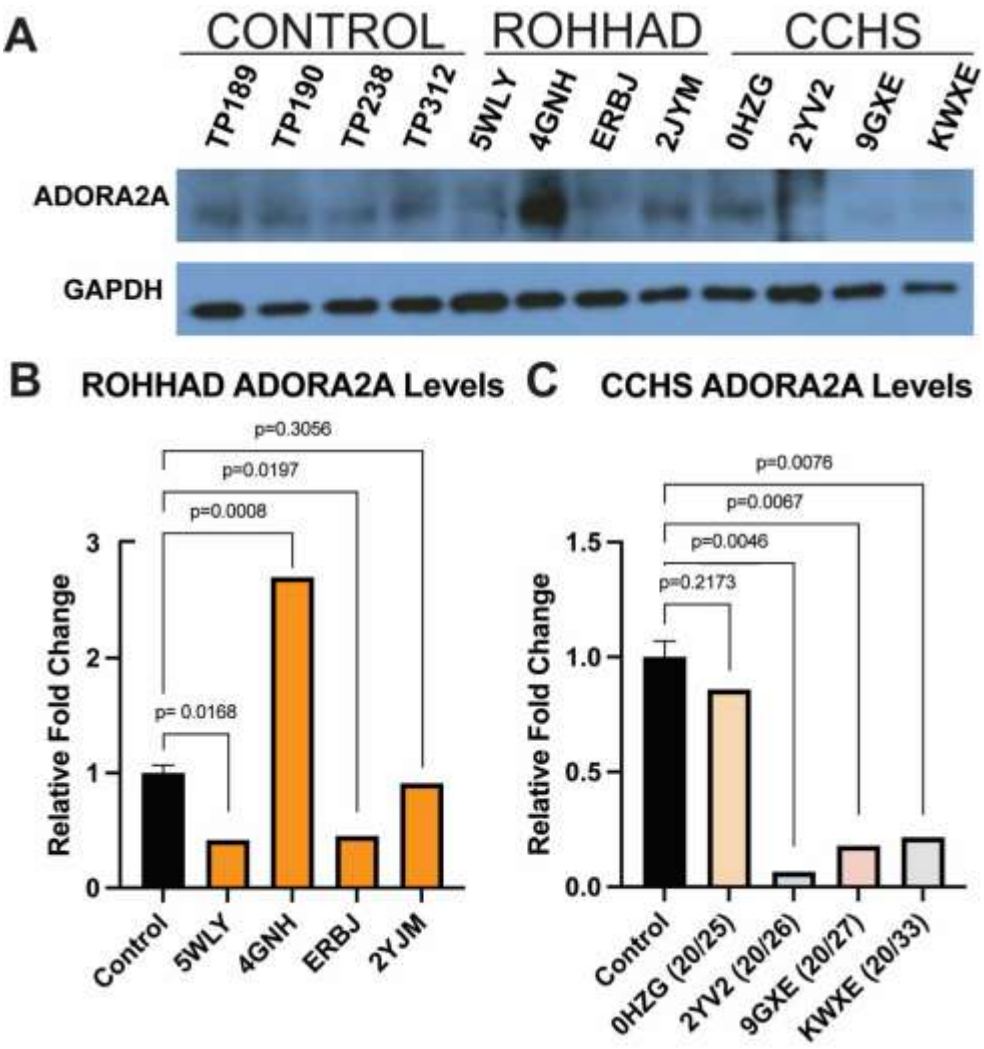

Figure A-5. Western blot analysis of ADORA2A levels in ROHHAD and CCHS DPSC-derived neurons.

(A) ECL western blot of ADORA2A in Control, ROHHAD, and CCHS groups. An average of all four controls was used for normalization and comparison against each of the four individual ROHHAD and the four individual CCHS cell lines. The graphs were scaled differently for ROHHAD versus CCHS comparisons, but the same control samples and averages were used in B and C. **(B)** Quantification of ADORA2A protein in ROHHAD individuals. 5WLY and ERBJ show a significant reduction, 4GNH shows increased ADORA2A protein, and 2JYM is statistically unchanged. **(C)** ADORA2A quantification in CCHS individuals. ADORA2A expression in 0HZG (20/25) is reduced but not significantly. 2YV2 (20/26), 9GXE (20/27) and KWXE (20/33) show a significant reduction in ADORA2A protein. Dental pulp stem cells (DPSC), Enhanced chemiluminescence (ECL), Rapid-onset obesity with hypothalamic dysfunction, hypoventilation, and autonomic dysfunction (ROHHAD), Congenital Central Hypoventilation syndrome (CCHS).

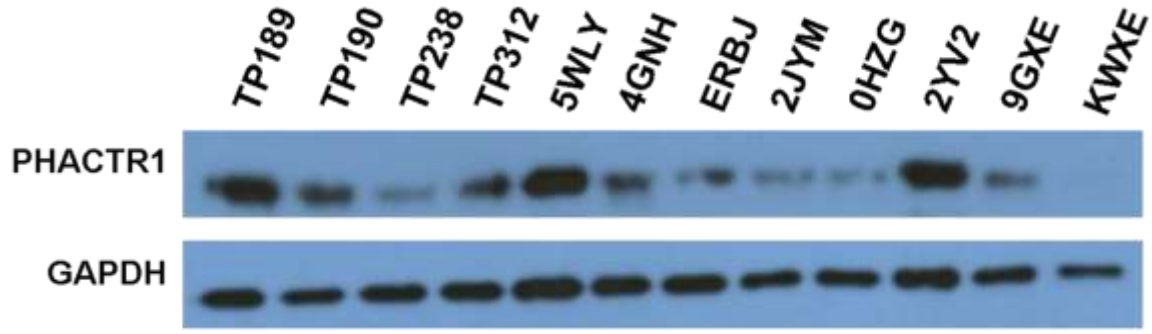

Figure A-6. Western blot analysis of PHACTR1 levels in ROHHAD and CCHS DPSC-derived neurons.

ECL western blot of PHACTR1 in Neurotypical Control (TP189, TP190, TP238, TP312), ROHHAD (5WLY, 4GNH, ERBJ, 2JYM), and CCHS (0HZG, 2YV2, 9GXE, KWXE) subjects. There was no consistent change of PHACTR1 amongst the controls, ROHHAD, and CCHS groups, although some individual subjects did show differing expression versus the average control values. Enhanced chemiluminescence (ECL), Rapid-onset obesity with hypothalamic dysfunction, hypoventilation, and autonomic dysfunction (ROHHAD), Congenital Central Hypoventilation syndrome (CCHS), dental pulp stem cell (DPSC).

Figure A-7. Graphic of the *ADORA2A* gene region on chr22 taken from the UCSC Genome Browser on Human (GRCh38/hg38).

The first exon of Isoform II of *ADORA2A* sits above a predicted promotor region by ENCODE cCRE (Candidate Cis-Regulatory Elements) and is in a region of open chromatin conformation as predicted by increased H3K27Ac (red bar, data from the Bernstein Lab at the Broad Institute). There are two predicted PHOX2B binding sites in this promotor region as well [385]. Homology to the consensus motif for PHOX2B is shown below the predicted binding sites in the genome browser image. University of California, Santa Cruz (UCSC).

Table A-6. Differentially expressed genes versus neurotypical controls in PW-UPD neurons.

Gene	Function
ATF7IP	Encodes a nuclear protein that acts as a transcriptional coactivator or corepressor.
ATPAF2	Encodes an assembly factor that plays a role in the assembly of mitochondrial ATP synthase.
ATP6V1B1	Encodes a component of vacuolar ATPase.
BBX	Encodes a transcription factor necessary for cell cycle progression.
CD2AP	Encodes a scaffolding protein that regulates the actin cytoskeleton.
CHD9	Encodes a transcriptional coactivator enables DNA and ATP-binding activity.
CPEB3	Encodes a protein involved in the cellular response to amino acid stimuli.
DDX28	Encodes a DEAD box protein that facilitates the assembly of the mitochondrial large ribosomal subunit.
DGKH	Encodes a diacylglycerol kinase enzyme involved in regulating intracellular concentrations of diacylglycerol and phosphatidic acid.
DUS1L	Encodes a protein that catalyzes the synthesis of dihydrouridine.
ERC1	Encodes a protein that regulates neurotransmitter release.
FER	Encodes a tyrosine kinase that regulates cell-cell adhesion and mediates signaling from the cell surface to the cytoskeleton via growth factor receptors.
FRYL	Encodes a protein involved in neuron projection development.
KATNB1	Encodes a protein that severs microtubules in an ATP-dependent manner.
LYSMD3	Encodes a protein that maintains Golgi structural integrity.
MARS2	Encodes a mitochondrial methionyl-tRNA synthetase protein.
MPHOSPH9	Encodes a phosphoprotein that negatively regulates cilia formation.
NAA60	Encodes an enzyme that localizes to the Golgi and transfers an acetyl group to the N-terminus of free proteins.
NCOR1	Encodes a protein that mediates ligand-independent transcription repression of thyroid-hormone and retinoic-acid receptors.
NDN	Encodes a protein that facilitates cell cycle arrest and acts as a transcription factor.
NF1	Encodes a protein that is a negative regulator of Ras transduction pathway.
PDS5A	Encodes a protein that regulates sister chromatid cohesion during mitosis.
PECAM1	Encodes an immunoglobulin that is involved in angiogenesis, leukocyte migration, and integrin activation.
PIK3CA	Encodes a phosphatidylinositol 3-kinase.
RELT	Encodes a receptor that plays a role in apoptosis.

Table A-6. Cont.

Gene	Function
RPTOR	Encodes a protein that regulates cell growth in response to nutrient and insulin levels.
SLC9A3R1	Encodes a sodium/hydrogen exchanger regulatory cofactor that regulates various proteins.
SMCHD1	Encodes a protein that plays a role in epigenetic silencing by regulating chromatin architecture.
SPATA33	Encodes a protein involved in fertilization and sperm motility.
TACC1	Encodes a protein that regulates transcription induced by nuclear receptors.
TGDS	Encodes a gene involved in the metabolism of a variety of compounds, including prostaglandins, retinoids, lipids, steroid hormones, and xenobiotics.
TMEM143	Encodes a transmembrane protein involved in hematopoietic progenitor cell differentiation.
TMEM115	Encodes a transmembrane protein involved in retrograde vesicle-mediated transport.
UBR2	Encodes an E3-ubiquitin ligase that targets proteins with destabilizing N-terminal residues for polyubiquitylation and proteasome-mediated degradation.
VWA8	Encodes a protein that enables ATP binding.
ZNF483	Encodes a zinc finger protein that enables DNA-binding transcription factor activity.
ZNF518A	Encodes a zinc finger protein that acts as a nuclear transcriptional regulator.

Prader-Willi syndrome uniparental disomy subtype (PW-UPD). *Data Source*: Safran, M., Rosen, N., Twik, M., BarShir, R., Stein, T. I., Dahary, D., Fishilevich, S., and Lancet, D. (2021) The GeneCards Suite. In *Practical Guide to Life Science Databases* (Abugessaisa, I., and Kasukawa, T., eds) pp. 27-56, Springer Nature Singapore, Singapore.

Table A-7. Differentially expressed genes in neurotypical control versus PW-del neurons identified by RNAseq and sc-RNAseq.

Gene	Function
ANGPTL4	Encodes a serum protein that regulates glucose homeostasis, lipid metabolism, and insulin sensitivity.
CTNNA2	Encodes a protein involved in the regulation of neuron migration and projection development.
CXCL12	Encodes a chemokine member of the intracrine family and functions as a ligand for G-protein coupled receptor chemokine receptor 4.
FBH1	Encodes an F-box protein that has both DNA-dependent ATPase and DNA unwinding activities.
FOXK1	Encodes a transcriptional regulator involved in different processes such as glucose metabolism, aerobic glycolysis, muscle cell differentiation and autophagy.
FOXO1	Encodes a transcription factor regulated by insulin signaling.
HERC2	Encodes an E3 ubiquitin-protein ligase that regulates ubiquitin-dependent retention of repair proteins on damaged chromosomes.
NOTCH2	Encodes a receptor that regulates cell fate determination.
PHF10	Encodes a protein that regulates transcription by chromatin remodeling.
RASGRF2	Encodes a calcium-regulated nucleotide exchange factor activating both RAS and RAS-related protein, RAC1, through the exchange of bound GDP for GTP
SNRPN	Encodes a component of the small nuclear ribonucleoprotein complex involved in tissue-specific alternative RNA processing events
SYNPO	Encodes a protein that plays a role in actin-based cell shaping and motility.
TNR	Encodes an extracellular matrix glycoprotein that plays a role in neurite outgrowth, neural cell adhesion and modulation of sodium channel function.
UBE3A	Encodes an E3-ubiquitin protein ligase.

Prader-Willi syndrome deletion subtype (PW-del). *Data Source*: Safran, M., Rosen, N., Twik, M., BarShir, R., Stein, T. I., Dahary, D., Fishilevich, S., and Lancet, D. (2021) The GeneCards Suite. In *Practical Guide to Life Science Databases* (Abugessaisa, I., and Kasukawa, T., eds) pp. 27-56, Springer Nature Singapore, Singapore.

VITA

Anna K. Victor was born in Memphis, Tennessee in 1991. After graduating from high school in 2010, she attended the University of Tennessee at Knoxville, obtaining a Bachelor of Science degree in Microbiology. Following graduation, she worked in the biomedical industry for several years at Meridian Biosciences in Memphis, Tennessee before attending graduate school at the University of Tennessee Health Science Center where she worked toward earning her PhD in the College of Graduate Health Sciences Biomedical Sciences Program, Neuroscience Track with her mentor Dr. Lawrence Reiter. She expects to receive her doctorate in April 2023.